August 12, 1961

To the Graduate Council:

I am submitting herewith a thesis written by George Marshall Drake, Jr. entitled "Heat and Momentum Transfer Within the Thermal Entrance Region for Non-Newtonian Fluids in Laminar Flow." I recommend that it be accept in partial fulfillment of the requirements for the degree of Doctor of Philosophy, with a major in Chemical Engineering.

John W. Prados
Major Professor

We have read this thesis and recommend its acceptance:

A H Jury
Edgar D Reaves
Donald C. Bogue
M Pickles
Harry F Rutrose
I Johnson
E E Stansbury

Accepted for the Council:

W. E. Spivey
Dean of the Graduate School

HEAT AND MOMENTUM TRANSFER WITHIN THE THERMAL ENTRANCE REGION FOR NON-NEWTONIAN FLUIDS IN LAMINAR FLOW

A Dissertation

Presented to

the Graduate Council of

The University of Tennessee

In Partial Fulfillment

of the Requirements for the Degree

Doctor of Philosophy

---

by

George Marshall Drake, Jr.

August 1961

ACKNOWLEDGEMENTS

The author wishes to acknowledge and express his appreciation to his major professor, Dr. John W. Prados, for the initial suggestions which led to the selection of this research problem and for the continued interest, suggestions, and constructive criticism which he has given throughout the investigation.

The members of the University's faculty have contributed materially to various facets of the authors education by their dedicated and enthusiastic instruction. The author is particularly grateful to the late Dr. R. M. Boarts for his counsel and financial assistance in the form of positions as a research assistant and later as an instructor of Chemical Engineering.

This research has been financially supported by the Phillips Petroleum Company and E. I. du Pont de Nemours and Company. The author wishes to express his sincere gratitude to both of these companies for their support.

Mr. E. H. Honeycutt, supervisor of the Chemical and Metallurgical Engineering Department's laboratories, and his staff have been of great assistance in the construction of experimental equipment for this work. The author is particularly indebted to Mr. O. V. Prater and Mr. H. B. Thompson for their numerous suggestions concerning the design and modification of equipment and for their craftmanship in constructing and assembling the various components.

The work of Mr. James A. Allen, who skillfully made the technical illustrations, is gratefully acknowledged.

525268

Sincere appreciation is extended to Mrs. Shirley Sue Brooks, who typed this manuscript; her great care with the many tables is particularly appreciated.

The author wishes to express his sincere gratitude to his wife, Margaret, who contributed immeasurably to the preparation of this thesis.

SUMMARY

Thermal conductivities were determined under non-isothermal laminar flow conditions for non-Newtonian fluids (aqueous, neutralized Carbopol solutions). The investigation was conducted with both vertically upward and vertically downward flow through a water-cooled, 1 inch schedule 40, stainless steel test section. Heat was supplied to the test fluid through a pair of steam heated concentric-pipe heat exchangers, and mixing and circulation were provided by a centrifugal pump.

Radial and axial temperature distribution data were obtained from the dynamic flow system through five thermocouple ports for eight different runs. These data were used with experimentally determined temperature-dependent rheological data to calculate: (a) velocity distributions and (b) thermal conductivities. The calculated thermal conductivity data qualitatively suggest that an increase in shear stress causes a slight decrease in thermal conductivity. It was not possible, however, to evaluate the effect of shear stress quantitatively because the constant shear stress regions essentially coincided with the isotherms.

Temperature profiles, calculated numerically under the assumption of constant thermal conductivity, agreed well with experimental results. Hence, it was concluded that any variations in thermal conductivity produced by shear stress and temperature variation were small enough not to affect the temperature distributions in the system studied.

Studies of the rheological behavior of the test fluids (aqueous, neutralized Carbopol solutions) were carried out using both a capillary and a rotational viscometer. These studies indicated that aqueous, neutralized Carbopol solutions obey the empirical power-law rheological model with some deviations at low shear stresses. The proportionality factor in the power law was found to decrease linearly with increasing temperature, while the shear-rate exponent was found to be temperature-independent.

Both direct experimental and calculated data served to indicate that free convectional effects were negligible in the viscous test fluids. The limited heat transfer data from this work were compared with literature correlations and found to be in reasonable agreement.

TABLE OF CONTENTS

CHAPTER		PAGE
I.	INTRODUCTION	1
II.	REVIEW OF PREVIOUS WORK	4
III.	DYNAMIC THERMAL CONDUCTIVITIES	11
IV.	EXPERIMENTAL EQUIPMENT	14
	General	14
	The Test Fluid	14
	The Rotational Viscometer	15
	The Flow System	15
V.	EXPERIMENTAL PROCEDURE	23
	General	23
	The Test Fluid	23
	The Flow Loop	24
VI.	PRESENTATION OF DATA AND RESULTS	26
	Data	26
	Results	29
VII.	DISCUSSION OF RESULTS	47
	Fluid Behavior	47
	Dynamic Thermal Conductivities	48
	Heat Transfer Considerations	50
	Experimental Errors	52
VIII.	CONCLUSIONS AND RECOMMENDATIONS	54

CHAPTER PAGE

REFERENCES 57

APPENDICES 62

A. The Capillary Viscometer 63

B. The Rotational Viscometer 76

C. Computer Programs 90

D. Explanation of Tabulated Data and Results 103

E. Nomenclature 130

VITA 135

LIST OF TABLES

TABLE		PAGE
I.	Summary of Temperature Profiles, Empirical Approximation, $T = T_{CL} - Ar^m$	30
II.	Rate of Axial Temperature Changes, Graphically Evaluated	36
III.	Pressure Gradient Data and Calculated Modifications Based on Continuity	37
IV.	Temperature-Dependent Rheological Parameters $C = C_o - BT$, where T is in ^oF	38
V.	Calculated Dimensionless Groups and Bulk Temperature	44
VI.	Dimensionless Groups for Heat Transfer Correlation	45
VII.	Reduced Temperature $\Theta = \frac{T - T_w}{T_i - T_w}$	46
VIII.	Capillary Viscometer Data	71
IX.	Brookfield Calibration Data, National Bureau of Standards Oil "N" at 77.0^oF	79
X.	Sample Rotational Viscometer Data	83
XI.	Sample Calculated Shear Stress on Spindle Wall	84
XII.	Sample Calculated Rheological Parameters as a Function of Temperature	85
XIII.	Experimental Temperature Distribution, Run 1	106
XIV.	Experimental Temperature Distribution, Run 2	107
XV.	Experimental Temperature Distribution, Run 3	108
XVI.	Experimental Temperature Distribution, Run 4	109
XVII.	Experimental Temperature Distribution, Run 5	110

TABLE		PAGE
XVIII.	Experimental Temperature Distribution, Run 6	111
XIX.	Experimental Temperature Distribution, Run 7	112
XX.	Experimental Temperature Distribution, Run 8	113
XXI.	Calculated Velocity and Thermal Conductivity Distribution, Run 1	114
XXII.	Calculated Velocity and Thermal Conductivity Distribution, Run 2	115
XXIII.	Calculated Velocity and Thermal Conductivity Distribution, Run 3	116
XXIV.	Calculated Velocity and Thermal Conductivity Distribution, Run 4	117
XXV.	Calculated Velocity and Thermal Conductivity Distribution, Run 5	118
XXVI.	Calculated Velocity and Thermal Conductivity Distribution, Run 6	119
XXVII.	Calculated Velocity and Thermal Conductivity Distribution, Run 7	120
XXVIII.	Calculated Velocity and Thermal Conductivity Distribution, Run 8	121
XXIX.	Calculated Temperature Profiles with Assumed Constant Thermal Conductivity, Run 1	122
XXX.	Calculated Temperature Profiles with Assumed Constant Thermal Conductivity, Run 2	123
XXXI.	Calculated Temperature Profiles with Assumed Constant Thermal Conductivity, Run 3	124

TABLE PAGE

XXXII. Calculated Temperature Profiles with Assumed Constant Thermal Conductivity, Run 4 125

XXXIII. Calculated Temperature Profiles with Assumed Constant Thermal Conductivity, Run 5 126

XXXIV. Calculated Temperature Profiles with Assumed Constant Thermal Conductivity, Run 6 127

XXXV. Calculated Temperature Profiles with Assumed Constant Thermal Conductivity, Run 7 128

XXXVI. Calculated Temperature Profiles with Assumed Constant Thermal Conductivity, Run 8 129

LIST OF FIGURES

FIGURE		PAGE
4.1	THE BROOKFIELD SYNCHRO-LECTRIC VISCOMETER	16
4.2	THE ROTATIONAL VISCOMETER ASSEMBLY	17
4.3	SCHEMATIC LAYOUT OF EXPERIMENTAL FLOW SYSTEM APPARATUS .	19
4.4	DETAILS OF THE EXPERIMENTAL TEST SECTION	20
4.5	THERMOCOUPLE PROBES AND CALIPER	21
6.1	THE EFFECT OF pH ON APPARENT VISCOSITY	27
6.2	TYPICAL CAPILLARY VISCOMETER DATA FOR POWER-LAW MODEL EVALUATION	28
6.3	OUTLET EXPERIMENTAL TEMPERATURE DISTRIBUTIONS FOR RUNS 3 AND 4	31
6.4	THERMAL CONDUCTIVITY VERSUS RADIAL POSITION (RUN 5) . .	32
6.5	THERMAL CONDUCTIVITY VERSUS RADIAL POSITION (RUN 8) . .	33
6.6	THERMAL CONDUCTIVITY VERSUS TEMPERATURE FOR VARIOUS SHEAR STRESS CONDITIONS (RUN 5)	34
6.7	THERMAL CONDUCTIVITY VERSUS TEMPERATURE FOR VARIOUS SHEAR STRESS CONDITIONS (RUN 8)	35
6.8	THE DEVELOPING TEMPERATURE AND VELOCITY PROFILES, RUN 8	40
6.9	CALCULATED TEMPERATURE DISTRIBUTIONS WITH EXPERIMENTAL DATA (RUN 5) ASSUMING CONSTANT THERMAL CONDUCTIVITY. .	41
6.10	CALCULATED TEMPERATURE DISTRIBUTIONS WITH EXPERIMENTAL DATA (RUN 8) ASSUMING CONSTANT THERMAL CONDUCTIVITY. .	42

FIGURE		PAGE
6.11	THEORETICAL TEMPERATURE DISTRIBUTIONS WITH EXPERIMENTAL DATA	43
A.1	CROSS SECTIONAL VIEW OF CAPILLARY VISCOMETER	64
A.2	SCHEMATIC DIAGRAM OF CAPILLARY VISCOMETER ASSEMBLY . . .	65
B.1	CALIBRATION DATA FOR THE BROOKFIELD SYNCHRO-LECTRIC VISCOMETER, 0.500 IN. SPINDLE	80
B.2	TYPICAL RHEOLOGICAL DATA, SAMPLE TAKEN AFTER RUN 6 . . .	86
B.3	TYPICAL SHEAR STRESS VERSUS TEMPERATURE DATA, SAMPLE TAKEN AFTER RUN 6	87
B.4	TYPICAL LOG-LOG PLOT OF SHEAR STRESS VERSUS SPINDLE SPEED DATA, SAMPLE TAKEN AFTER RUN 6	88
B.5	TYPICAL CONSISTENCY INDEX VERSUS TEMPERATURE DATA, SAMPLE TAKEN AFTER RUN 6	89

CHAPTER I

INTRODUCTION

The variety and number of recent publications on facets of non-Newtonian fluid behavior manifest the growing importance of this area of scientific research. Current literature abounds with descriptions of peculiar fluid behavior (1)(6)(23)(32)(34)(43)(51); and, although quantities of research have been done on non-Newtonian rheology, many questions remain unanswered.

A multitude of isothermal, laminar flow analyses of non-Newtonian fluid behavior have appeared in the literature (8)(17)(31)(36)(50). Some of these analyses have semi-theoretical foundation while the remainder are based on empirical observation alone. To date there has been no general formulation made of a non-Newtonian fluid theory which adequately describes and explains the various types of fluid behavior. Consequently, the methods currently employed for engineering design depend on the rheological behavior of the particular type of non-Newtonian fluid in question.

The realm of non-isothermal laminar flow is complicated by temperature dependent fluid properties. Even for Newtonian fluids, which are relatively uncomplicated, one finds that the addition of heat (positive or negative) to fluids in laminar flow generates problems so complex mathematically that solutions are all but impossible except by numerical means or the inclusion of severe, simplifying assumptions (20)(30). The situation is the same for non-Newtonian fluids with the further difficulty of a more complex rheological model. As a result,

the empirical methods commonly employed have inherently lacked the generality required for application to changes in variables such as shear stress, temperature, viscosity, thermal conductivity, etc. in laminar, non-Newtonian fluid flow.

Based on the premise that transport phenomena in fluids (gases and liquids) are functions of the same variable (6)(15)(42) and knowledge that molecular viscosity is a non-proportional function of shear stress in non-Newtonian fluids (liquids) (1)(23)(32), it is conceivable that the thermal conductivity of non-Newtonian fluids (liquids) may be some function of shear stress also. Experimental thermal conductivity data for liquids are conventionally determined by using thin layers of liquid in static test equipment (12)(18)(19)(44). There are certain obvious reasons for making measurements in this manner, such as: (a) the measurements are simple and standardized, (b) the equipment is easy to calibrate, and (c) convectional effects can be eliminated or accurately estimated (19)(44). However, static tests cannot show any shear stress dependence of the thermal conductivity, should such exist.

It was felt that a technique of experimentally evaluating thermal conductivities of liquids from a dynamic flow system was necessary for the analysis of functional relationships between thermal conductivity and shear stress for non-Newtonian fluids, and the present work was undertaken in an attempt to develop such a technique. Specifically, the objectives were: (a) to develop an experimental and mathematical method to evaluate point values of thermal conductivity as a function of temperature and shear stress, and (b) to evaluate the effect of liquid

thermal conductivity variation on temperature profiles observed in laminar non-isothermal flow.

To achieve these objectives, a mathematical analysis was made to relate the desired fluid properties to quantities which could be measured experimentally. Next a series of rheological experiments were carried out to evaluate aqueous solutions of carboxypolymethylene (Carbopol-934) for use as the non-Newtonian fluid to be tested. Then a series of steady-state, laminar, pipe-flow experiments were made to determine actual temperature profiles in the thermal entrance region. Finally the data were analyzed with the aid of the IBM 1620 digital computer in the University of Tennessee Computer Center. This analysis yielded thermal conductivity values as functions of temperature and shear stress and also demonstrated the effect of thermal conductivity variations on the temperature profiles.

Those who are not familiar with non-Newtonian fluids in general are referred to one of the general references on the subject (1)(6)(23)(32)(34)(43)(51). The following chapter is a general review of related literature. The next chapter is devoted to the technique of determining experimental thermal conductivities from a dynamic flow system. This is then followed by descriptions of the experimental equipment and procedures, and finally the experimental results are presented. Mathematical derivations, explanation of calculations, experimental data, computer programs, and notation are found in the appendices.

CHAPTER II

REVIEW OF PREVIOUS WORK

A - Isothermal, Laminar Flow

The theory of isothermal, laminar flow of Newtonian fluids is comparatively well understood and mathematically developed. The Navier-Stokes equations of fluid motion with friction

$$\rho \frac{D\vec{w}}{Dt} = \rho \vec{g} - \nabla P - (\nabla \cdot \vec{\tau}) \quad , \qquad (2\text{-}1)$$

the continuity equation

$$\frac{D\rho}{Dt} = - \nabla \cdot (\vec{w} \rho) \quad , \qquad (2\text{-}2)$$

and suitable boundary conditions provide sufficient information to determine velocity profiles in isothermal laminar flow. However, the complex non-linear nature of the equations makes it impossible to obtain analytical solutions except for very simple geometries or in regions where boundary layer simplifications apply. In equations (2-1) and (2-2), t is time, ρ is the fluid density, $\vec{\tau}$ is the shear stress tensor, $\vec{g}$ is the external force vector, $\vec{w}$ is the velocity vector, and P is static pressure. For further information the reader is referred to one of the standard texts on hydrodynamic theory (14)(22)(38)(41)(46).

The same general hydrodynamic equations are used for isothermal, laminar flow of non-Newtonian fluids; however, some very useful results have been obtained for particular non-Newtonian fluids in circular pipe flow. Analysts desiring to predict certain flow quantities for non-

Newtonian fluids in circular pipe flow may use one of the following approaches rather than the more complex general Navier-Stokes equations (from which these methods come).

One method of analyzing flow behavior is to use rheological data to determine the local shear rate, $(-dw/dr)$, as a function of shear stress, τ.

$$\frac{-dw}{dr} = f(\tau) \qquad (2\text{-}3)$$

The resulting expression is then integrated twice to determine volumetric flow rate, Q,

$$Q = 2\pi \int_0^{R_w} r \left[\int_r^{R_w} f(\tau)\, d\, y_r \right] dr, \qquad (2\text{-}4)$$

where: R_w is the pipe radius, y_r is the dummy integration symbol for distance from the centerline, and r is the actual distance from the centerline.

Equation (2-4) has been evaluated for Bingham plastics by Buckingham (7); for power-law fluids by Weltman, McGinnis, and others (23)(31)(50); for Eyring's simple hyperbolic sine relation by Tobolsky and Eyring (48); and for the more complex Powell-Eyring equation by Stevens (8).

An alternate method of evaluating flow parameters, proposed by Metzner and Reed (36), is somewhat more general since no particular rheological model need be assumed for the actual test fluid. The power-law parameters C and n in equation (2-5)

$$\tau = C \left(\frac{-dw}{dr} \right)^n , \qquad (2\text{-}5)$$

are replaced by the modified parameters C' and n' where

$$\frac{1}{n'} = \frac{d \ln(8V/D)}{d \ln(D \Delta P/4L)} , \qquad (2\text{-}6)$$

$$C' = \frac{D \Delta P}{4L} \Big/ \left(\frac{8V}{D}\right)^{n'} , \qquad (2\text{-}7)$$

V is the average linear velocity, D is the inside pipe diameter, and $\Delta P/L$ is the linear pressure gradient. Thus, by evaluating the constants C' and n' from experimental capillary data, one can use equations (2-4), (2-5), and (2-7) to evaluate the flow parameters directly. This technique has proven useful over wide ranges of shear stress since the modified parameters C' and n' do not change appreciably for many fluids (5)(9)(35)(36).

B - Non-Isothermal Laminar Flow

The absence of any general expressions for accurately depicting the temperature dependence of fluid properties has caused the development of mathematical theories of non-isothermal, laminar flow to lag behind the corresponding theory for isothermal flow. Even in those cases where temperature dependence of properties can be taken into account, the mathematical solution appears to be impossible except by numerical means unless severe simplifying assumptions are made.

Non-isothermal, laminar flow can be described with equations (2-1) and (2-2), and the energy equation,

$$C_p \rho \frac{DT}{Dt} = -(\nabla \cdot \vec{q}) - (\tau : \nabla \vec{v}) . \qquad (2\text{-}8)$$

In equation (2-8), T is temperature, C_p is heat capacity, $\vec{q}$ is the heat flux vector, and $(\tau:\nabla\vec{w})$ is heat production due to viscous dissipation. The role of the heat production by the viscous dissipation term is not important under many conditions (27) and is generally neglected (10)(16)(27).

In the general case, the density, ρ ; the viscous friction term of equation (2-1), $(\nabla\cdot\vec{\tau})$; the heat flux term of equation (2-8), $(\nabla\cdot\vec{q})$; and heat capacity, C_p, will be functions of the temperature distribution, and therefore of the coordinate system chosen. Equation (2-8) also involves the velocities for which equation (2-2) is the differential equation. Consequently, to solve the general problem, one must solve two non-linear partial differential equations, each of which involves the integrated result of the other. The complexity of this problem defies rigorous solution except by numerical means.

Several attempts have been made to solve equations (2-1), (2-2) and (2-8). The classical solutions first obtained by Graetz, Leveque, Nusselt, and Russell for Newtonian fluids generally involved assumptions of some particular form of velocity distribution for use in Equation (2-8). These solutions and their limitations are reviewed and discussed at great length by Drew (10) and Boelter et al. (4), and the reader is referred to these papers for further information.

In the above classical solutions to equations (2-1), (2-2), and (2-8), no attempt was made to take the effect of temperature on fluid properties into account, i. e., constant fluid properties were assumed. Some of the more recent investigators of the problem have attempted to take the variation of fluid properties into account. Boelter et al. (4)

and Lee (25) attempted to allow for Newtonian viscosity variations by a series of successive approximations to determine pressure gradients in non-isothermal flow, and Yamagata (52) made similar calculations in which he attempted to evaluate heat transfer characteristics. Yamagata found it necessary to add an emperical correction for density variation in addition to his incorporated Newtonian viscosity variation. Martinelli and Boelter (29) and Boelter (3) allowed for the temperature dependence of density but not viscosity; and, therefore, accounted for natural convection only. Their results proved successful in accounting for non-isothermal effects in mass transfer (3) but proved inadequate when applied to data for heated laminar flow of oils (29). Pigford (40) treated the case of laminar, Newtonian fluid flow in vertical tubes in which both density and fluidity (the recripocal of viscosity) were assumed to be linear functions of temperature. However, it was necessary to assume Leveque's temperature distribution for the boundary near the wall in order to solve the differential equation for pressure gradients. Therefore, Pigford's results are limited to flows with high Graetz moduli (short heated lengths and high linear velocities). Pigford also suggests modifications to his theoretical solution which might be used to account for non-isothermal effects in the flow of power-law, non-Newtonian fluids. Lyche and Bird (27) solved equations (2-1), (2-2) and (2-8) for the limiting case of "isothermal" heat transfer (i. e., the difference between the tube wall and the bulk of the fluid is small, and the variation of fluid properties is small enough to be neglected) for power-law, non-Newtonian fluids. They reduced these equations to a Sturm-Liouville problem for which they tabulated eigenvalue solutions for the cases of

$n = 1/3$ and $n = 1/2$. Several numerical solutions for the temperature distribution or pressure gradient from equations (2-1), (2-2), and (2-8) have recently been obtained for the power-law type of non-Newtonian fluids with digital computers (13)(16)(49). Gee and Lyon (13) made the most general allowances for temperature dependent fluid properties reported to date. They included temperature dependence of apparent viscosity, thermal conductivity, and heat capacity in addition to internal frictional generation of heat.

In addition to the above analytical and numerical solutions, there have also been several empirical investigations of the problem of non-isothermal, laminar flow. Perhaps the first was that of Keevil and McAdams (21) who developed empirical curves of friction factor versus Reynolds number as functions of temperature. Sieder and Tate (47) obtained equation (2-9) for laminar non-isothermal Newtonian fluid flow.

$$\frac{f_{iso}}{f_{ni}} = 1.1 \left(\frac{\mu_b}{\mu_w}\right)^{1/4} , \qquad (2\text{-}9)$$

where: f_{iso} is the isothermal Fanning friction factor,

f_{ni} is the non-isothermal Fanning friction factor,

μ_b is the viscosity evaluated at the bulk temperature,

and

μ_w is the viscosity evaluated at the wall temperature.

By means of equation (2-9) it is possible to bring non-isothermal laminar friction factors into superposition with the isothermal form of Poiseuille's equation. Although the Sieder-Tate empirical correlation

was proposed over twenty years ago, it is still the best available empirical method of incorporating non-isothermal effects into engineering design equations. Metzner (37) attempted to modify the Sieder-Tate correlation for extension to non-Newtonian fluids and was able to show some correlation. Metzner also made some empirical heat transfer correlations for non-Newtonian fluids in laminar flow.

In the work reviewed above, there has been little effort made to incorporate the variation of thermal conductivity into a solution of equations (2-1), (2-2), and (2-8). Only one investigation has been conducted where a temperature dependent thermal conductivity was used (13). Apparently no work, either theoretical or experimental, has previously been done on evaluating thermal conductivity data for liquids under conditions other than those in static test equipment described in many standard reference works (18)(19)(30)(39). All thermal conductivity data reported in the open literature have been concerned with its temperature dependence while assuming it to be unaffected by shear stress or any other flow parameter (even for non-Newtonian fluids). The work presented in the remainder of this thesis was undertaken to clarify this situation.

CHAPTER III

DYNAMIC THERMAL CONDUCTIVITIES

The equations of motion (2-1), continuity (2-2), and energy (2-8) presented in the preceding chapter provide the mathematical framework for extracting experimental liquid thermal conductivity data from a dynamic test system for non-Newtonian fluids. Consider the non-isothermal flow of a fluid through a cylindrical tube where it may be assumed that: (a) steady state has been attained, (b) radial velocity components are negligibly small, (c) heat conduction in the axial direction is negligible in comparison with heat transport in the axial direction by the over-all fluid motion, (d) heat produced by viscous dissipation is neglected, (e) the fluid obeys a non-Newtonian, temperature dependent, rheological model known as the pseudoplastic power-law, (f) there are no external (body) forces acting on the fluid, and (g) heat is removed from the fluid through the tube wall.

For cylindrical tubes (and incorporating the above assumptions) equations (2-1), (2-2), and (2-8) may be simplified to:

Motion:

$$0 = -\frac{dp}{dz} - \frac{1}{r}\frac{d}{dr}(r\tau_{rz}). \qquad (3\text{-}1)$$

Energy:

$$C_p \rho v_z \frac{\partial T}{\partial z} = -\frac{1}{r}\frac{\partial (rq_r)}{\partial r} \qquad (3\text{-}2)$$

in which τ_{rz} is the shear stress in the axial, z, direction per unit area on an element of fluid surface of constant radius, r, and q_r is the heat flux in the radial direction, r. In order to solve these equations,

the fluxes τ_{rz} and q_r are expressed in terms of velocity and temperature gradients as follows:

Power-law:

$$\tau_{rz} = -C \left| \frac{dw_z}{dr} \right|^{n-1} \frac{dw_z}{dr} \qquad (3\text{-}3)$$

Fourier's law:

$$q_r = -K \frac{\partial T}{\partial r} \qquad (3\text{-}4)$$

in which C and n are parameters in the modification of Newton's Law, obtainable as a function of temperature from analysis of flow data in various types of viscometers (1)(6)(23)(32)(34)(43)(51) and K is the coefficient of thermal conductivity. The use of the power-law has been discussed in detail in the above references. For Newtonian liquids C is the coefficient of viscosity, μ, and n is unity.

Substitution of equation (3-3) into equation (3-1) gives an equation for velocity distribution which can be numerically integrated (an analytical solution is possible in certain cases):

$$w_z = \int_r^{Rw} \left(\frac{\tau_{rz}}{C} \right)^{1/n} dy_r \qquad (3\text{-}5)$$

where τ_{rz} is evaluated from the pressure gradient by a simple force balance.

$$\tau_{rz} = \left(\frac{\Delta P}{L} \right) \frac{r}{2} \qquad (3\text{-}6)$$

Fourier's Law, equation (3-4), substituted into equation (3-2) gives the partial differential equation:

$$\frac{\partial}{\partial r}\left[r K \frac{\partial T}{\partial r}\right] = r C_p \rho w_z \frac{\partial T}{\partial z} \quad . \quad (3\text{-}7)$$

By integrating the above with respect to the radial distance, one obtains:

$$K(R) = \frac{\int_0^R r C_p \rho w_z \frac{\partial T}{\partial z} \, dr}{R\left(\frac{\partial T}{\partial r}\right)_R} \quad (3\text{-}8)$$

or, from substitution of equations (3-5) and (3-6) into equation (3-8):

$$K(R) = \frac{\int_0^R r C_p \rho \frac{\partial T}{\partial z}\left[\int_r^{R_w}\left(\frac{\Delta Pr}{2LC}\right)^{1/n} dy_r\right] dr}{R\left(\frac{\partial T}{\partial r}\right)_R} \quad . \quad (3\text{-}9)$$

The integral in equation (3-9) can be numerically evaluated from temperature dependent rheological data, the pressure gradient, and an experimental evaluation of the temperature distribution in both axial and radial directions.

CHAPTER IV

EXPERIMENTAL EQUIPMENT

I. GENERAL

The equipment used in this investigation consisted of a flow system and associated fluid testing equipment. A non-isothermal flow loop, measuring and regulating apparatus, and a fluid reservoir comprised the flow system. The fluid testing equipment included a MacBeth continuous indicating pH meter, a capillary viscometer with continuously varying pressure head used for a preliminary fluid behavior study (described in Appendix A), a Brookfield Synchro-Lectric viscometer used for a study of the temperature dependent rheological properties, and assorted laboratory glassware.

II. THE TEST FLUID

Carbopol 934 is the commercial name for a high molecular weight, carboxy vinyl polymer manufactured by the B. F. Goodrich Chemical Company and used in this investigation. It was obtained as a fluffy, white, water-soluble, acid powder which required neutralization for the development of maximum viscosity. The powdered form was dissolved in water and then neutralized with sodium hydroxide.

A Brookfield viscometer, with standard spindles, was used with a MacBeth continuous indicating pH meter to study the effect of pH on viscous properties and to establish the approximate range of concentrations to be used later in the flow system. It was found that concentrations of about 0.25 weight percent Carbopol had the

desired physical properties; and, consequently, the test fluids used in this work were near that composition.

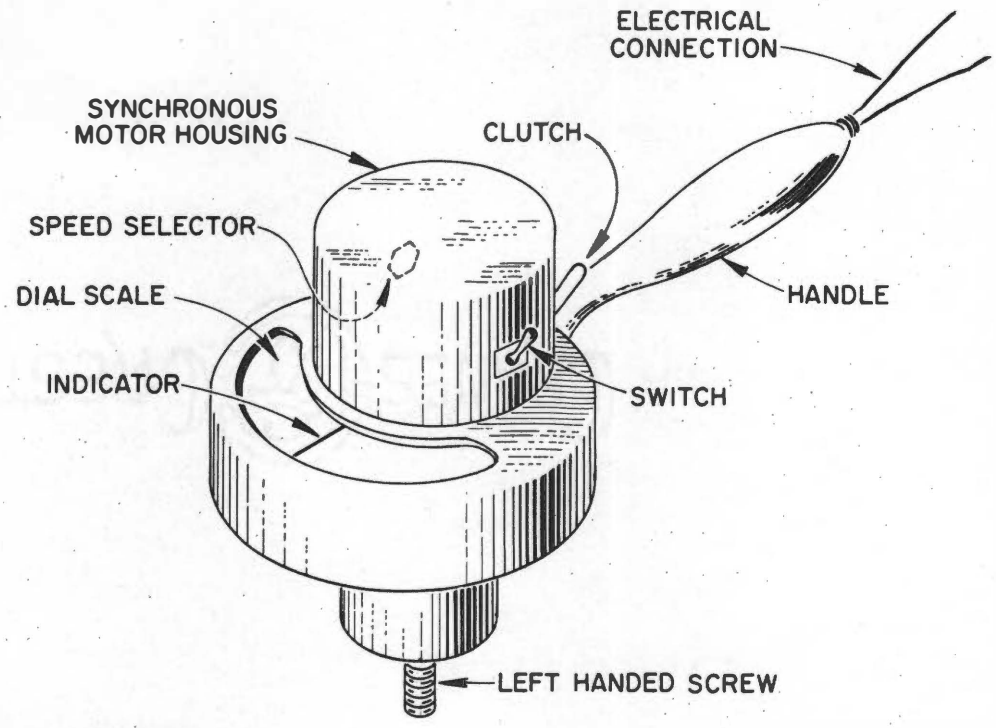
III. THE ROTATIONAL VISCOMETER

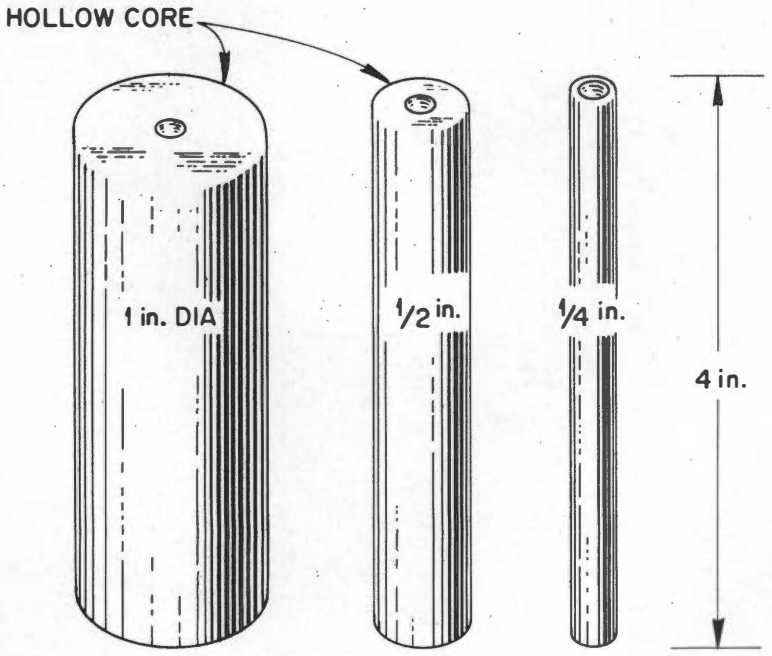
The Brookfield Synchro-Lectric Viscometer (No. 1474, U.T. Ch.E. 678) was used to measure quantities for calculating the temperature dependent rheological parameters of test fluids. The spindles normally used with the Brookfield viscometer were not of the cylindrical geometry most amenable to mathematical analysis; therefore, three cylindrical spindles (1.000, 0.500, and 0.250 inch outside diameter) were made and used, Figure 4.1.

The Brookfield viscometer was mounted on a steady, variable height table, Figure 4.2. The table height was adjusted by means of a vertical, threaded shaft geared to 0.01 inch of travel per turn of the feed handle. Elevation changes were measured with a spring dial, since there was some gear backlash in the feed mechanism. A small heat exchanger was mounted directly onto the table base and used to maintain the sample temperature at a constant value while the viscometer was in use. The heat exchanger circulated constant temperature ($\pm$ 0.2°C) water from a bath manufactured by Forma-Scientific, Inc.

IV. THE FLOW SYSTEM

All parts of the flow system that made contact with the test fluid were either stainless steel or glass. The upstream piping to the centrifugal pump (1/2 horsepower) was 1-1/2 inch schedule 40 pipe, and the downstream piping through the test section to the reservoir was





CYLINDRICAL SPINDLES

FIGURE 4.1

THE BROOKFIELD SYNCHRO-LECTRIC VISCOMETER

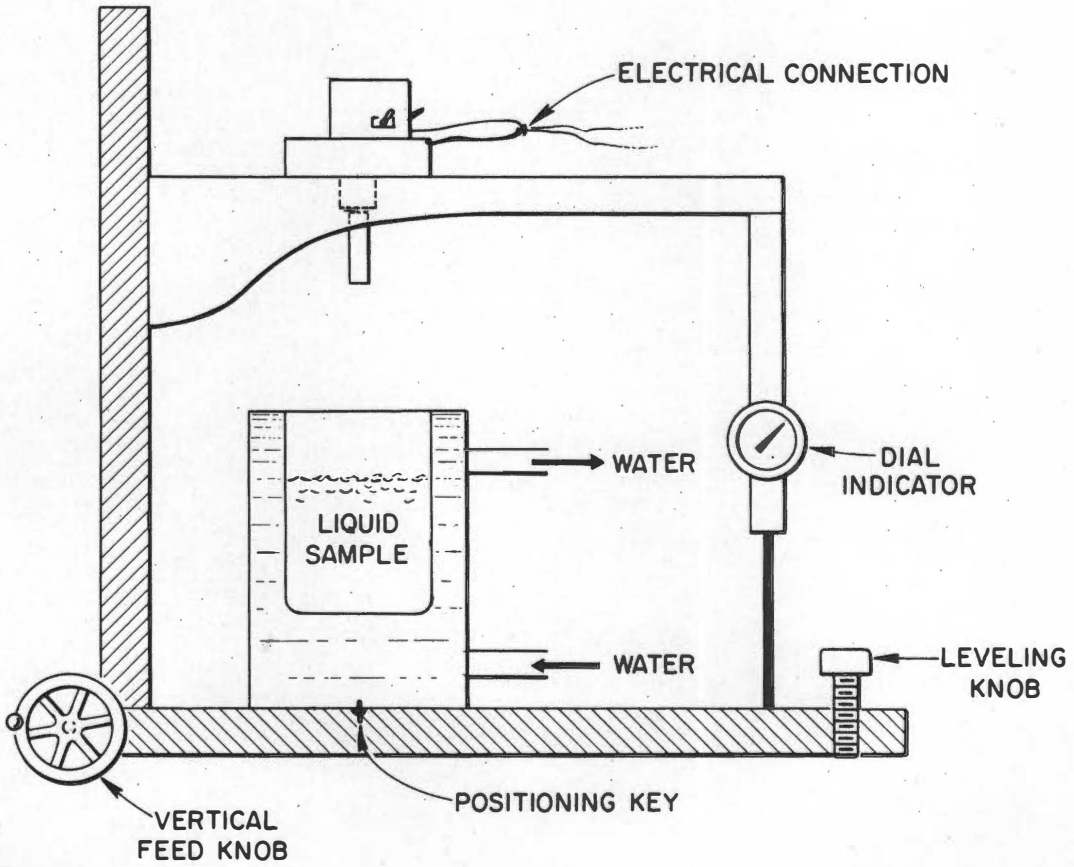


FIGURE 4.2

THE ROTATIONAL VISCOMETER ASSEMBLY

1 inch schedule 40 pipe.

The schematic diagram, Figure 4.3 shows the arrangement of the various components in the system. The check valve in the reservoir on the upstream side of the pump prevented the system from draining after shut-down, and the funnel on the upstream side was used to prime the pump for start-up. Two concentric pipe heat exchangers were installed upstream (2.25 feet vertical and 1.50 feet horizontal) to heat the test fluid. A rotameter was used with a manual control valve to maintain steady flow rates and to determine the approximate volumetric flows. Gate valves were arranged so that the direction of flow through the test section, Figure 4.4, could be reversed between runs, and a siphon-breaking vent was provided in the return line to the reservoir. City water was passed through the concentric pipe heat exchanger on the test section in a direction countercurrent to the test fluid for cooling.

An inverted differential manometer was used to measure the pressure drop across the test section. Temperature profiles were measured radially at 0.75 foot axial intervals along the cooled test section with thermocouples inserted through ports in the concentric pipe heat exchanger, Figure 4.4. The 30 gage copper-constantan thermocouples were sheathed in 0.072 inch outside diameter hypodermic tubing. An angular rotation of 90° was made between each thermocouple port.

The thermocouple probes, Figure 4.5, were bent inside the test section to form the "L" shape shown with the beaded point extending in a direction parallel to the pipe wall and into the flow direction of the fluid. The small conical nylon seal prevented leaks between the sheath and the pipe fittings pictured while epoxy resin cement was

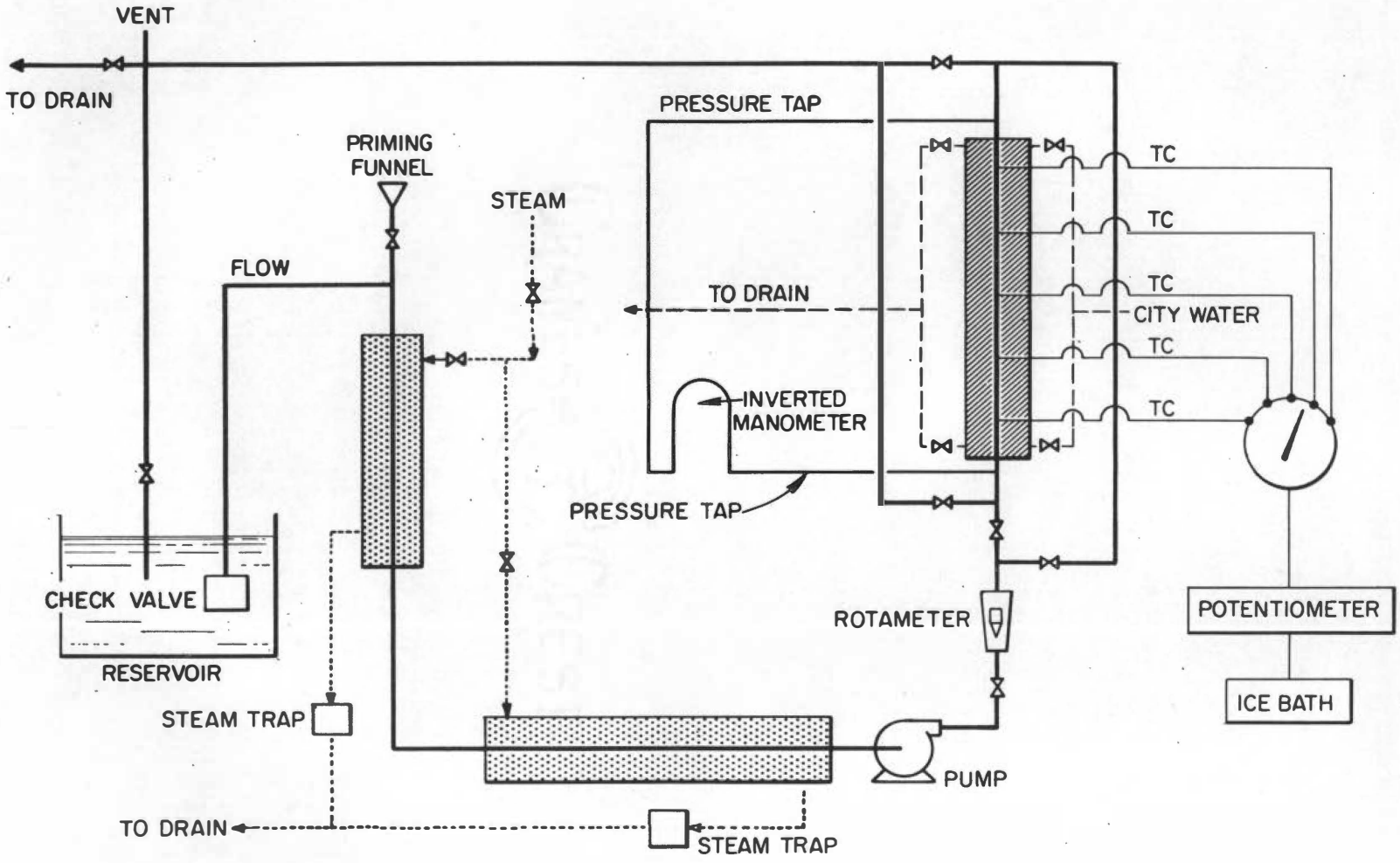


FIGURE 4.3

SCHEMATIC LAYOUT OF EXPERIMENTAL FLOW SYSTEM APPARATUS

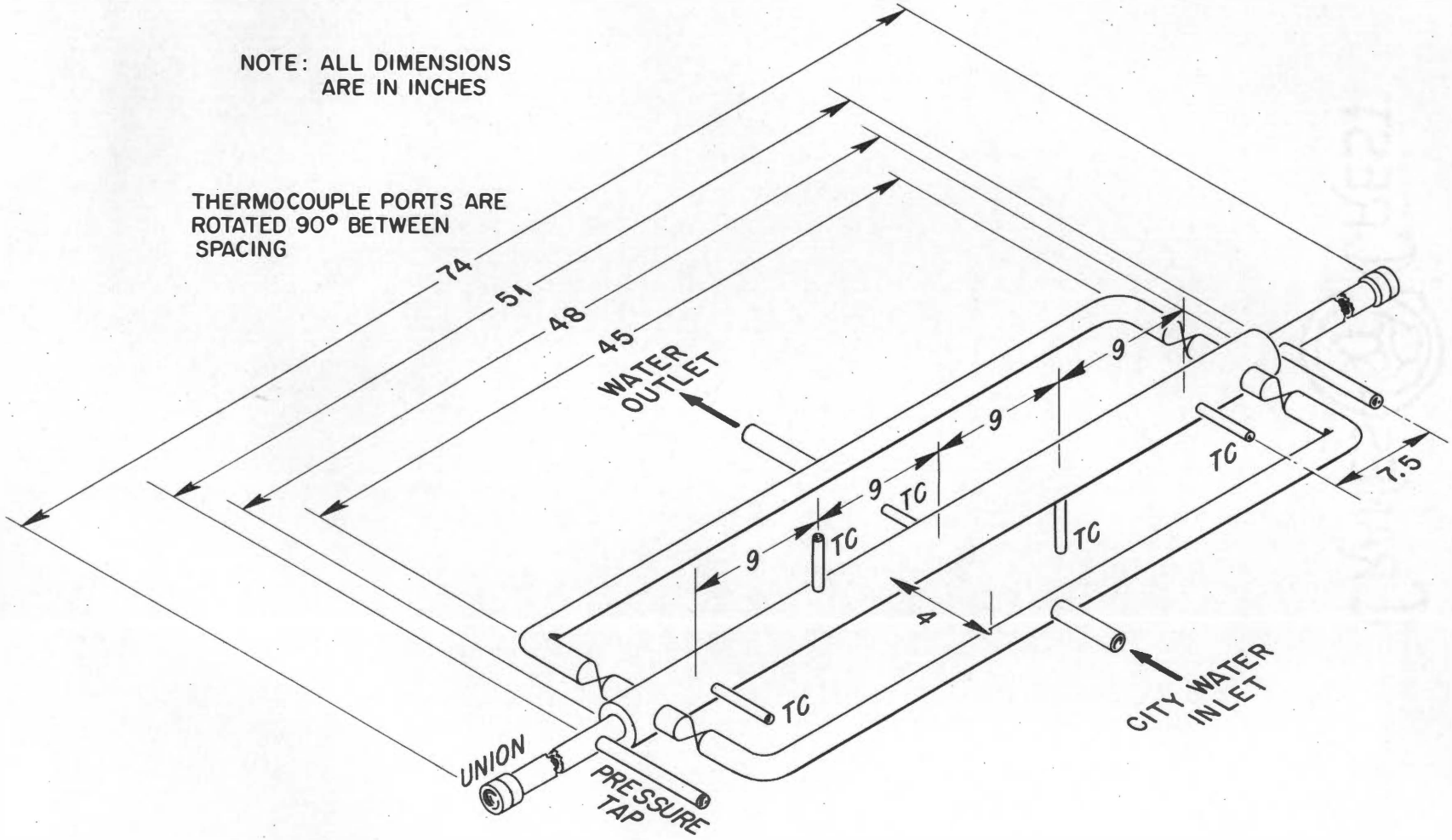


FIGURE 4.4

DETAILS OF THE EXPERIMENTAL TEST SECTION

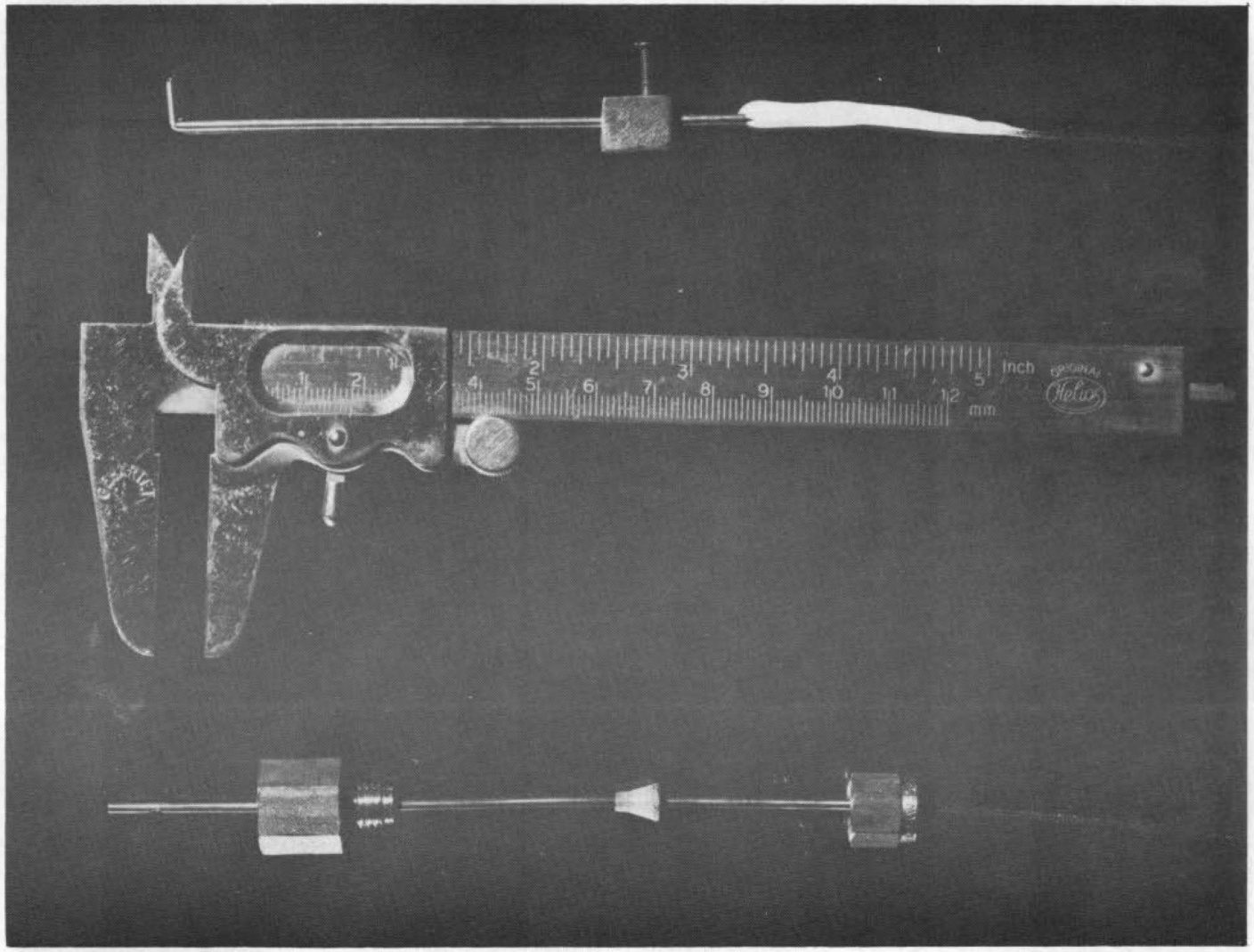


FIGURE 4.5

THERMOCOUPLE PROBES AND CALIPER

used to seal the thermocouple wire to the sheath as shown. This probe geometry eliminated steep temperature gradients along the thermocouple wires near the bead, and also minimized flow disturbances in the immediate vicinity of the bead. Radial distances were determined from measurements made with the vernier scale caliper shown in Figure 4.5 on the length of the thermocouple probe extending outside the pipe. The thermocouple emfs were determined with the aid of a Leeds and Northrup potentiometer (No. 319790, U.T. Ch.E. 117) and a Leeds and Northrup galvanometer (No. 1062928, U.T. Ch.E. 496).

CHAPTER V

EXPERIMENTAL PROCEDURE

I. GENERAL

There were two experimental objectives in this investigation: (a) to evaluate the rheological properties of the test fluid used and (b) to obtain steady-state temperature profile data from the test fluid in the flow loop. Rheological properties were evaluated through isothermal viscometric experiments carried out at a series of temperatures. Temperature profiles were obtained from movable probes inserted in the test loop.

II. THE TEST FLUID

Aqueous solutions of carboxypolymethylene (Carbopol-934) were investigated in a series of laboratory experiments. Solutions exhibiting non-Newtonian behavior were easily prepared with Carbopol concentrations less than a half of one percent by weight as noted by Metzner (33). Small amounts of standardized sodium hydroxide solution were added to various concentrations of Carbopol solutions after which the pH and apparent, or Brookfield, viscosity were measured. The general rheological behavior of several neutralized Carbopol solutions was studied by testing the pseudoplastic power-law model with capillary viscometer data, Appendix A. The densities of Carbopol solutions were found to be indistinguishable from those of water at the same temperature.

The Brookfield Synchro-Lectric viscometer, Figure 4.1, was used to evaluate the temperature-dependent rheological properties of test fluid samples taken before and after each run in the flow loop. The experimental method used to obtain these data was to place the sample in a small, constant-temperature heat exchanger mounted on the base of a variable height table, Figure 4.2, and measure the torque on a cylindrical spindle at various spindle speeds for a number of immersion depths. The power-law constants were determined from the data by the method outlined in Appendix B for several temperatures.

III. THE FLOW LOOP

The experimental flow loop was described in the preceding chapter, Figure 4.3. The steps involved in obtaining steady-state conditions and data from this equipment are best considered in four separate groups: (a) preliminary, (b) start-up, (c) steady-state, and (d) shut-down procedures.

A preliminary maintenance check of the equipment prefaced the normal start-up procedure. This maintenance check included repairing or replacing defective thermocouple probes, flushing the system if necessary, and checking the manometer lines. Flushing the system was periodically necessary to remove accumulated dirt or to use new solutions in the system. New solutions were made up directly in the flow loop by adding powdered Carbopol to the reservoir, circulating the mixture until the powdered Carbopol dissolved, and neutralizing with additions of measured quantities of a standard sodium hydroxide solution.

The start-up procedure included operations for each of the control and instrumentation units. The pump was started, the rotameter float level adjusted, cooling water turned on, and the steam rate regulated. The reference junction for the potentiometer was then prepared and preliminary thermocouple emf readings were noted. After the thermocouple readings became steady, final adjustments were made on the test solution, cooling water, and steam flow rates.

The steady-state operational procedure involved the manual maintenance of a steady rotameter level and the collection of data. Rotameter control was unpredictable and required close attention to prevent a wide variation in volumetric flow rates. During steady-state operation the following data were recorded for each test run: (a) the static pressure drop across the test section, (b) radial temperature profiles at 0.75 foot axial intervals, (c) the flow direction, and (d) the rotameter reading. In addition, two samples of the test solution were taken to evaluate the temperature-dependent rheological parameters for each run.

The shut-down procedure required turning off the steam about five minutes before stopping circulation. This short delay prevented the stagnant test fluid from becoming overheated in the flow loop. Overheating was undesirable because of "vapor locks" and "bubbles" formed by boiling the test fluid.

CHAPTER VI

PRESENTATION OF DATA AND RESULTS

I. DATA

The experimental data obtained in this investigation were those required to evaluate temperature, velocity, shear stress, and thermal conductivity distributions in the dynamic test system. An average pressure gradient and sets of experimental temperature profiles at five axial positions were measured for each test run. Liquid samples taken before and after each test run were analyzed for temperature-dependent rheological parameters. Complete tabulations of these and other pertinent experimental data are recorded in notebooks entitled "Original Record of Research" on file in the Chemical and Metallurgical Engineering Department of the University of Tennessee. These records are on pages 2552 to 2568, 3501 to 3519, 4551 to 4556, 16501 to 16550, 16851 to 16872, and 16901 to 16934, inclusive.

An index of viscous behavior (i.e. Brookfield or apparent viscosity) is plotted as a function of pH in Figure 6.1 for three aqueous Carbopol solutions. This figure is representative of those data taken in that portion of the investigation. The validity of the power-law rheological model was examined with data from a capillary viscometer and typical data from this analysis are shown in Figure 6.2. The method used and data for Figure 6.2 are given in Appendix A.

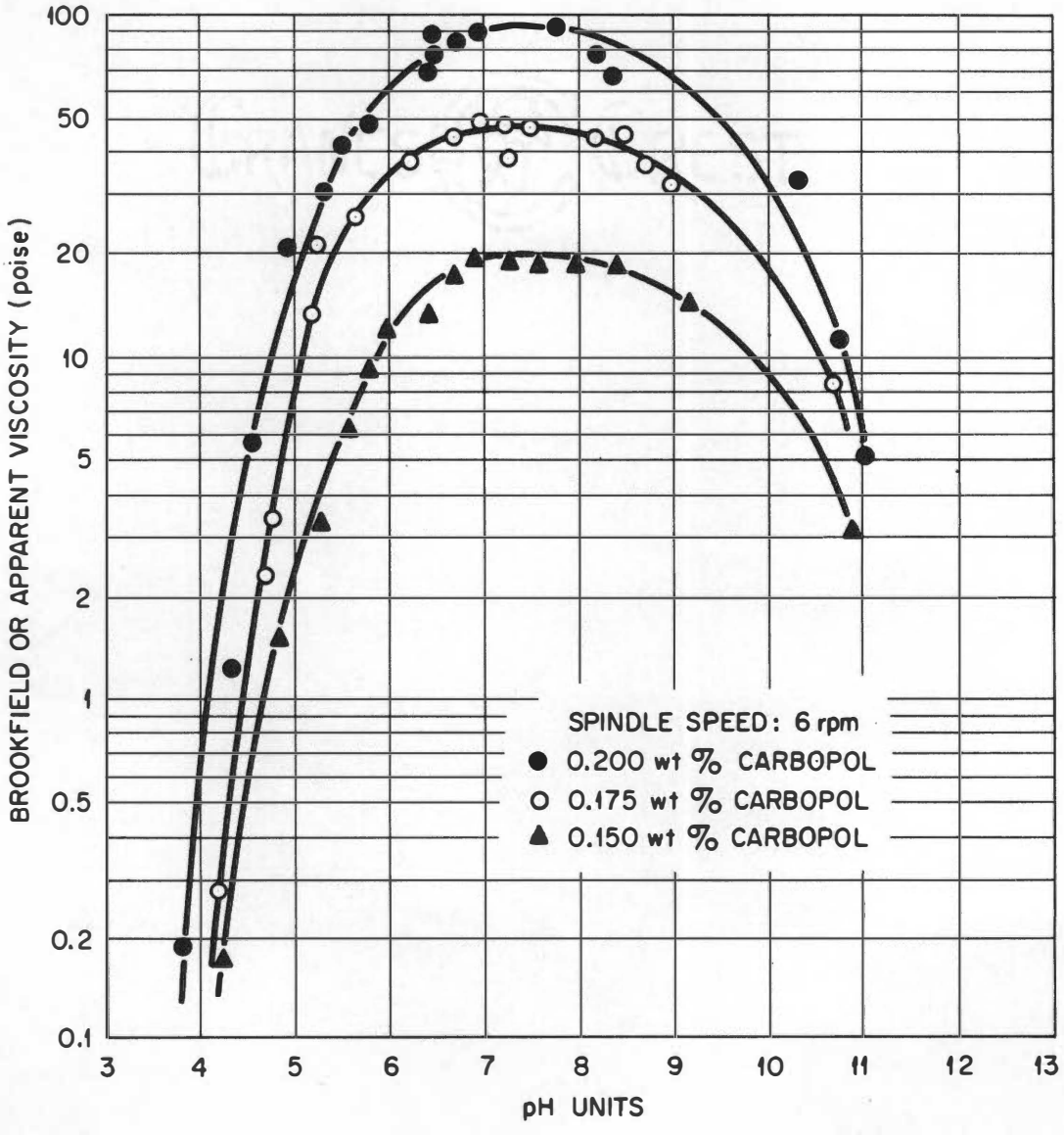


FIGURE 6.1

THE EFFECT OF pH ON APPARENT VISCOSITY

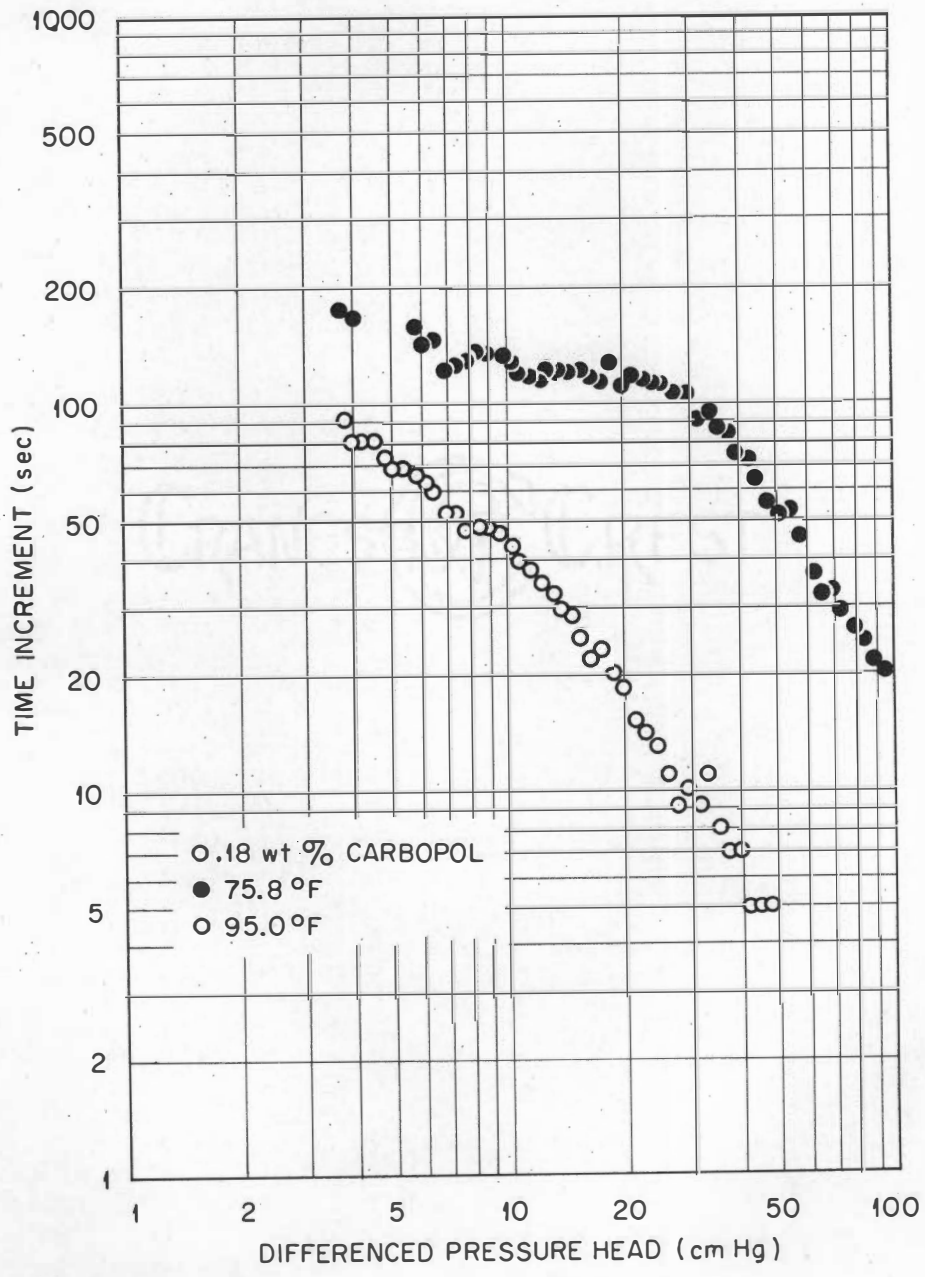


FIGURE 6.2

TYPICAL CAPILLARY VISCOMETER DATA FOR
POWER-LAW MODEL EVALUATION

Complete experimental temperature distributions are tabulated in Appendix D, and empirical equations fitted to these data are given in Table I. Graphically evaluated constants used to calculate axial temperature gradients are tabulated in Table II. The measured pressure gradient and calculated pressure gradients at intermediate points along the test section are tabulated in Table III for each run. The reduced radial distance variable used in many of the tabulations is defined as the radial distance from the centerline divided by the pipe radius which was 1.332 centimeters in this work. The temperature-dependent parameters in the power-law rheological equation are tabulated in Table IV for each test run. These constants represent average values obtained from two or more liquid samples tested at several temperatures in the range encountered in the experimental test run. All temperatures, linear measurements, and force units in the above tables are given in degrees Fahrenheit, centimeters, and dynes, respectively.

The direction of flow through the test section in the flow loop was changed between runs, and the experimental temperature distributions at the outlet position are shown in Figure 6.3 for runs 3 and 4. The lines represent the empirical equations fitted to the data points.

II. RESULTS

Four radial thermal conductivity and velocity profiles were calculated for each run, and these values are tabulated in Appendix D. The thermal conductivity profiles are presented graphically for runs 5 and 8 in Figures 6.4 and 6.5. Figures 6.6 and 6.7 show thermal conductivity data as functions of temperature for various experimental

TABLE I

SUMMARY OF TEMPERATURE PROFILES,
EMPIRICAL APPROXIMATION, $T = T_{CL} - Ar^m$

where: r = radial position in cm
T = temperature in °F

Run	Position	T_{CL}, °F	A, °F/cm^m	m	Run	Position	T_{CL}, °F	A, °F/cm^m	m
(1)	(2)	(3)	(4)	(5)	(1)	(2)	(3)	(4)	(5)
1	(1) Inlet	138.0	30.5	3.58	2	(1) Inlet	129.6	27.5	4.44
1	(2)	136.3	45.0	2.47	2	(2)	128.2	32.5	2.84
1	(3) Middle	130.0	39.5	2.14	2	(3) Middle	126.6	35.1	2.84
1	(4)	122.3	35.2	1.87	2	(4)	122.0	34.5	1.78
1	(5) Outlet	116.7	34.5	1.87	2	(5) Outlet	117.5	34.2	1.78
3	(1) Inlet	145.7	30.5	3.85	4	(1) Inlet	146.9	30.5	3.86
3	(2)	146.8	38.0	3.45	4	(2)	146.9	43.0	3.27
3	(3) Middle	145.1	41.0	2.69	4	(3) Middle	144.7	50.0	2.43
3	(4)	142.5	43.0	2.42	4	(4)	142.8	50.5	2.21
3	(5) Outlet	138.3	48.0	2.47	4	(5) Outlet	138.3	53.5	2.23
5	(1) Inlet	133.0	23.0	4.70	6	(1) Inlet	152.3	35.0	3.84
5	(2)	132.6	31.0	3.45	6	(2)	150.2	40.0	3.40
5	(3) Middle	132.1	36.8	2.82	6	(3) Middle	149.4	44.2	2.71
5	(4)	130.3	40.0	2.30	6	(4)	149.3	50.0	2.30
5	(5) Outlet	127.5	40.5	2.29	6	(5) Outlet	145.9	51.0	2.25
7	(1) Inlet	157.0	35.0	4.13	8	(1) Inlet	170.0	45.3	3.33
7	(2)	155.1	47.0	2.99	8	(2)	169.3	55.0	2.75
7	(3) Middle	153.0	55.0	2.47	8	(3) Middle	166.8	64.2	2.20
7	(4)	149.1	54.5	2.26	8	(4)	162.9	64.5	2.25
7	(5) Outlet	145.8	57.0	2.26	8	(5) Outlet	157.5	64.5	2.25

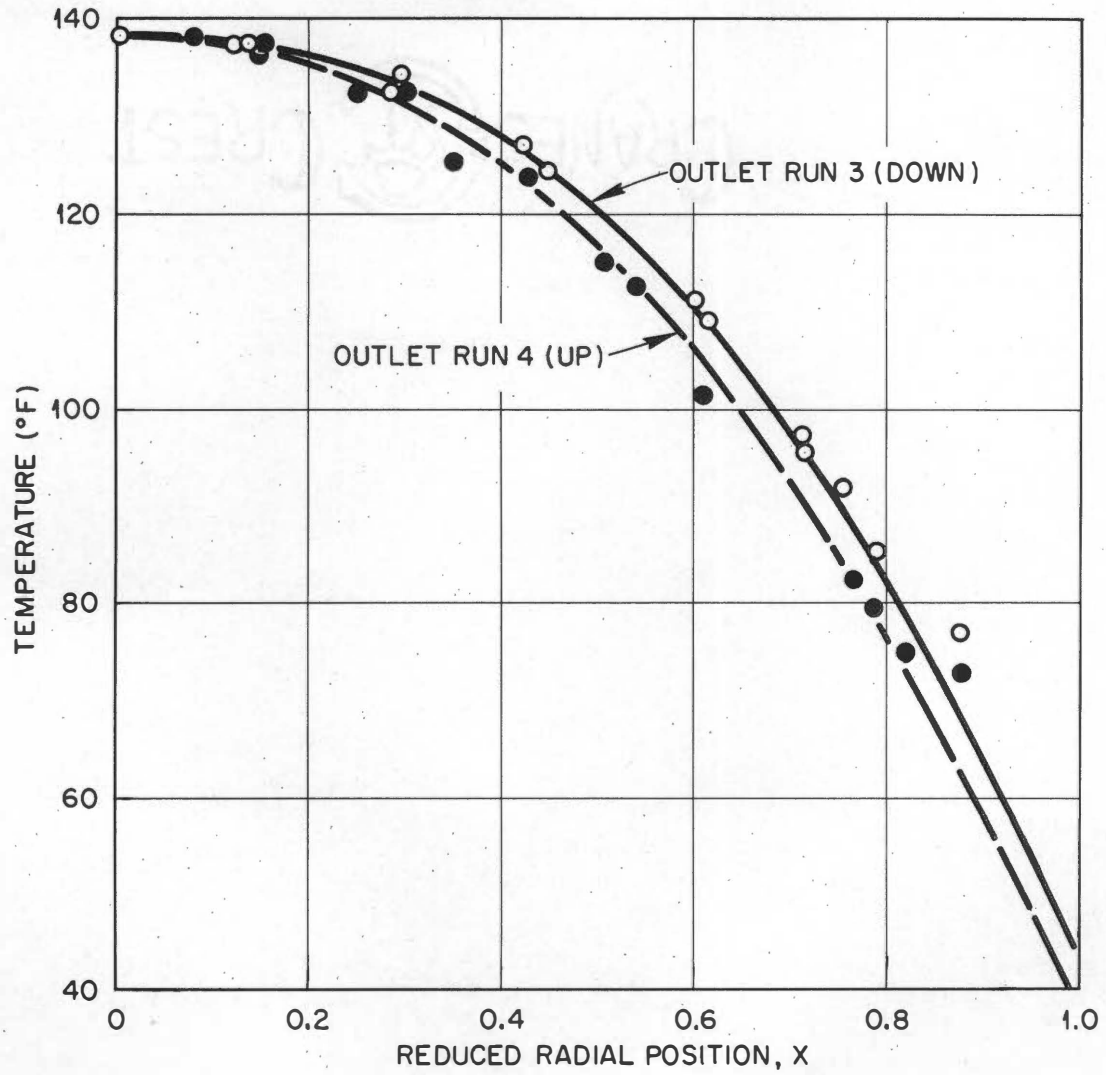


FIGURE 6.3

OUTLET EXPERIMENTAL TEMPERATURE DISTRIBUTIONS FOR RUNS 3 AND 4

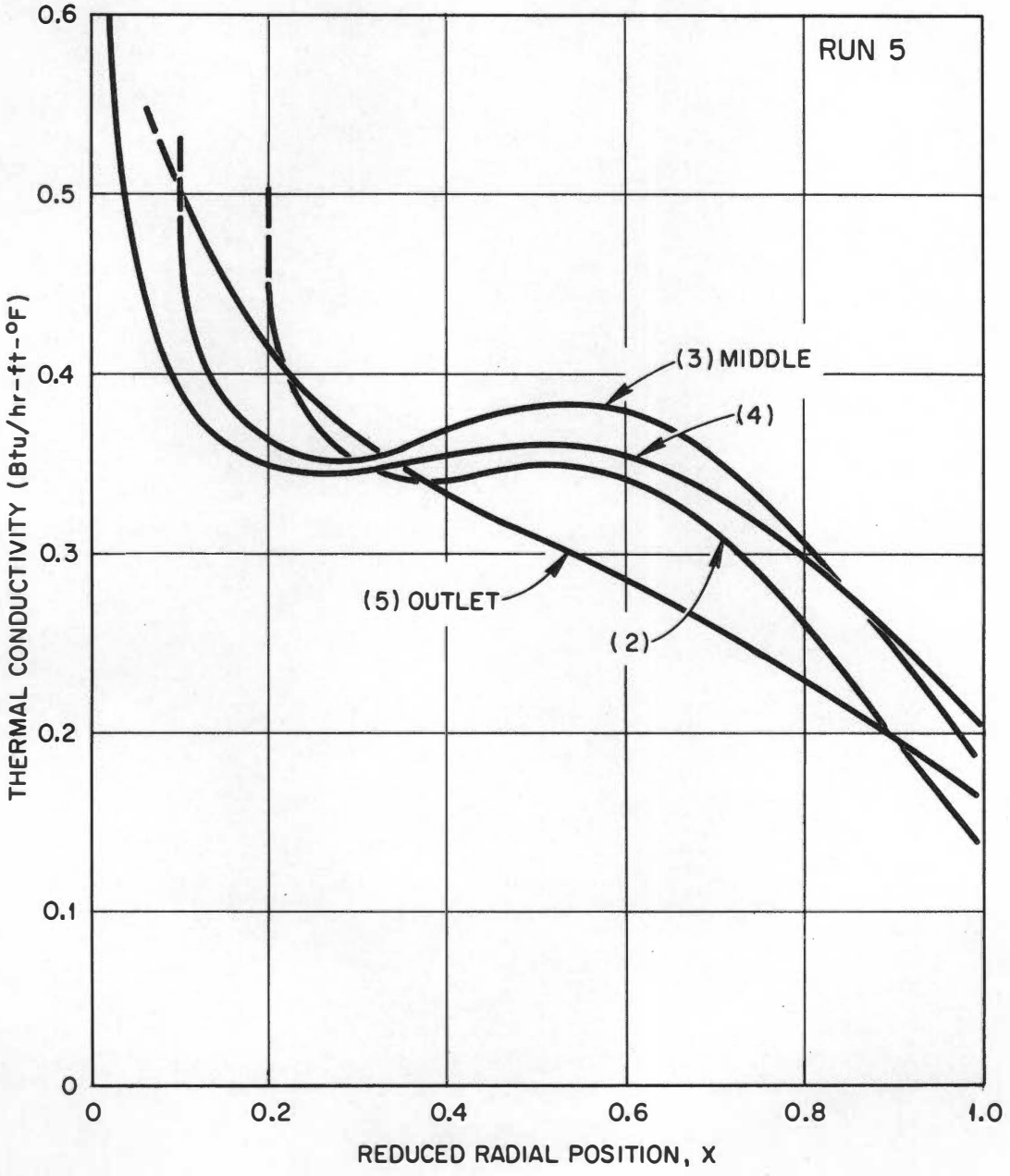


FIGURE 6.4

THERMAL CONDUCTIVITY VERSUS RADIAL POSITION (RUN 5)

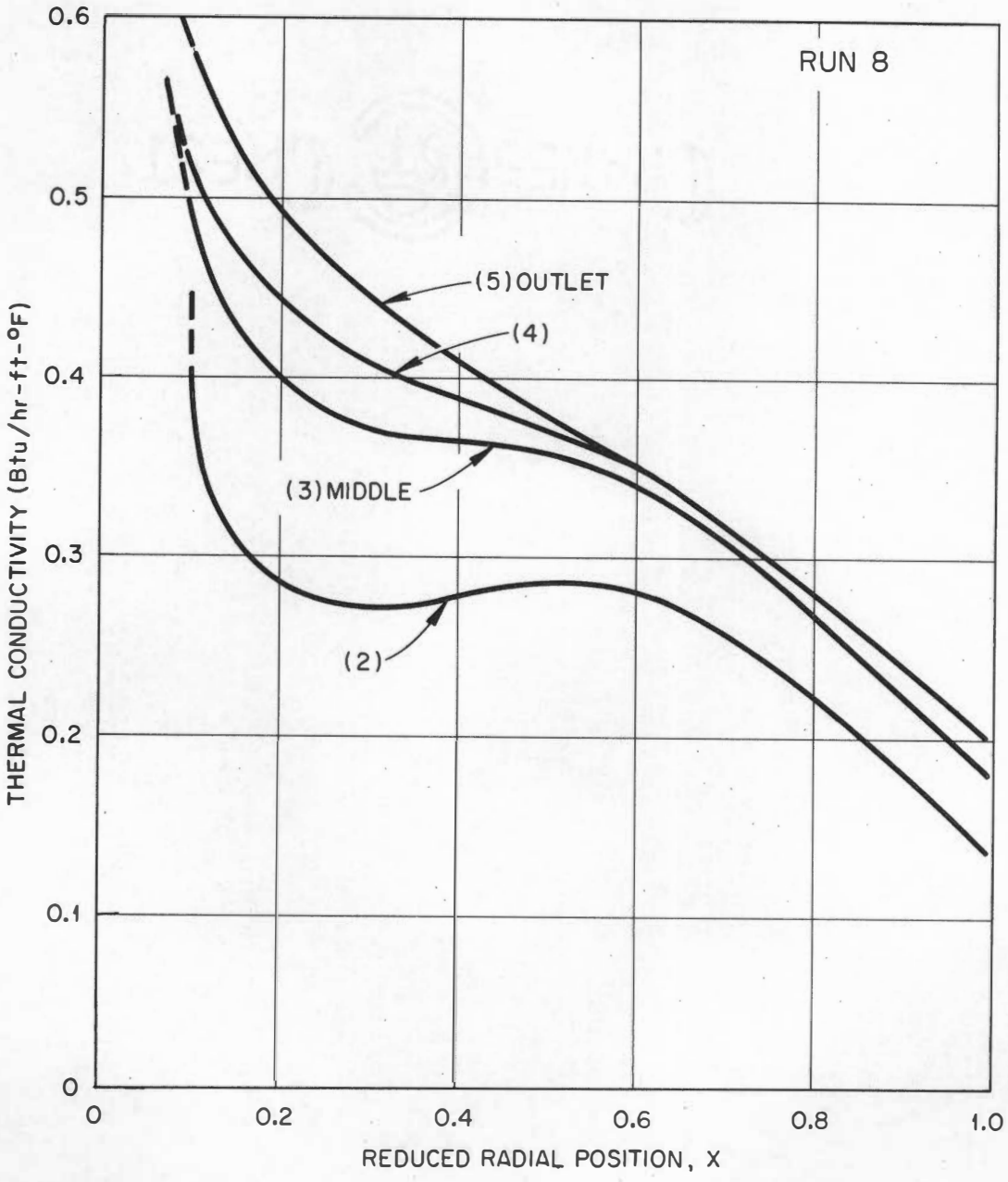


FIGURE 6.5

THERMAL CONDUCTIVITY VERSUS RADIAL POSITION (RUN 8)

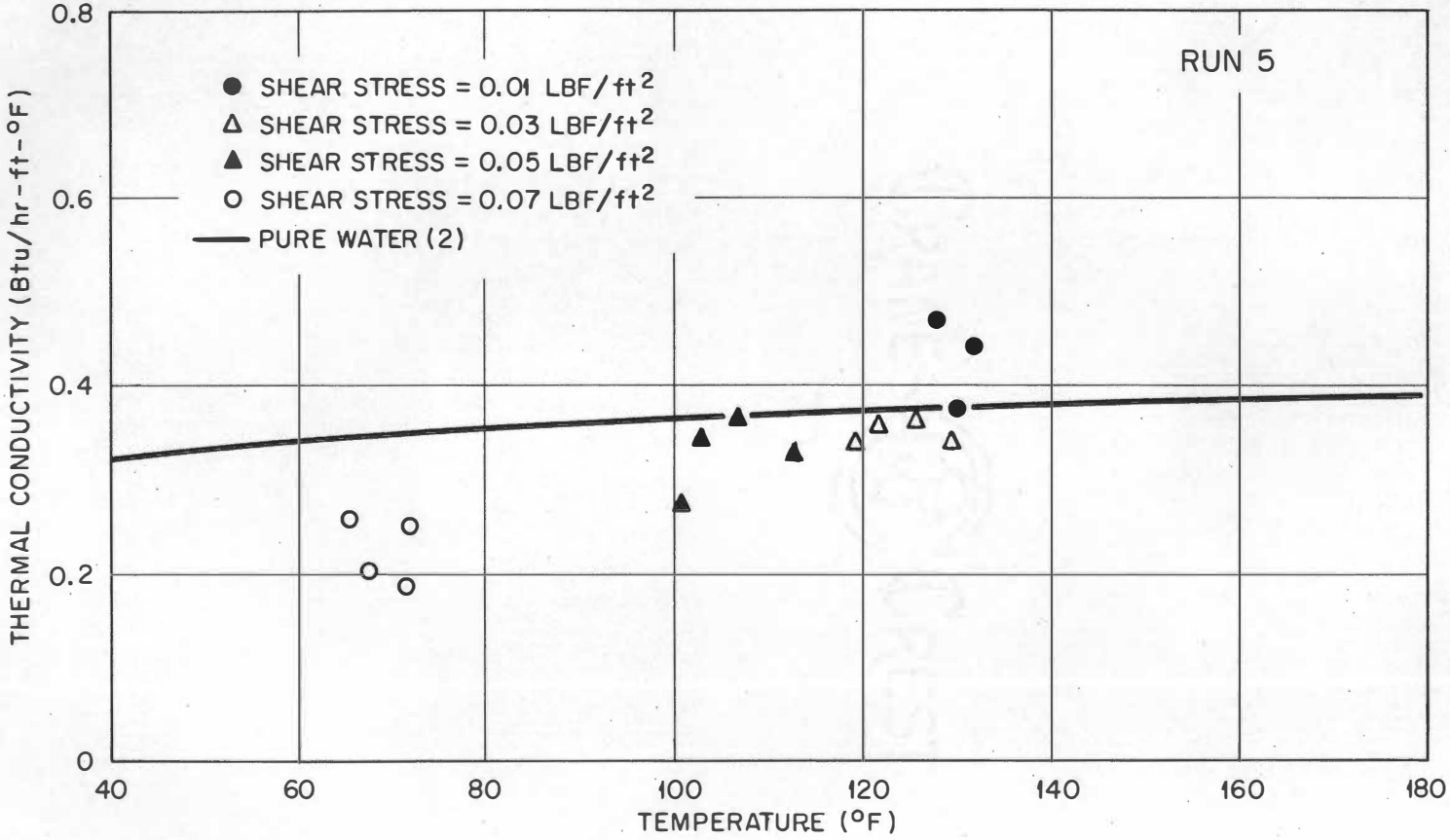


FIGURE 6.6

THERMAL CONDUCTIVITY VERSUS TEMPERATURE FOR VARIOUS SHEAR STRESS CONDITIONS (RUN 5)

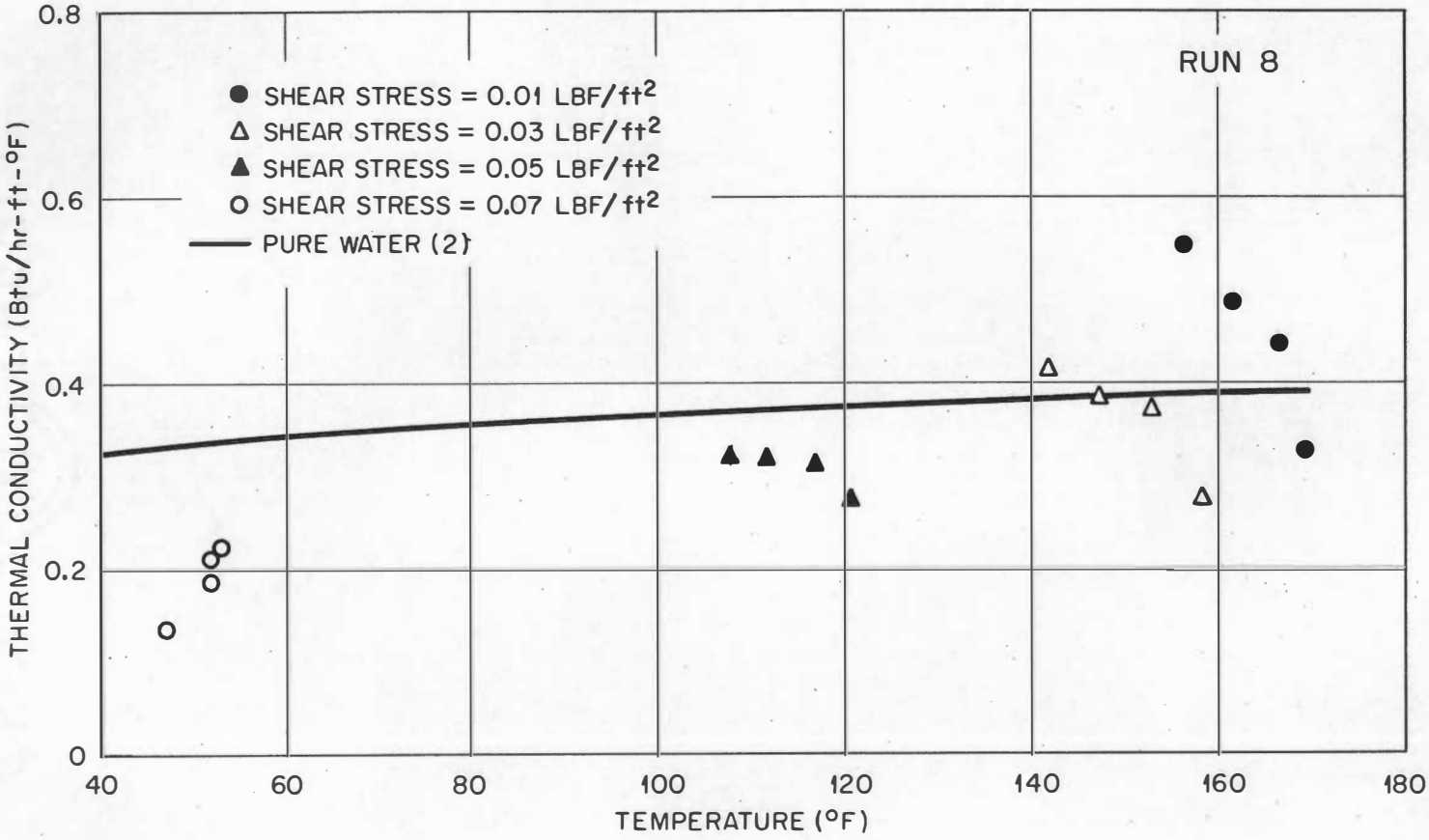


FIGURE 6.7

THERMAL CONDUCTIVITY VERSUS TEMPERATURE FOR VARIOUS SHEAR STRESS CONDITION (RUN 8)

TABLE II

RATE OF AXIAL TEMPERATURE CHANGES, GRAPHICALLY EVALUATED

Run	Position	$\frac{\partial T_{CL}}{\partial Z}$, °F/cm	$\frac{\partial A}{\partial Z}$, °F/cm^{m+1}	$\frac{\partial m}{\partial Z}$, cm^{-1}
(1)	(2)	(3)	(4)	(5)
1	(2)	-0.1608	0.1137	-0.0236
1	(3) Middle	- .2100	.0481	- .0139
1	(4)	- .2556	.0000	- .0019
1	(5) Outlet	- .2556	.0000	.0000
3	(2)	- .0869	.2799	- .0271
3	(3) Middle	- .1159	.1968	- .0241
3	(4)	- .1816	.1268	- .0101
3	(5) Outlet	- .2056	.0394	.0000
5	(2)	- .0306	.2931	- .0416
5	(3) Middle	- .0612	.2056	- .0262
5	(4)	- .1094	.1006	- .0109
5	(5) Outlet	- .1531	.0000	.0000
7	(2)	- .1050	.3149	- .0289
7	(3) Middle	- .1312	.1793	- .0157
7	(4)	- .1662	.0656	- .0057
7	(5) Outlet	- .2318	.0000	.0000

Run	Position	$\frac{\partial T_{CL}}{\partial Z}$ °F/cm	$\frac{\partial A}{\partial Z}$ °F/cm^{m+1}	$\frac{\partial m}{\partial Z}$ cm^{-1}
(1)	(2)	(3)	(4)	(5)
2	(2)	-0.1162	0.1037	-0.0346
2	(3) Middle	- .1687	.0219	- .0197
2	(4)	- .2443	.0000	- .0083
2	(5) Outlet	- .2493	.0000	.0000
4	(2)	- .0875	.3000	- .0367
4	(3) Middle	- .1256	.1925	- .0262
4	(4)	- .1675	.1443	- .0219
4	(5) Outlet	- .1968	.0000	.0000
6	(2)	- .0569	.2712	- .0427
6	(3) Middle	- .0744	.1881	- .0262
6	(4)	- .0919	.1094	- .0105
6	(5) Outlet	- .1225	.0219	.0000
8	(2)	- .0744	.2756	- .0201
8	(3) Middle	- .1750	.1706	- .0127
8	(4)	- .2581	.0787	- .0048
8	(5) Outlet	- .3193	.0044	.0000

TABLE III

PRESSURE GRADIENT DATA AND CALCULATED MODIFICATIONS BASED ON CONTINUITY

	Pressure Gradient, Dynes/Cm^3							
Position	Run 1	Run 2	Run 3	Run 4	Run 5	Run 6	Run 7	Run 8
(1)	(2)	(3)	(4)	(5)	(6)	(7)	(8)	(9)
Measured Value	62.22	47.00	52.96	52.96	54.94	54.28	52.96	50.31
(2)	62.22	47.00	52.96	52.96	54.94	54.28	52.96	50.31
(3) Middle	63.91	47.14	53.68	53.95	55.77	54.78	54.06	51.55
(4)	65.94	47.78	54.86	54.95	56.45	55.26	55.18	52.85
(5) Outlet	67.35	48.47	56.12	55.76	57.09	55.94	56.28	54.19

TABLE IV

TEMPERATURE-DEPENDENT RHEOLOGICAL PARAMETERS
$C = C_o - BT$, WHERE T IS IN ^oF

Run	C_o, Dynes-Seconds^n/cm^2	B, Dynes-Seconds^n/cm^2-^oF	n, Dimensionless
(1)	(2)	(3)	(4)
1	45.44	0.134	0.314
2	31.58	0.093	0.329
3	31.00	0.091	0.332
4	31.00	0.091	0.332
5	30.60	0.090	0.328
6	30.60	0.090	0.328
7	30.00	0.089	0.332
8	30.00	0.089	0.332

shear stress conditions (ranging from 0.01 to 0.07 lbf/ft^2) for runs 5 and 8 with the thermal conductivity of pure water (2) shown by smooth curves for reference. The experimental temperature profiles and calculated velocity distributions are shown in Figure 6.8 for four axial positions along the test section.

Temperature distributions were calculated for the three positions downstream from the second thermocouple port (1.25 feet from initial cooling) for each run by assuming an average constant thermal conductivity. The data from the second thermocouple port and an approximate wall temperature distribution were used as boundary conditions for Equation (2-8). The calculated temperature profiles are completely tabulated in Appendix D and graphically presented in Figures 6.9 and 6.10 for runs 5 and 8.

Experimental data were also used to calculate dimensionless groups commonly employed in hydrodynamics and heat transfer. These data are given in Tables V and VI. Experimental temperature profiles from this investigation were recalculated and tabulated in Table VII for runs 5 and 8 in terms of reduced temperature. These data are compared with theoretical curves of Lyche and Bird (27) in Figure 6.11 where β is the reciprocal Graetz number, $xK_z/C_p\rho Q$, Q is volumetric flow rate, and z is the cooled length.

The calculated results are given in terms of degrees Fahrenheit, feet, and pounds force. The linear velocities are given in feet per minute and the thermal conductivities in $Btu/hr\text{-}ft\text{-}^{o}F$.

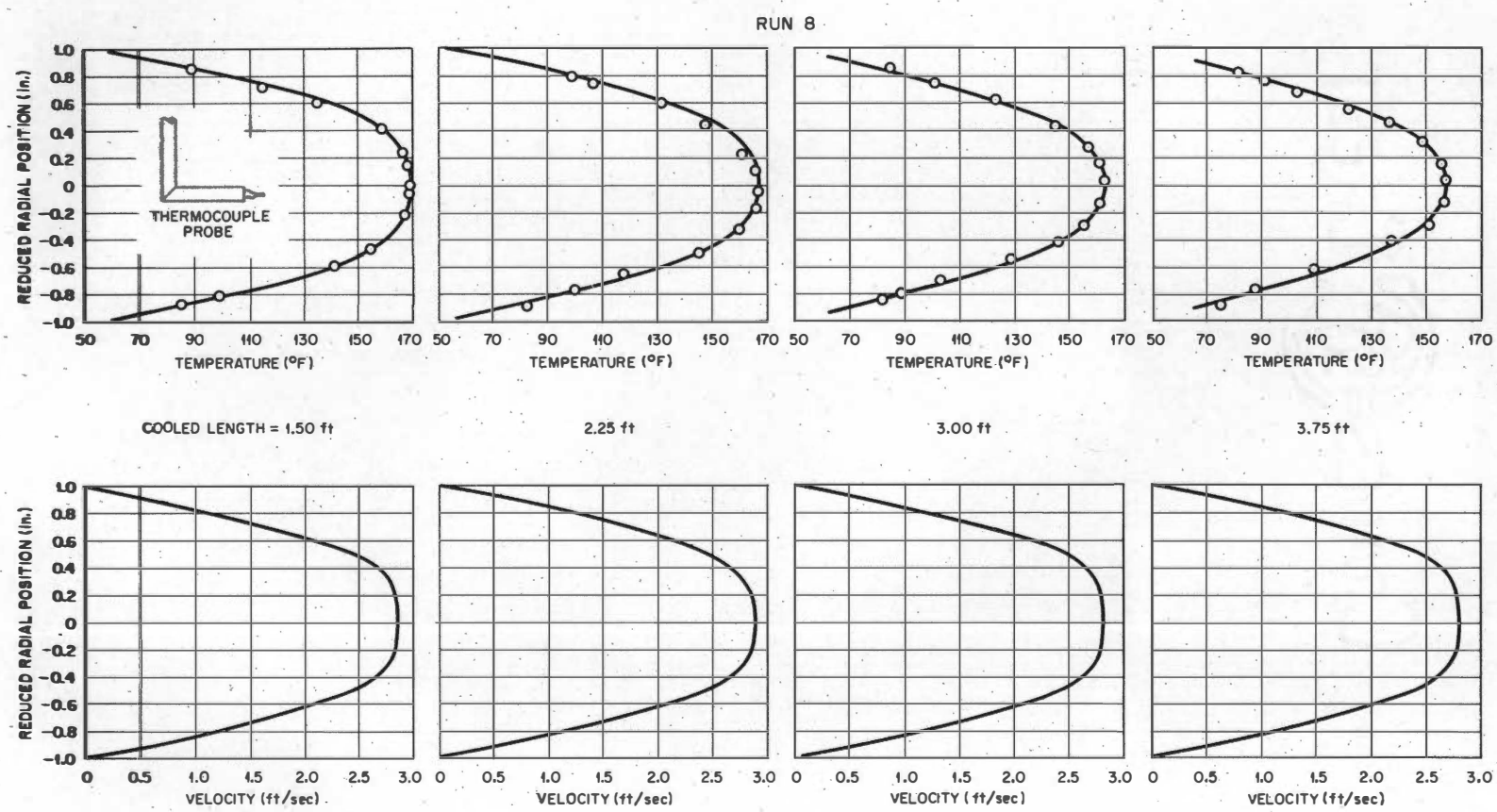


FIGURE 6.8

THE DEVELOPING TEMPERATURE AND VELOCITY PROFILES, RUN 8

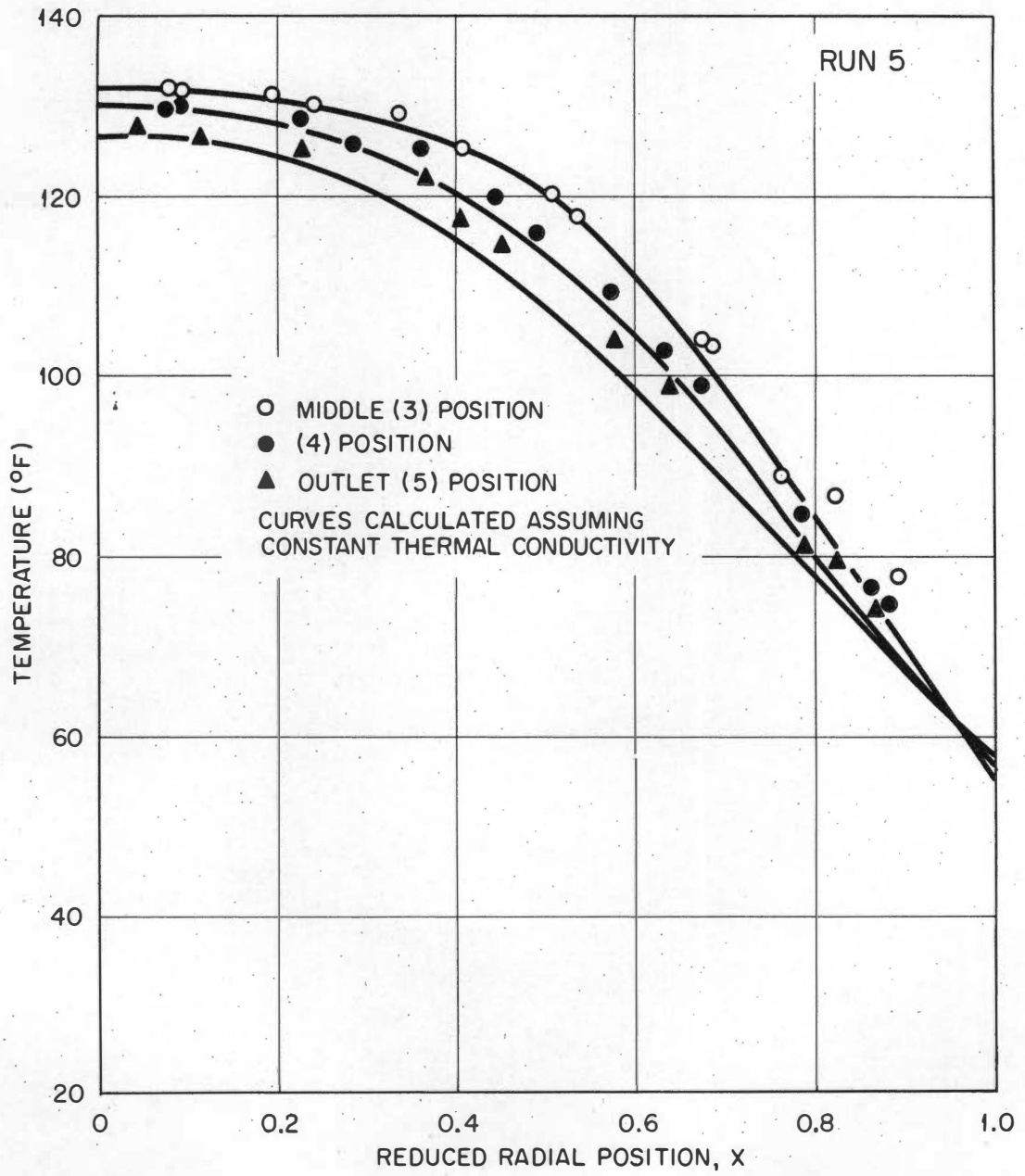


FIGURE 6.9

CALCULATED TEMPERATURE DISTRIBUTIONS WITH EXPERIMENTAL DATA (RUN 5) ASSUMING CONSTANT THERMAL CONDUCTIVITY

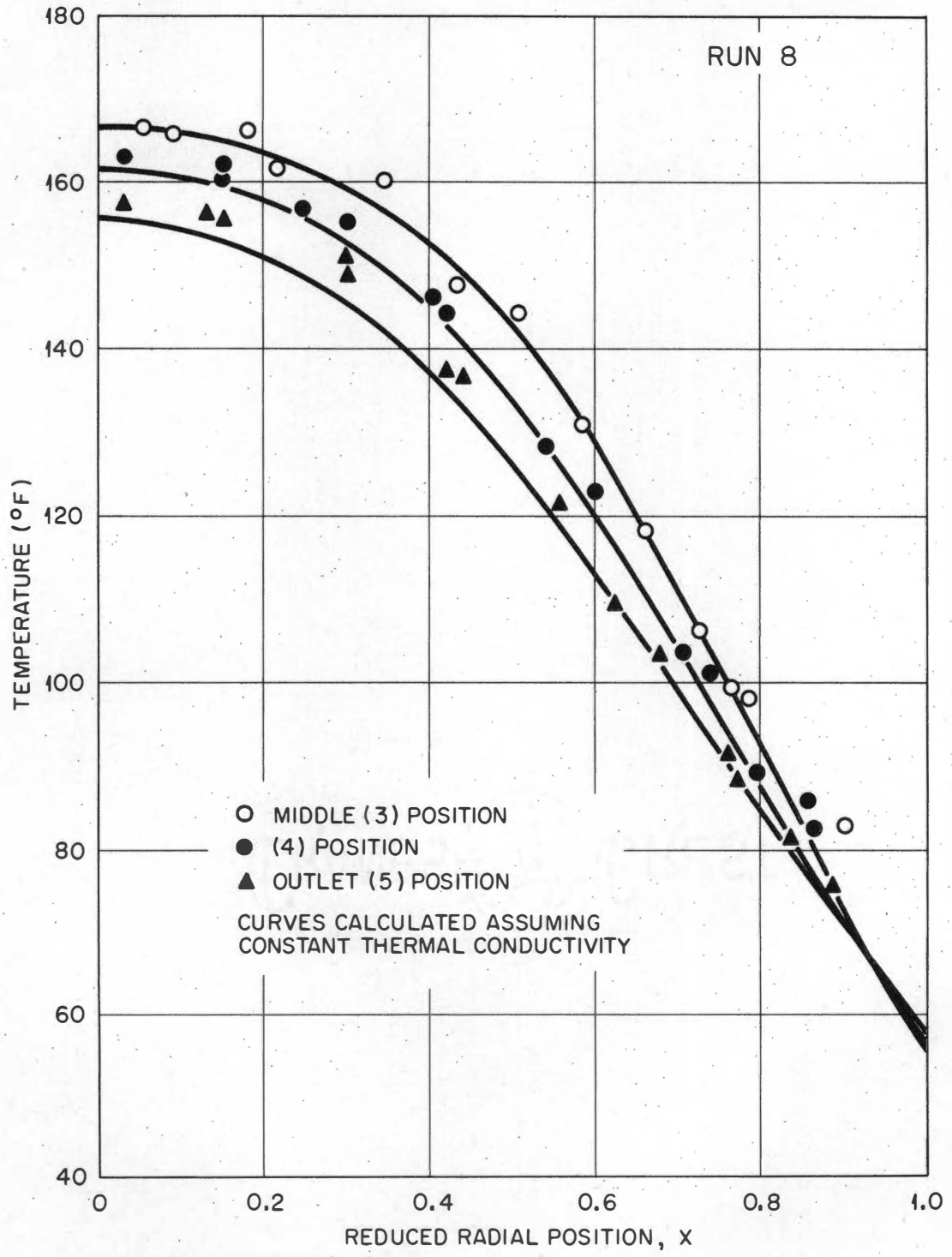


FIGURE 6.10

CALCULATED TEMPERATURE DISTRIBUTIONS WITH EXPERIMENTAL DATA (RUN 8) ASSUMING CONSTANT THERMAL CONDUCTIVITY

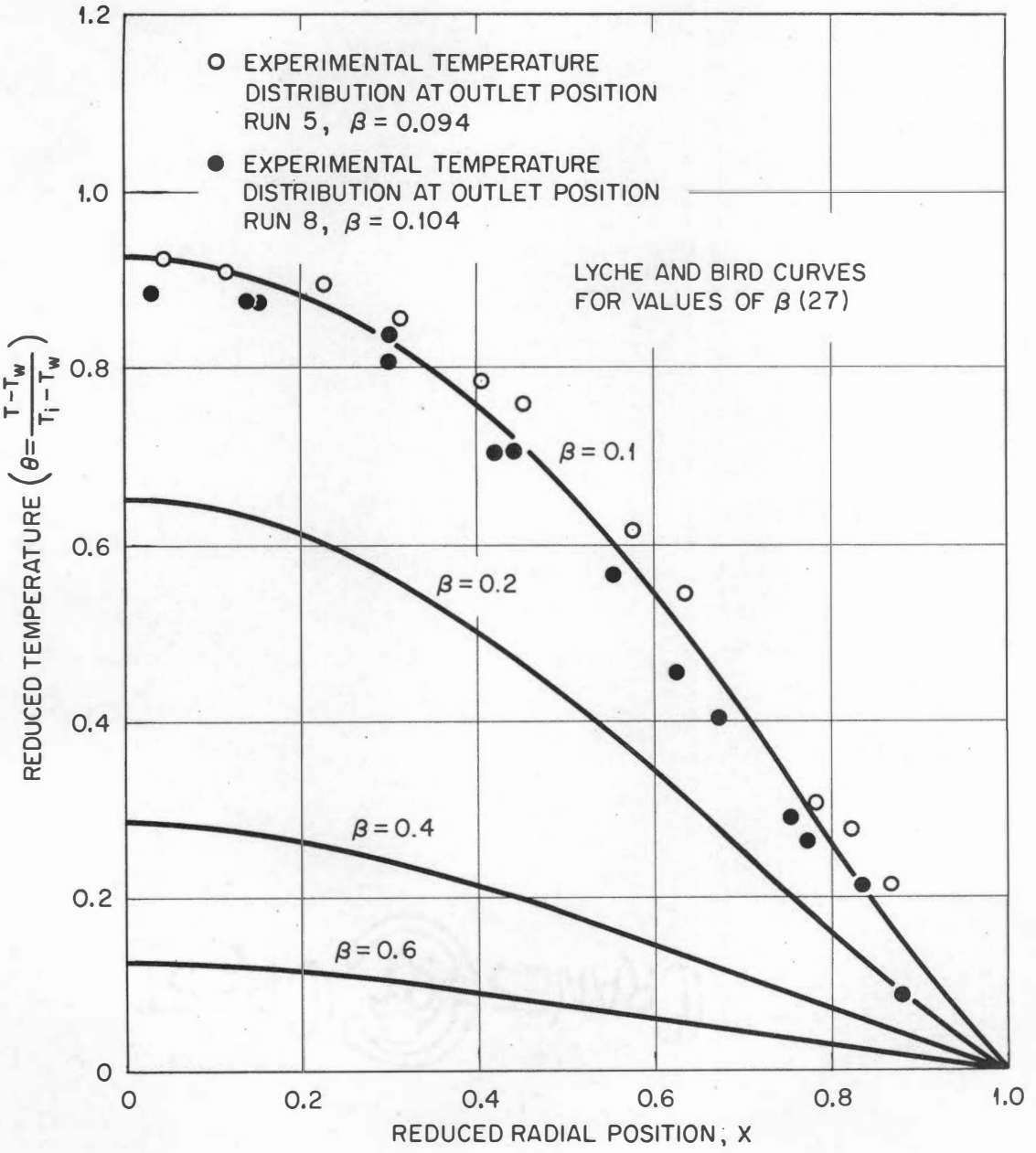


FIGURE 6.11

THEORETICAL TEMPERATURE DISTRIBUTIONS WITH EXPERIMENTAL DATA

TABLE V

CALCULATED DIMENSIONLESS GROUPS
AND BULK TEMPERATURE

Run	Position	Reynold's Number	Nusselt Number	Prandtl Number, Bulk	Prandtl Number, Wall	Bulk Temperature °F
(1)	(2)	(3)	(4)	(5)	(6)	(7)
1	(5) Outlet	0.0376	3.210	20,950	16,745	93.64
1	(4)	0.0376	14.483	20,652	17,801	99.40
1	(3) Middle	0.0388	4.715	20,230	19,344	102.26
1	(2)	0.0410	9.645	19,200	20,817	114.30
2	(5) Outlet	0.0666	6.113	13,386	11,179	94.59
2	(4)	0.0682	9.818	13,113	11,678	99.08
2	(3) Middle	0.0705	11.791	12,641	12,177	108.27
2	(2)	0.0707	13.583	12,613	12,426	108.72
3	(5) Outlet	0.1621	14.271	8,922	7,950	110.33
3	(4)	0.1660	2.778	8,710	8,440	115.91
3	(3) Middle	0.1698	7.229	8,522	8,943	120.56
3	(2)	0.1741	1.928	8,305	9,318	126.37
4	(5) Outlet	0.1400	9.399	9,547	8,054	106.87
4	(4)	0.1422	11.187	9,402	8,413	110.38
4	(3) Middle	0.1452	4.479	9,205	8,853	115.29
4	(2)	0.1509	7.444	8,855	9,318	123.85
5	(5) Outlet	0.1903	5.452	8,430	7,247	103.30
5	(4)	0.1924	8.257	8,340	7,524	105.83
5	(3) Middle	0.1963	3.068	8,173	7,825	110.54
5	(2)	0.2006	3.680	7,995	8,185	115.55
6	(5) Outlet	0.1993	3.558	8,018	7,556	115.46
6	(4)	0.1913	9.595	8,096	7,860	117.95
6	(3) Middle	0.2059	5.762	7,754	8,116	122.98
6	(2)	0.2112	8.896	7,562	8,390	128.27
7	(5) Outlet	0.2002	4.523	7,945	7,115	113.60
7	(4)	0.2039	7.442	7,806	7,510	117.48
7	(3) Middle	0.2087	7.975	7,622	7,758	122.72
7	(2)	0.2154	4.282	7,387	8,392	129.30
8	(5) Outlet	0.1786	6.329	8,132	7,677	121.81
8	(4)	0.1827	4.579	7,950	8,190	126.61
8	(3) Middle	0.1879	8.741	7,725	8,735	132.68
8	(2)	0.1939	7.619	7,488	9,304	138.93

TABLE VI

DIMENSIONLESS GROUPS FOR HEAT TRANSFER CORRELATION

Run Number	Average Values Based on Fluid Temperature Gradient at the Pipe Wall		Average Values Based on Axial Bulk Temperature Change		Empirical Predictions of Metzner, Vaughn, and Houghton (37)		Theoretical "Isothermal" Predictions of Lyche-Bird (27)	
	Nusselt Number	Graetz Number	Nusselt Number	Graetz Number	Nusselt Number	Graetz Number	Nusselt Number	Graetz Number
(1)	(2)	(3)	(4)	(5)	(6)	(7)	(8)	(9)
1	8.0	24.0	3.2	16.3	4.9	24.0	3.25	15.7
2	10.3	27.3	1.8	18.5	5.1	27.0	----	----
3	6.6	44.2	4.5	30.0	6.0	44.0	----	----
4	8.1	40.9	4.4	27.7	5.8	41.0	----	----
5	5.2	49.1	3.8	33.3	6.1	49.0	----	----
6	7.0	48.8	4.0	33.1	6.1	49.0	----	----
7	6.1	48.7	4.9	33.0	6.1	49.0	----	----
8	6.8	49.4	4.9	30.1	6.2	49.5	4.59	31.4

TABLE VII

REDUCED TEMPERATURE, $\theta = \frac{T - T_W}{T_i - T_W}$

T = Point Temperature
T_W = Wall Temperature = 58°F
T_i = Inlet Fluid Temperature

Run 5, T_i = 133°F			Run 8, T_i = 170°F		
Reduced Radius, X	Temperature, °F	Reduced Temp, θ	Reduced Radius, X	Temperature, °F	Reduced Temp, θ
(1)	(2)	(3)	(4)	(5)	(6)
-0.871	74.4	0.213	-0.886	75.7	0.089
- .788	81.0	.307	- .773	88.0	.268
- .578	104.0	.613	- .623	109.3	.455
- .405	117.2	.787	- .420	137.1	.705
- .225	125.0	.893	- .143	156.2	.875
- .045	127.4	.920	- .300	151.7	.839
.113	126.4	.907	.030	157.4	.884
.368	122.0	.853	.150	155.5	.875
.450	114.5	.760	.300	148.2	.804
.638	98.7	.547	.443	136.5	.705
.826	79.4	.280	.535	121.1	.563
			.676	103.1	.402
			.758	91.2	.295
			.833	81.7	.214

CHAPTER VII

DISCUSSION OF RESULTS

I. FLUID BEHAVIOR

The viscous behavior of aqueous Carbopol was found to be a function of the solution's pH as well as its concentration, temperature, and shear stress. An index of viscous behavior, the apparent or Brookfield viscosity, was used to study the effect of pH in various solutions at constant temperature ($80^{\circ}F$) and spindle speed. This study revealed that apparent viscosity reaches a maximum and remains essentially constant for solutions of given concentration with pH's between 6.5 and 8.0. This facet of aqueous Carbopol behavior proved helpful in preparing solutions in the flow system.

The capillary viscometer data showed that the isothermal rheological behavior of Carbopol solutions could be described with a pair of power-law models: (a) one for low shear stresses and/or temperatures and (b) another for higher shear stresses and/or temperatures. Fortunately, a single power-law model proved adequate for describing the rheological behavior of the Carbopol solutions in the shear stress and temperature ranges encountered in the non-isothermal flow loop. It was also fortunate that the consistency index, C, of the power-law model exhibited a linear temperature dependence while the flow-behavior index, n, was unaffected by temperature.

A slight decrease in the consistency index was noted after high temperature runs or the passage of several days. This effect occured over periods of time much longer than the test run duration, so it was

felt that the average rheological properties of samples taken before and after each run would be adequate.

II. DYNAMIC THERMAL CONDUCTIVITIES

An examination of Figures 6.4 and 6.5 reveals that unusual changes in the calculated thermal conductivities occur in the neighborhood of both the pipe wall and the centerline. The unusual changes near the pipe centerline resulted from the high amplification of experimental error at small radial distances in calculation with Equation (3-9), since both the numerator and denominator are small when the distance from the centerline is small. A large portion of the unusual changes in the neighborhood of the pipe wall are believed to result from the extrapolation of experimental temperature distributions to the pipe wall by means of the empirical equations in Table I. Figure 6.3 indicates that this extrapolation provides a poor estimate of wall temperature in some cases and points out the need for an experimental evaluation of wall temperature.

It was not possible to show any quantitative effect of shear stress on thermal conductivity because the experimental isotherms and constant shear stress lines almost coincided with each other. However, the data qualitatively suggest that thermal conductivity decreases slightly with an increase in shear stress as indicated in Figures 6.6 and 6.7 by a comparison of calculated dynamic thermal conductivity data from runs 5 and 8 with static thermal conductivity data for pure water (2).

The flow direction through the test section was alternated between runs in an effort to determine whether or not convectional effects were involved. One set of these paired runs was obtained under essentially the same thermal and flow conditions. Experimental temperature distributions from the outlet axial position for runs 3 and 4 are shown in Figure 6.3 and indicate that there were no significant free convectional effects involved since the distributions have essentially the same shape.

The continuity equation (Equation 2-2) was used to calculate the radial velocity component at a number of radial and axial positions for each run. The maximum radial velocities calculated were less than 5×10^{-4} feet per minute (run 6) as compared to axial velocities of about 3 feet per minute. No significant radial convectional effects were expected because of the highly viscous nature of the test fluid, and these data and calculations substantiated this opinion.

The temperature profiles calculated by assuming a constant thermal conductivity with the experimental boundary conditions were in good agreement with the experimentally measured temperature distributions as illustrated in Figures 6.9 and 6.10. Therefore, it would appear that neither shear stress nor temperature affected the thermal conductivity sufficiently to cause appreciable changes in the experimental temperature profiles. This opinion is further supported by the close agreement of data from this investigation with the theoretical temperature distributions of Lyche and Bird (27) for "isothermal" heat transfer.

III. HEAT TRANSFER CONSIDERATIONS

The scope of this experimental investigation was limited as indicated by the non-Newtonian heat transfer and hydrodynamic dimensionless groups given in Tables V and VI. Prandtl numbers were calculated for both bulk and wall conditions. Nusselt numbers were tabulated in three ways: (a) point values based on the temperature gradient in the fluid at the wall (Table V), (b) an average of the point values from (a) for each run (Table VI), and (c) those based on the bulk temperature change in each run (Table VI). The Nusselt-Graetz numbers from Table VI were compared with the modified Leveque equation for heat transfer to Newtonian fluids in laminar flow (40) and,

$$\frac{h_A D}{K} = N_{NU} = 1.75 \left(\frac{Q \rho C_p}{Kz}\right)^{1/3} = 1.75 N_{Gz}^{1/3} \quad (7\text{-}1)$$

with the exception of those data from runs 1 and 2, showed good agreement for (c). The non-Newtonian modification of Equation (7-1) presented by Pigford (40) and experimentally verified by Metzner, Vaughn, and Houghton (37) for non-Newtonian fluids

$$\frac{N_{NU}}{\Delta^{1/3}} = 1.75 N_{Gz}^{1/3} \quad (7\text{-}2)$$

where $\Delta^{1/3} = \frac{3n' + 1}{4n'}$

fits the data calculated for (b) slightly better than Equation (7-1), but, since those data incorporate the errors of an estimated wall

temperature, the use of the non-Newtonian correction term cannot be justified from the experimental data of this work. Metzner, Vaughn, and Houghton (37) also recommended an empirical viscosity correction term similar to the one developed by Sieder and Tate for Newtonian fluids (47) to modify Equation (7-2).

$$\frac{N_{Nu}}{\Delta^{1/3}} = 1.75\, N_{Gz}^{1/3} \left(\frac{C_{cup}}{C_{wall}}\right)^{0.14} \qquad (7\text{-}3)$$

where: C_{cup} = the consistency index evaluated at the bulk temperature, and

C_{wall} = the consistency index evaluated at the wall temperature.

This additional correction amounts to about 2.5% for the limited data of this work and cannot be justified here although some degree of success has been claimed for extensive correlation of several investigators' data (37).

A comparison of the Nusselt numbers calculated for (c) above with the theoretical values calculated by Lyche and Bird (27) indicates that the experimental data of this work are also in good agreement on this point. This was to be expected since the Lyche-Bird theoretical temperature profiles agree with the experimental profiles of this investigation.

IV. EXPERIMENTAL ERRORS

There were multiple opportunities for error in this investigation; however, it is believed that most of these errors were minimized by careful experimentation. The usual measurement errors involved in the temperature, distance, and rheological determinations were subject to some "smoothing" in the preliminary data analysis steps, and it is felt that most of the random errors were eliminated or "averaged out".

The greatest observed experimental variation occurred in runs 1 and 2 where the source of heating was different from that employed in the other runs. During these initial runs a pair of electrical immersion heaters were placed in the reservoir for heating, and the steam heat exchangers were not used. At the end of both runs 1 and 2 it was found that an appreciable quantity of the test fluid had evaporated. The rheological properties of the samples taken before and after these runs were quite different, and it was suspected that some accelerated "aging" effects were involved. Some results obtained from runs 1 and 2 were inconsistent with those obtained from the remaining runs.

Most experimentally determined temperatures and pressure differentials were reproducible within 5 percent with only a few larger variations. The rheological data were somewhat less consistent, and it is believed that most of the error was due to accelerated "aging" of the samples while heating them to the higher temperatures for testing. Instead of measuring the pressure drop as was done in this work, it would be preferable to measure the volumetric flow rate and compute the pressure gradient since errors in measuring the pressure gradient

are greatly amplified in calculating velocities for power-law fluids.

The need for experimental temperature data near the pipe wall was emphasized repeatedly by the abnormal results calculated for quantities in that neighborhood.

CHAPTER VIII

CONCLUSIONS AND RECOMMENDATIONS

The conclusions of the investigations reported here are summarized in the following paragraphs.

The dynamic non-Newtonian thermal conductivity data qualitatively suggest that an increase in shear stress causes a slight decrease in thermal conductivity for aqueous Carbopol solutions. However, it is not possible to show any quantitative shear stress effects because the constant shear regions almost coincide with the experimental isotherms. Supplementary temperature profile calculations assuming constant thermal conductivity show that the effects of a shear stress and temperature on the thermal conductivity of aqueous Carbopol are small enough to have no effect on the temperature distribution in the fluid.

The limited heat transfer data from this investigation agree with the theoretical calculations of Lyche and Bird (27) and the experimental correlation of Metzner, Vaughn, and Houghton (37). Hence, it is felt that accurate heat transfer calculations can be made for laminar non-Newtonian flow using constant values of thermal conductivity.

Both experimental and calculated data indicate that free convectional effects are negligible in such highly viscous, non-Newtonian fluids for the range of conditions investigated.

The rheological behavior of neutralized aqueous Carbopol solutions is well described by an empirical, temperature-dependent,

power-law relation. The consistency index of the power-law, C, decreases linearly with increasing temperature, while the exponent, n, is independent of temperature.

Although it proved impossible to determine an exact relation between shear stress and the thermal conductivity of non-Newtonian fluids in the equipment of the present investigation, it is felt that the equipment modifications recommended in the following paragraphs would enable future workers to determine the nature of such a relation if one exists.

Experimental non-Newtonian thermal conductivity data should be obtained under conditions where the constant shear lines and isotherms do not coincide, e.g., in non-isothermal test sections where the residence time of the test fluid is long enough to allow the bulk fluid temperature to approach the wall temperature. Under these conditions the effect of temperature and shear stress would be separable, and it would be possible to show quantitative effects of shear stress on thermal conductivity.

Experimental determinations of wall temperature should be carried out using thermocouples imbedded in the pipe wall. This would eliminate the necessity of extrapolating experimental temperature data, a questionable procedure at best. In addition, it may also be possible to reduce the thermocouple probe size slightly. This would enable one to obtain experimental temperature data in a neighborhood somewhat nearer the pipe wall.

An accurate (magnetic) flowmeter should be obtained for work with non-Newtonian fluids. Such a measuring device would allow one to

calculate pressure gradient data for various axial positions in an experimentally measured temperature field from a knowledge of the fluid's rheological behavior. It would also provide an independent check on calculated velocity profiles.

Experimental techniques for the direct experimental evaluation of velocity profiles should also be considered. Velocity profile data, determined experimentally, would eliminate the need for the extensive rheological study of the present investigation and the calculation of velocity profiles.

REFERENCES

REFERENCES

1. Alves, G. E., Boucher, D. F., and Pigford, R. L., "Pipe-Line Design for Non-Newtonian Solutions and Suspensions," Chem. Eng. Progr. 48, 385 (1952).

2. Anderson, F. A., and Castleberry, B. W., "Physical Properties of Water," Department of Chemical Engineering, University of Mississippi (1957).

3. Boelter, L. M. K., "Note on the Diffusion of Vapors into an Air Stream Flowing Viscously and Vertically," Trans. A. I. Ch. E. 39, 557 (1943).

4. _____, Cherry, V. H., and Johnson, H. A., "Heat Transfer Notes," University of Cal fornia Syllabus Series, X-16 - X-36 (1948).

5. Bogue, D. C., "Velocity Profiles in Turbulent Non-Newtonian Pipe Flow," University of Delaware (Ph.D. thesis), 1960.

6. Bird, R. V., Stewart, W. E., and Lightfoot, E. N., Transport Phenomena. New York: John Wiley and Sons, 1960.

7. Buckingham, E., Proc. A. S. T. M. 21, 1154 (1921). Reference taken from Metzner (32).

8. Christiansen, E. B., Ryan, N. W., and Stevens, W. E., "Pipe-Line Design for Non-Newtonian Fluids," A. I. Ch. E. Journal 1, 544 (1955).

9. Dodge, D. W., "Turbulent Flow of Non-Newtonian Fluids in Smooth Round Tubes," University of Delaware (Ph. D. thesis), 1958.

10. Drew, T. B., "Mathematical Attacks on Forced Convection Problems," Trans. A. I. Ch. E. 26, 26 (1931).

11. Drew, T. B., Koo, E. C., and McAdams, W. H., "The Friction Factor for Clean Round Pipes," Trans. A. I. Ch. E. 28, 56 (1932).

12. Eckert, E. R. G. and Drake, R. M. Heat and Mass Transfer. New York: McGraw-Hill Book Company, 1959.

13. Gee, R. E. and Lyon, J. B., "Nonisothermal Flow of Viscous Non-Newtonian Fluids," Ind. Eng. Chem. 49, 956 (1957).

14. Goldstein, S. Modern Developments in Fluid Dynamics Vol. I. Oxford, England: Oxford University Press, 1938.

15. Green, H. S. The Molecular Theory of Fluids. Amsterdam, Holland: North-Holland Publishing Company, 135-145, 1952.

16. Hanks, R. W., "The Non-Isothermal Flow of Non-Newtonian Fluids," University of Utah (Ph.D. thesis), 1960.

17. Hedstrom, V. O. A., "Flow of Plastics Materials in Pipes," Ind. Eng. Chem. 44, 651 (1952).

18. Ingersoll, L. R., Zobel, O. J., and Ingersoll, A. C., Heat Conduction. Madison, Wisconsin: University of Wisconsin Press, 234-239, 1954.

19. Jakob, M., Heat Transfer, Vol. I. New York: John Wiley and Sons, 1949.

20. Kay, J. M., An Introduction to Fluid Mechanics and Heat Transfer. Cambridge, 1957.

21. Keevil, C. S. and McAdams, W. H., "How Heat Transmission Affects Fluid Friction in Pipes," Chem. and Met. Eng. 36, 464 (1929).

22. Lamb, H., Hydrodynamics, Sixth Ed. New York: Dover Publications, 1932.

23. Lapple, C. E., et. al. Fluid and Particle Mechanics. Newark, Delaware: University of Delaware Press, 115, 1954.

24. Larkin, F. L., "Visual Study of the Laminar-Turbulent Transition Region for a Non-Newtonian Fluid," The University of Tennessee (M. S. thesis), 1959.

25. Lee, A., et al., Proc. 5th Int. Cong. Appl. Mech., Cambridge, 571 (1939). Reference taken from Pigford (40).

26. Lo, H. S., "A Wide Shear Range Capillary Viscometer for Non-Newtonian Fluids," The University of Tennessee (M. S. thesis), 1959.

27. Lyche, B. C. and Bird, R. B., "The Graetz-Nusselt Problem for a Power-Law Non-Newtonian Fluid," Chem. Eng. Sci. 6, 35, (1956).

28. Maron, S. H., Kreiger, I. M., and Sisko, A. W., "A Capillary Viscometer with Continuously Varying Pressure Head," J. Applied Phys. 23, 971 (1954).

29. Martinelli, R. C., et al., "Heat Transfer and Pressure Drop for a Fluid Flowing in the Viscous Region Through a Vertical Pipe," Trans. A. E. Ch. E. 38, 493 (1942).

30. McAdams, W. H., Heat Transmission, Third Ed. New York: McGraw-Hill Book Company, 1954.

31. McGinnis, P. H., "A Study of Velocity Distributions and Rheograms for Laminar Pipe Flow of Pseudoplastic Fluids," North Carolina State College (Ph. D. thesis), 1960.

32. Metzner, A. B. Advances in Chemical Engineering, Vol. I. (Drew, T. B. and Hoopes, J. W. Editors) New York: Academic Press, 77-153, 1956.

33. _____, Personal Communication (1959).

34. _____, "Flow of Non-Newtonian Fluids," Handbook of Fluid Dynamics. McGraw-Hill Book Company, (in press).

35. _____, and Friend, P. S., "Heat Transfer to Turbulent Non-Newtonian Fluids," Ind. Eng. Chem. 51, 879 (1959).

36. _____, and Reed, J. C., "Flow of Non-Newtonian Fluids - Correlation for the Laminar, Transition, and Turbulent Flow Regions," A. I. Ch. E. Journal 1, 434 (1955).

37. _____, Vaughn, R. D. and Houghton, G. L., "Heat Transfer to Non-Newtonian Fluids," A. I. Ch. E. Journal 3, 92, (1957).

38. Pai, S. I., Viscous Flow Theory, Vol. I. Princeton, New Jersey: D. Van Nostrand Company, 1956.

39. Perry, J. H., Chemical Engineers' Handbook, Third Ed., New York: McGraw-Hill Book Company, 175, 225, and 459, 1950.

40. Pigford, R. L., "Nonisothermal Flow and Heat Transfer Inside Vertical Tubes," Chem. Eng. Prog. Symposium Ser. No. 17, 51, 79 (1955).

41. Prandtl, L., Fluid Dynamics. New York: Hafner Publishing Company, 1952.

42. Present, R. D., Kinetic Theory of Gases. New York: McGraw-Hill Book Company, 27-47 (1958).

43. Reiner, M. Deformation and Flow. London, England: Interscience, 1949.

44. Sakiadis, B. C., and Coats, J., "Studies of Thermal Conductivities of Liquids, Parts I and II," A. I. Ch. E. Journal I, 275-88(1955) and Part III, A. I. Ch. E. Journal 3, 121 (1957)

45. Scarborough, J. B., Numerical Mathematical Analysis. Baltimore: Johns Hopkins Press, 64-8 and 128-30, 1955.

46. Schlichting, H., Boundary Layer Theory. London, England: Pergamon Press, 1955.

47. Sieder, E. N. and Tate, G. E., "Heat Transfer and Pressure Drop of Liquids in Tubes," Ind. Eng. Chem. 28, 1429 (1936).

48. Tobolsky, A. and Eyring, H. J., "Mechanical Properties of Polymeric Materials," J. Chem. Phys. 11, 125 (1943).

49. Toor, H. L., "The Energy Equation for Viscous Flow," Ind. Eng. Chem. 48, 922 (1956).

50. Weltman, R. N., "Friction Factors for Flow of Non-Newtonian Materials in Pipelines," Ind. Eng. Chem. 48, 386 (1956).

51. Wilkinson, W. L., Non-Newtonian Fluids. London, England: Pergamon Press, 1960.

52. Yamagata, K., Mem. Fac. Eng., Kyushu Imp. Univ. 8, 365 (1940). Reference taken from Pigford (40).

APPENDICES

APPENDIX A

THE CAPILLARY VISCOMETER

Determinations of non-Newtonian viscosity data are frequently made with a capillary viscometer. Maron, Kreiger, and Sisko (28) described an absolute viscometer with continuously varying pressure head which had a wide operating range and was simple to use. A viscometer of similar design was constructed by Lo (26) and modified slightly by Larkin (24) at the University of Tennessee. The modified viscometer is shown in Figures A.1 and A.2.

The capillary unit is installed inside a Plexiglas cylinder which can be removed and completely disassembled for cleaning or changing capillary tubes, Figure A.1. The capillary unit contains two reservoirs which are approximately 2 inches in diameter and 1 inch deep jointed by the side arm and capillary tubes. Two Plexiglas strips provide support to remove strain from the glass capillary tube. The sidearm tube is used to fill the bottom reservoir with the sample and facilitate the rapid attainment of hydrostatic balance at the end of a test. Viscosity determinations in this investigation involved the use of a precision bore Pyrex capillary tube with an inside diameter of 0.1019 cm., obtained from the Wilmad Glass Company.

The manometer unit was made from a Meriam manometer with a 0.718 cm. inside diameter, 128 cm. long glass tube. The manometer unit was connected to the capillary unit by clear Plexiglas containing nylon stopcock valves. A twenty ml. hypodermic syringe

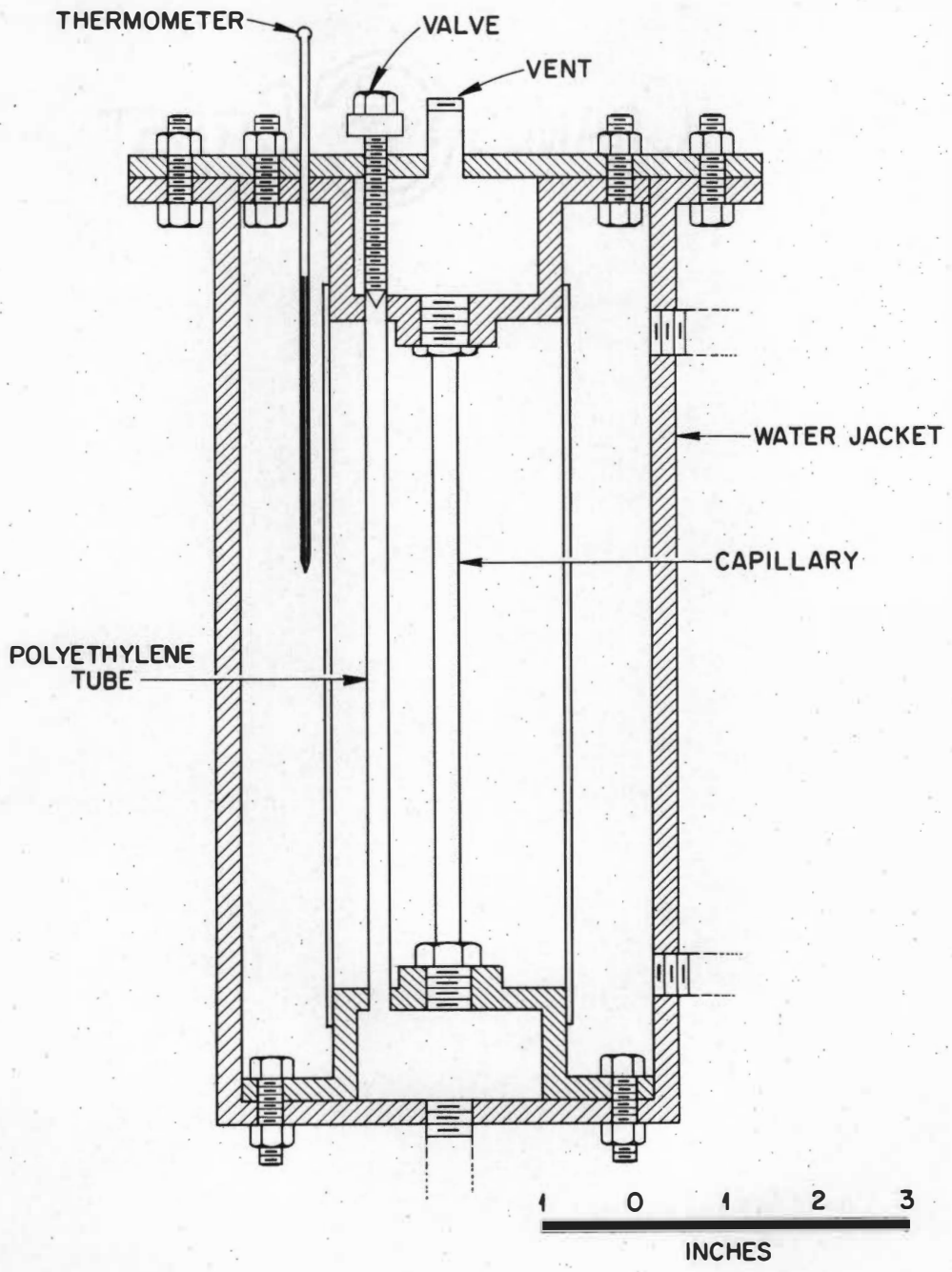


FIGURE A.1

CROSS SECTIONAL VIEW OF THE CAPILLARY VISCOMETER

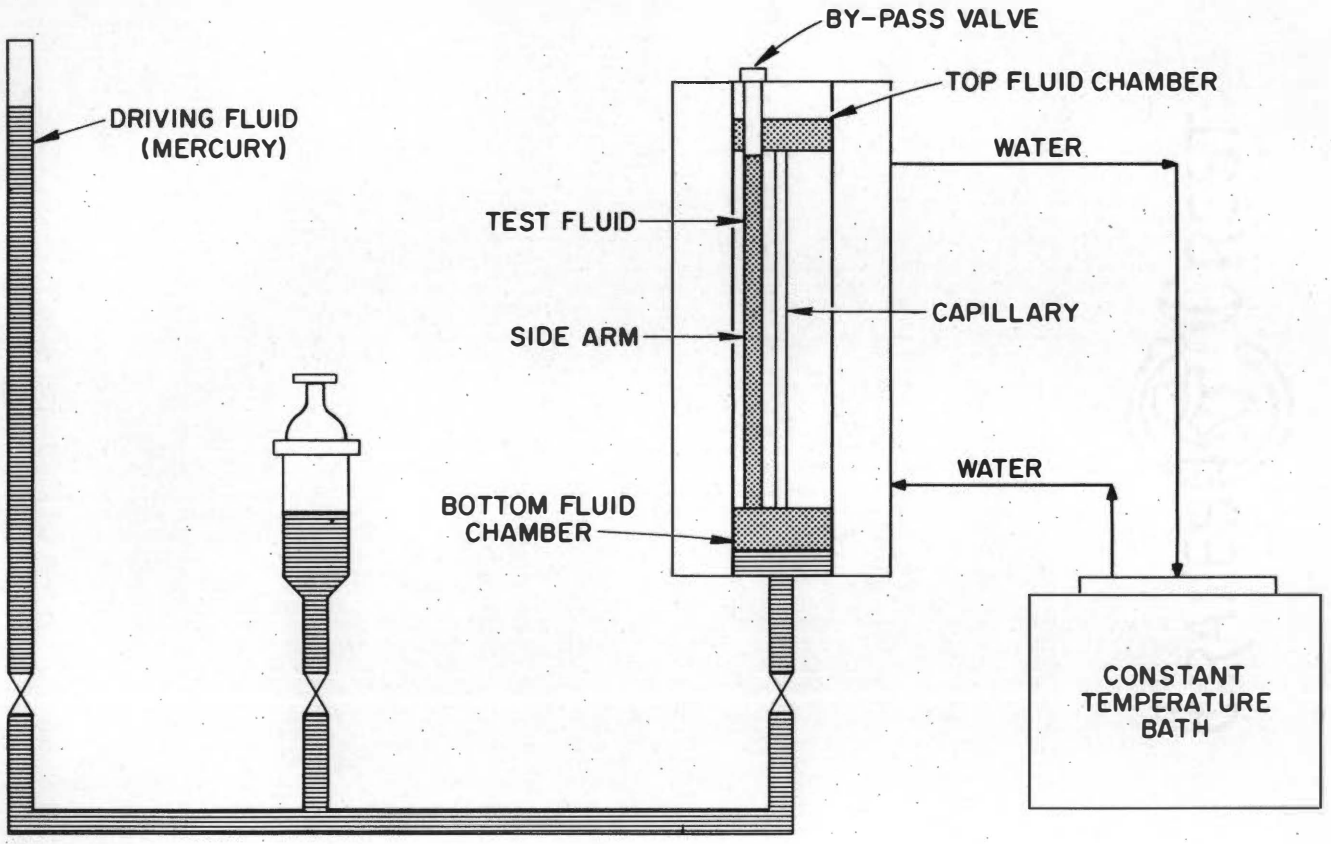


FIGURE A.2

SCHEMATIC DIAGRAM OF CAPILLARY VISCOMETER ASSEMBLY

was used to adjust the mercury level in the manometer leg and to purge air from the bottom reservoir of the capillary unit before each test. Both the capillary unit and manometer were mounted on the rigid grillwork of a laboratory bench. Water circulated from a constant temperature bath, manufactured by the American Scientific Instrument Company, was used to maintain isothermal conditions during each run. The vertical height of the mercury in the manometer tube was measured during the tests with a cathetometer manufactured by the Fredrich C. Henson Company. Mercury levels were read to the nearest 0.001 cm. by use of a dial indicator on the cathetometer's base. The time corresponding to the various mercury levels was obtained with two electrical timers manufactured by the Standard Electric Timer Company.

I. METHOD OF ANALYSIS

The physical parameters of the viscometer are designated as follows:

R_M = radius of the manometer tube

R_C = radius of the capillary

R_R = radius of the reservoirs in the capillary unit

L = length of the capillary tube.

Since both reservoirs have the same cross-sectional area, (when the by-pass valve is closed), the height of the sample column, s, remains constant during a test. The heights y and z' will be used to designate the heights of the mercury columns in the capillary unit reservoir and in the manometer, respectively, above the horizontal

interconnecting mercury flow line.

The pressure drop across the capillary, ΔP, can be expressed as:

$$\Delta P = \frac{z' \rho_m g}{g_c} - \left(\frac{y \rho_m g}{g_c} + \frac{s \rho_s g}{g_c} \right) \quad \text{(A-1)}$$

where: ρ_m = density of mercury,

ρ_s = density of test liquid,

g = acceleration due to gravity,

g_c = units constant.

When the system is brought into hydrostatic balance, $y = y_o$ and $z' = z'_o$ and:

$$\Delta P = 0 = \frac{z'_o \rho_m g}{g_c} - \left(\frac{y_o \rho_m g}{g_c} + \frac{s \rho_s g}{g_c} \right) \quad \text{(A-2)}$$

Equation (A-2) is substracted from Equation (A-1):

$$\Delta P = \left[(z' - z'_o) - (y - y_o) \right] \frac{\rho_m g}{g_c} \quad \text{(A-3)}$$

Since the volume of mercury in the system remains constant, one can write:

$$y - y_o = -\frac{R_M^2}{R_R^2} (z' - z'_o) \quad \text{(A-4)}$$

and substitute (A-4) into (A-3) to obtain:

$$\Delta P = (z' - z'_o) \frac{\rho_m g}{g_c} \left(1 + \frac{R_M^2}{R_R^2} \right). \quad \text{(A-5)}$$

Now, let $z' - z'_o = h$ so:

$$\Delta P = \frac{\rho_m g}{g_c} \left(1 + \frac{R_M^2}{R_R^2} \right) h \qquad \text{(A-6)}$$

and the volumetric flow rate, Q, is:

$$Q = -\pi R_M^2 \frac{dh}{dt} \qquad \text{(A-7)}$$

An inspection of equations (A-6) and (A-7) reveals that an experimental determination of h as a function of time, t, will permit one to calculate both ΔP and Q. The density of the sample fluid does not appear in either of the equations and need not be known.

The power-law constants, C and n, can be evaluated from capillary viscometer data using Equations (A-6) and (A-7) with the similar expressions obtained from the power-law rheological model.

A simple force balance on power-law fluids in pipe flow gives:

$$\tau = \frac{\Delta P}{2L} = C \left[-\frac{dw}{dr} \right]^n \qquad \text{(A-8)}$$

Equation (A-8) can be rearranged and integrated to determine the point velocity, w, as a function of radial position, r.

$$w = -\left[\frac{\Delta P}{2CL}\right]^{1/n} \int_{R_C}^{r} r^{1/n}\, dr = \frac{n}{n+1} \left[\frac{\Delta P}{2CL}\right]^{1/n} \left[R_w^{\frac{n+1}{n}} - r^{\frac{n+1}{n}} \right] \qquad \text{(A-9)}$$

The volumetric flow rate can then be determined by an additional integration.

$$Q = \int_0^{R_c} 2\pi r w dr = \left(\frac{\Delta P}{2CL}\right)^{1/n} \frac{\pi n}{3n+1} R_w^{\frac{3n+1}{n}} \qquad \text{(A-10)}$$

Now, substituting Equations (A-6) and (A-7) into Equation (A-10),

$$-\pi R_M^2 \frac{dh}{dt} = \frac{\pi n}{3n+1} \left[\frac{h \rho_m g}{2CLg_c}\right] \left(1 + \frac{R_M^2}{R_R^2}\right)^{1/n} \left(R_c^{\frac{3n+1}{n}}\right), \qquad \text{(A-11)}$$

an expression is obtained which involves only: (a) the power-law parameters, (b) the instrument dimensions, and (c) experimental data from the capillary viscometer.

For simplification, define:

$$E = \frac{n}{R_M^2(3n+1)} \left[\frac{\rho_m g}{2CLg_c} \left(1 + \frac{R_M^2}{R_R^2}\right)\right]^{1/n} \left[R_c^{\frac{3n+1}{n}}\right] \qquad \text{(A-12)}$$

Thus, Equation (A-11) becomes:

$$\frac{dh}{dt} = -E h^{1/n} \qquad \text{(A-13)}$$

which can also be integrated to give:

$$t = \frac{n}{E(1-n)} \left[h^{\frac{n-1}{n}} - h_1^{\frac{n-1}{n}}\right] \qquad \text{(A-14)}$$

where h_1 is the driving height at $t = 0$.

Equation (A-14) is of the form:

$$t = a + bh^d \qquad \text{(A-15)}$$

where:

$$a = - \frac{n\, h_1^{\frac{n-1}{n}}}{E(1-n)}$$

$$b = \frac{n}{E(1-n)}$$

$$d = \frac{n-1}{n}$$

Now, define:

$$h_2 = Gh_1 \qquad \Delta t_1 = t_2 - t_1$$

$$h_3 = Gh_2 \qquad \Delta t_2 = t_3 - t_2$$

$$h_4 = Gh_3 \qquad \Delta t_3 = t_4 - t_3$$

$$h_j = G^{j-1} h_1 \qquad \Delta t_j = t_{j+1} - t_j$$

$$\Delta t_j = b \left[G^d - 1 \right] h_j^d \qquad \text{(A-16)}$$

Where: $0 < G < 1$ (= 0.944 for the data analyzed in this investigation). Equation (A-15) is of a form for which data can be arranged to determine all three constants (since they are interdependent upon only two unknown parameters, C and n). By plotting the capillary viscometer data, h versus t, and differencing as defined above, it is possible to evaluate both C and n from the slope and intercept on a log-log plot of h_j versus Δt_j, since the slope of such a plot is equal to d and the intercept is equal to $\log b \left[G^C - 1 \right]$.

Data from a typical sample of neutralized Carbopol are presented in Table VIII and shown in Figure 6.2 for this analysis. This technique was not employed for the evaluation of temperature-

TABLE VIII

CAPILLARY VISCOMETER DATA
0.18 WEIGHT % CARBOPOL AT 75.8°F

Counting Index, J	Differenced Pressure Head, cm. Hg., $G^J h_1$	Time, Seconds	Time Increment, Seconds
(1)	(2)	(3)	(4)
1	94.400	16	20
2	88.360	36	21
3	83.058	57	24
4	78.075	81	26
5	73.391	107	29
6	68.988	136	32
7	64.849	168	32
8	60.958	200	36
9	57.301	236	45
10	53.863	281	52
11	50.631	333	51
12	47.593	384	55
13	44.737	439	64
14	42.053	503	70
15	39.530	573	73
16	37.158	646	82
17	34.929	728	85
18	32.833	813	94
19	30.863	907	91
20	29.011	998	105
21	27.270	1103	106
22	25.634	1209	111
23	24.096	1320	111
24	22.650	1431	114
25	21.291	1545	116
26	20.014	1661	110
27	18.813	1771	125
28	17.684	1896	112
29	16.623	2008	117
30	15.626	2125	118
31	14.688	2243	118
32	13.807	2361	118
33	12.979	2479	118
34	12.200	2597	116
35	11.468	2713	118
36	10.780	2831	119
37	10.133	2950	122
38	9.525	3072	128
39	8.954	3200	132
40	8.416	3332	133

TABLE VIII (CONTINUED)

Counting Index, J	Differenced Pressure Head, cm. Hg., $G^J h_1$	Time, Seconds	Time Increment, Seconds
(1)	(2)	(3)	(4)
41	7.911	3465	128
42	7.437	3593	125
43	6.990	3718	122
44	6.571	3840	142
45	6.177	4082	140
46	5.806	4222	156
47	5.458	4378	---
48	5.130	----	---
49	4.822	----	---
50	4.533	----	---
51	4.261	----	---
52	4.005	4968	164
53	3.765	5132	173
54	3.539	5305	---

TABLE VIII (CONTINUED)

CAPILLARY VISCOMETER DATA
0.18 WEIGHT % CARBOPOL AT 95.0°F

Counting Index, J	Differenced Pressure Head, cm. Hg., $G^J h_j$	Time, Seconds	Time Increment, Seconds
(1)	(2)	(3)	(4)
12	47.593	6	5
13	44.737	11	5
14	42.053	16	5
15	39.530	21	7
16	37.158	28	7
17	34.929	35	8
18	32.833	43	11
19	30.863	54	9
20	29.011	63	10
21	27.270	73	9
22	25.634	82	11
23	24.096	93	13
24	22.650	106	14
25	21.291	120	15
26	20.014	135	18
27	18.813	153	20
28	17.684	173	23
29	16.623	196	22
30	15.626	218	25
31	14.688	243	28
32	13.807	271	29
33	12.979	300	32
34	12.200	332	34
35	11.468	336	37
36	10.780	403	39
37	10.133	442	42
38	9.525	484	46
39	8.954	530	47
40	8.416	577	48
41	7.911	625	47
42	7.437	672	53
43	6.990	725	53
44	6.571	778	59
45	6.177	837	63
46	5.806	900	65
47	5.458	965	68

TABLE VIII (CONTINUED)

Counting Index, J	Differenced Pressure Head, Δ_j cm. Hg.,	Time, Seconds	Time Increment, Seconds
(1)	(2)	(3)	(4)
48	5.130	1033	68
49	4.822	1101	71
50	4.533	1172	80
51	4.261	1252	80
52	4.005	1332	80
53	3.765	1412	96
54	3.539	1508	--

dependent rheological parameters of the solutions used in the flow system primarily because of the temperature limitation imposed by the low softening point of the Plexiglas construction material. However, it was felt that the experimental and analytical techniques used provided an adequate general knowledge about the validity of the power-law model for neutralized aqueous Carbopol solutions.

APPENDIX B

THE ROTATIONAL VISCOMETER

A Brookfield Synchro-Lectric viscometer shown in Figures 4.1 and 4.2 was used to evaluate the rheological properties of the fluid samples obtained from the dynamic flow system. Three cylindrical spindles were made for use with the Brookfield viscometer since the spindles supplied with the instrument did not have geometries amenable to mathematical analysis.

I. CALIBRATION

The Brookfield viscometer required calibration to determine absolute rheological data, and a viscometer calibration fluid was obtained from the National Bureau of Standards (oil N, Lot No. 31) for this purpose. The calibration fluid was obtained with a set of temperature-viscosity data, and the Brookfield viscometer was calibrated at one of these temperatures ($77^{\circ}F$) by using the Newtonian viscosity of the oil at that temperature (9.054 poise) as follows.

The relation between shear stress and shear rate for Newtonian fluids is defined by

$$\tau = - \frac{\mu}{g_c} \upsilon \qquad \text{(B-1)}$$

where μ is the viscosity, and υ is the shear rate.

Consider a section through the viscometer of unit height in the region of uniform flow (away from the end effects). The measured couple per unit height is H.

The shear stress $\tau(r)$ at radius r is given by

$$\tau(r) = \frac{H}{2\pi r^2} \qquad \text{(B-2)}$$

and the rate of shear by

$$\nu = r\frac{d\Omega}{dr} \qquad \text{(B-3)}$$

where Ω is the angular velocity.

Therefore, for Newtonian fluids

$$d\Omega = -\frac{g_c\tau}{\mu}\frac{dr}{r} = -\frac{g_c H dr}{\mu 2\pi r^3} \qquad \text{(B-4)}$$

The solution of this differential equation depends on the boundary conditions at the cylinder surface and the width of the fluid gap. If there is no slipping either at the cylinder or the container walls, the boundary conditions become

$\Omega = \Omega_s$ at $r = r_s$, spindle radius

$\Omega = 0$ at $r = r_c$, container radius

Hence, integrating Equation (B-4), the angular velocity at the spindle surface is

$$\Omega_s = \frac{g_c H}{4\pi\mu r_s^2}\left[1 - \left(\frac{r_s}{r_c}\right)^2\right] \qquad \text{(B-5)}$$

which reduces to

$$\Omega_s = \frac{g_c H}{4\pi\mu r_s^2} \qquad \text{(B-6)}$$

for $r_c >> r_s$, e.g., if $r_s = 0.250$ and $r_c = 2.50$, then $1 - \left(\frac{r_s}{r_c}\right)^2 = 0.99$

and Equation (B-6) is only in 1% error.

Rearranging Equation (B-6),

$$H = \frac{4\pi \mu r_s^2 \Omega_s}{g_c} , \qquad \text{(B-7)}$$

and by definition the spring constant is equal to the meter deflection divided by torque on the spindle. It is also known (by a simple force balance on the spindle) that the torque is equal to the product of the measured couple per unit height, H, and the spindle immersion depth, z_1, Therefore,

$$\text{Spring Constant} = \frac{\text{Meter Deflection}}{Hz_1} \qquad \text{(B-8)}$$

Combining Equations (B-7) and (B-8)

$$\text{Spring Constant} = \left(\frac{\text{Meter Deflection}}{z_1}\right)\left(\frac{g_c}{4\pi \mu r_s^2 \Omega_s}\right) \qquad \text{(B-9)}$$

Equation (B-9) can now be used to determine the value of the spring constant from experimental data since all terms are readily available.

II. EXPLANATION OF BROOKFIELD CALIBRATION DATA, TABLE IX

Data for calibrating the spring constant of the Brookfield viscometer are given in Table IX, and those data for the 0.500 in. O.D. spindle are plotted in Figure B.1. The slopes of the lines are equal to the "Meter Deflection per unit immersion depth" required for Equation (B-9). The calibration fluid viscosity at 77°F was

TABLE IX

BROOKFIELD CALIBRATION DATA
NATIONAL BUREAU OF STANDARDS OIL "N" AT 77.0°F

Immersion Depth, in.	1.00 in. O.D. Spindle Scale Deflection, Units				0.500 in. O.D. Spindle Scale Deflection, Units				0.250 in. O.D. Spindle Scale Deflection, Units			
	6 RPM	12 RPM	30 RPM	60 RPM	6 RPM	12 RPM	30 RPM	60 RPM	6 RPM	12 RPM	30 RPM	60 RPM
0.300	9.8	21.8	53.5	---	---	---	---	---	---	---	---	---
0.400	15.4	31.9	78.0	---	---	---	---	---	---	---	---	---
0.500	21.8	43.0	---	---	---	---	---	---	---	---	---	---
0.600	27.3	52.8	---	---	3.6	7.9	21.7	42.7	---	---	---	---
0.700	31.8	62.3	---	---	---	---	---	---	---	---	---	---
0.800	37.1	71.6	---	---	5.7	12.3	32.3	64.8	1.2	2.6	8.3	16.3
1.000	46.2	90.7	---	---	8.2	17.0	43.8	86.0	---	---	---	---
1.200	---	---	---	---	10.3	21.7	54.9	---	2.4	4.8	13.4	26.8
1.400	---	---	---	---	12.8	26.2	65.3	---	---	---	---	---
1.600	---	---	---	---	15.3	30.7	76.1	---	3.4	7.3	19.2	38.0
1.800	---	---	---	---	17.8	35.7	88.3	---	4.1	8.4	21.9	43.3
2.000	---	---	---	---	---	---	---	---	4.6	9.7	24.7	48.9

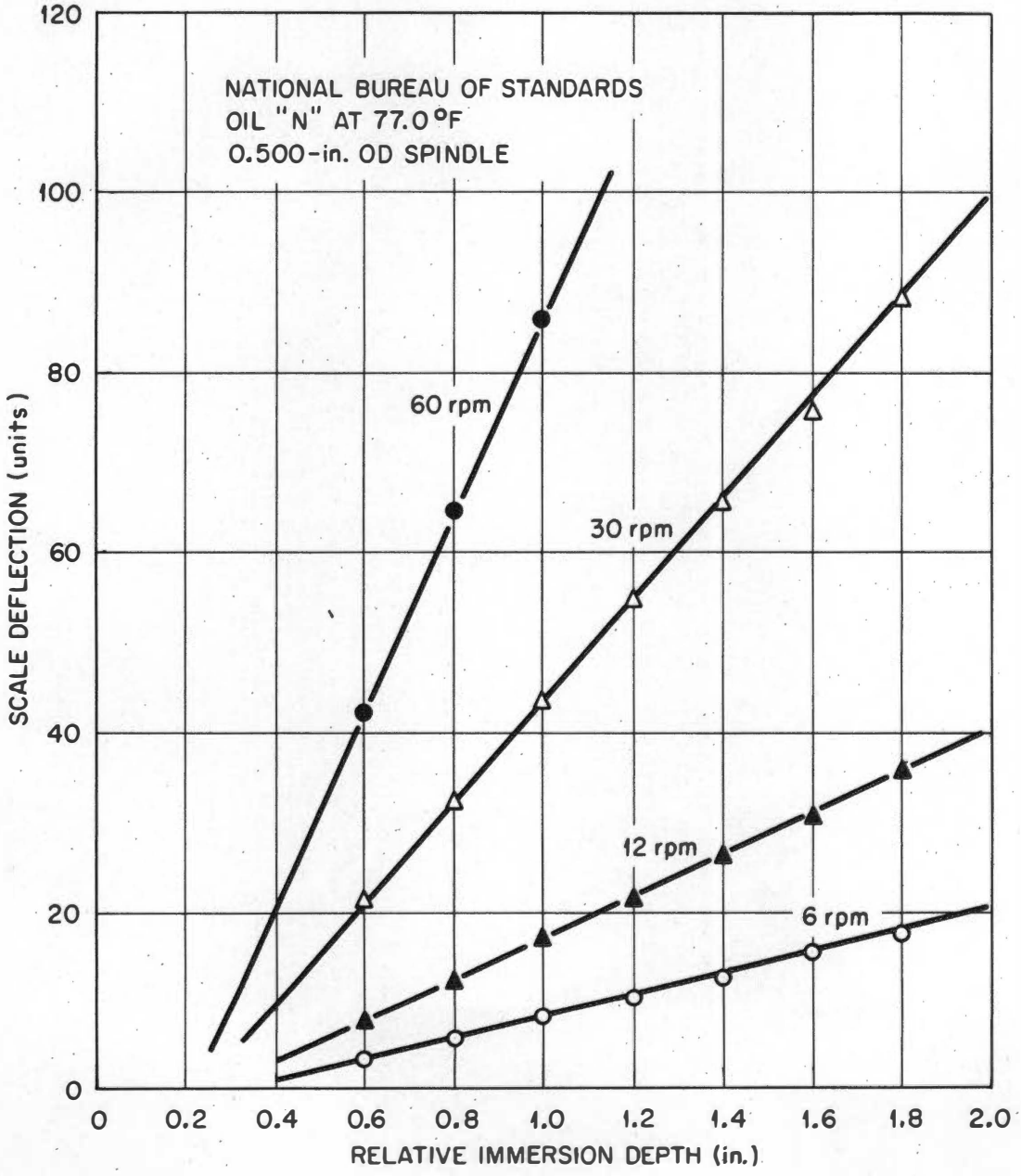


FIGURE B.1

CALIBRATION DATA FOR THE BROOKFIELD SYNCHRO-LECTRIC VISCOMETER, 0.500 IN. SPINDLE

9.054 poise, and the instrument parameters are given in Table IX.

The spring constants calculated from the data were

Spindle Speed RPM	Spring Constant Deflection Units/Dyne-cm.
6	0.1520
12	0.1537
30	0.1538
60	0.1545
Average	0.1535

The average spring constant for all three spindles and four speeds was 0.1551 Deflection Units per Dyne-cm.

III. POWER-LAW FLUIDS

The relation between shear stress and shear rate for power-law fluids is defined by

$$\tau = c \left[- \nu \right]^{n} . \qquad \text{(B-10)}$$

and combining Equations (B-10), (B-2), and (B-3) one obtains

$$d\Omega = - \left(\frac{\tau}{c}\right)^{1/n} \frac{dr}{r} = \frac{1}{2} \left(\frac{\tau}{c}\right)^{1/n} \frac{d\tau}{\tau} \qquad \text{(B-11)}$$

The boundary conditions for this differential equation are

$$\Omega = \Omega_s \text{ at } r = r_s$$
$$\Omega = 0 \quad \text{at } r = r_c .$$

Hence, integrating Equation (B-11), the angular velocity at the spindle surface is

$$\Omega_s = \frac{n}{2} \left(\frac{M}{2\pi r_s^2 c}\right)^{1/n} \left(1 - \left(\frac{r_s}{r_c}\right)^{2/n}\right) \qquad \text{(B-12)}$$

For $n << 1$ Equation (B-12) becomes

$$\Omega_s = \frac{n}{2}\left(\frac{H}{2\pi r_s^2 C}\right)^{1/n} = \frac{n}{2}\left[\frac{\tau_s}{C}\right]^{1/n} \qquad \text{(B-13)}$$

Therefore, a log-log plot of shear stress versus angular velocity must be a straight line with slope, n, and intercept, $\left(\frac{2}{n}\right)^n C$.

Explanations of sample data for these equations are given below.

IV. SAMPLE BROOKFIELD ROTATIONAL VISCOMETER DATA, TABLES X, XI, AND XII

Scale deflection (Table X, columns (2), (3), (4), and (5)) is plotted versus relative immersion depth (Table X, column (1)) in Figure B.2. The slopes of these curves are used to calculate the wall shear stress on the spindle (Table XI, column (3)) as a function of spindle speed (Table XI, Column (1)) by use of Equations (B-2) and (B-8). These shear stress-temperature-spindle speed data are presented graphically as: (a) a rectangular plot of shear stress versus temperature for each speed (this figure hints strongly of a linear temperature dependence), Figure B.3, and (b) a log-log plot of shear stress versus angular velocity (which shows the linear relation indicated by Equation (B-13)), Figure B.4. The slopes and intercepts of plots similar to Figure B.4 were calculated by least mean squares and tabulated in Table XII as a linear function of temperature, see Figure B.5. These data were then averaged with similar data for other samples to obtain the temperature-dependent rheological data in Table IV.

TABLE X

SAMPLE ROTATIONAL VISCOMETER DATA - 80.6°F
SAMPLE TAKEN AFTER RUN 6
SPINDLE DIAMETER = 0.500"

Relative Immersion Depth, Inches	Scale Deflection, Units			
	6 RPM	12 RPM	30 RPM	60 RPM
(1)	(2)	(3)	(4)	(5)
0.800	16.0	19.6	26.5	32.5
1.008	24.5	30.2	40.2	51.3
1.216	32.9	40.5	54.4	69.2
1.424	41.0	50.6	67.6	87.4
1.632	49.5	60.7	81.9	----

TABLE XI

SAMPLE CALCULATED SHEAR STRESS ON SPINDLE WALL
SAMPLE TAKEN AFTER RUN 6
SPINDLE DIAMETER = 0.500 INCHES

Spindle Speed, Radians/Second	Shear Stress on Spindle Wall, Dynes/cm^2				
	54.5°F	80.6°F	102.4°F	127.4°F	145.4°F
(1)	(2)	(3)	(4)	(5)	(6)
0.628	42.35	40.05	37.43	31.16	33.16
1.256	53.93	49.64	46.34	37.85	38.65
3.14	73.51	65.82	61.02	49.14	48.84
6.28	95.88	84.89	76.60	61.32	60.33

TABLE XII

SAMPLE CALCULATED RHEOLOGICAL PARAMETERS
AS A FUNCTION OF TEMPERATURE
SAMPLE TAKEN AFTER RUN 6

Temperature, °F	Consistency Index, C, Dynes Sec^n/cm^2	n
(1)	(2)	(3)
54.5	26.7	0.352
80.6	25.3	.325
102.4	24.0	.329
127.4	20.0	.331
145.4	21.3	.306

$$C = 28.16 - 0.0704T \quad \frac{\text{Dynes sec}^n}{\text{cm}^2}$$

$$n_{avg} = 0.329$$

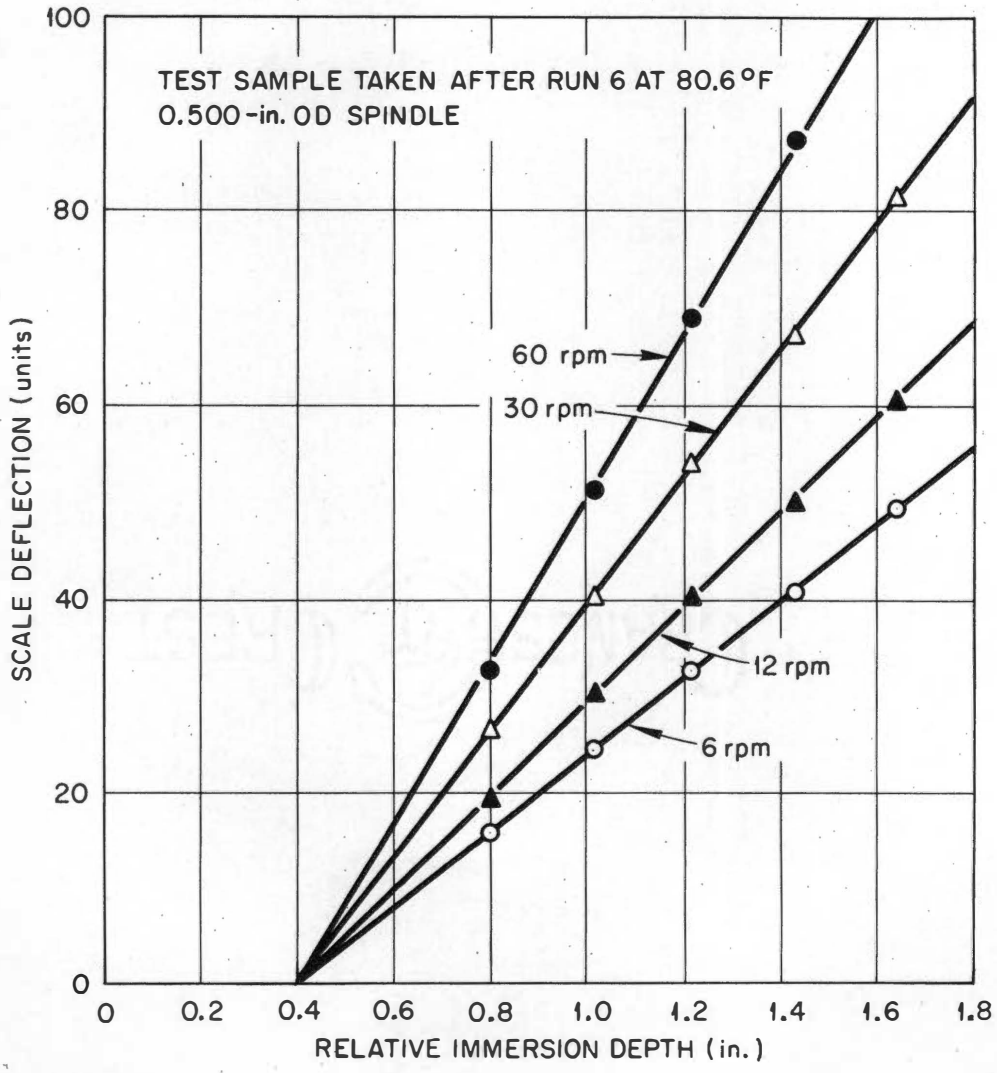


FIGURE B.2

TYPICAL RHEOLOGICAL DATA, SAMPLE TAKEN AFTER RUN 6

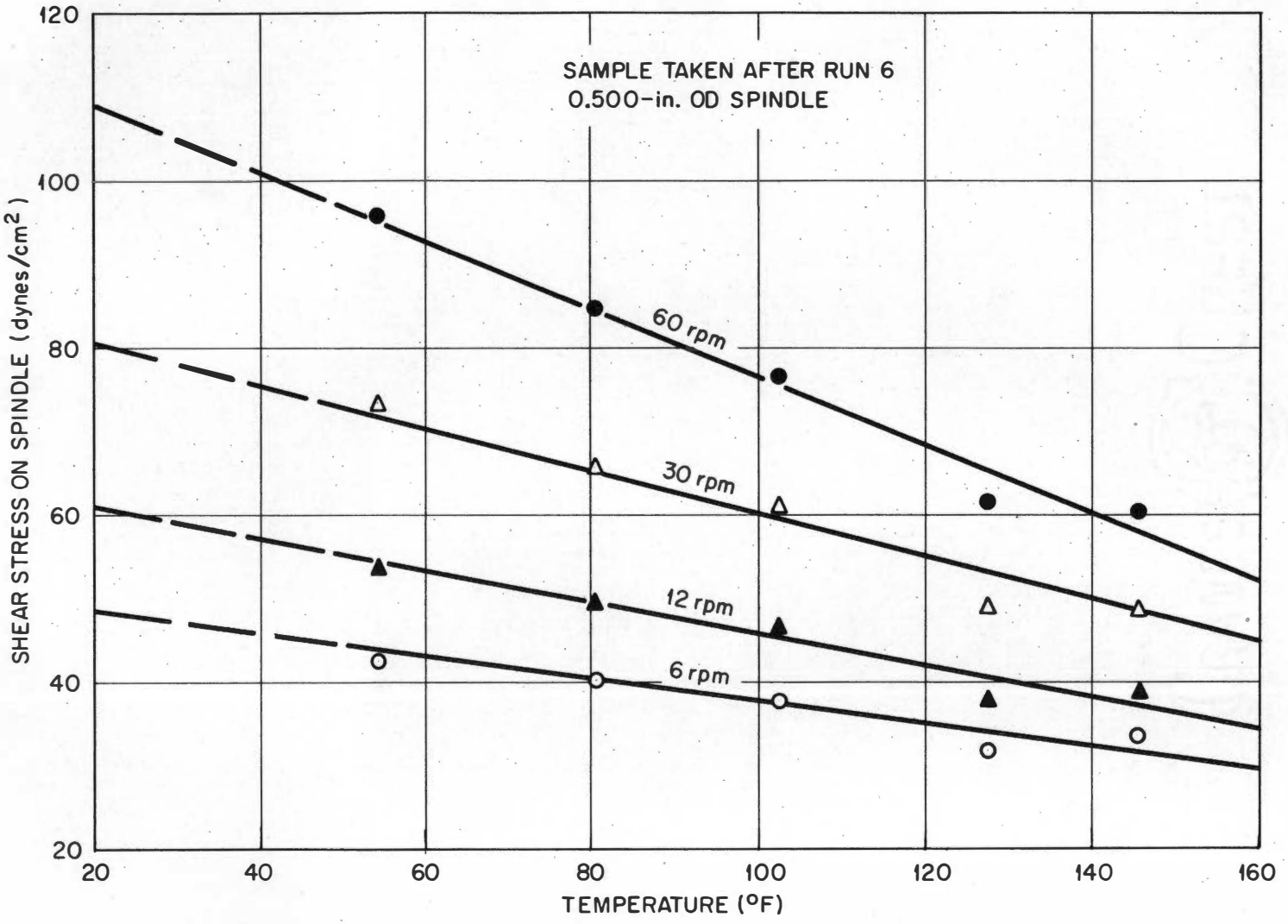


FIGURE B.3

TYPICAL SHEAR STRESS VERSUS TEMPERATURE DATA, SAMPLE TAKEN AFTER RUN 6

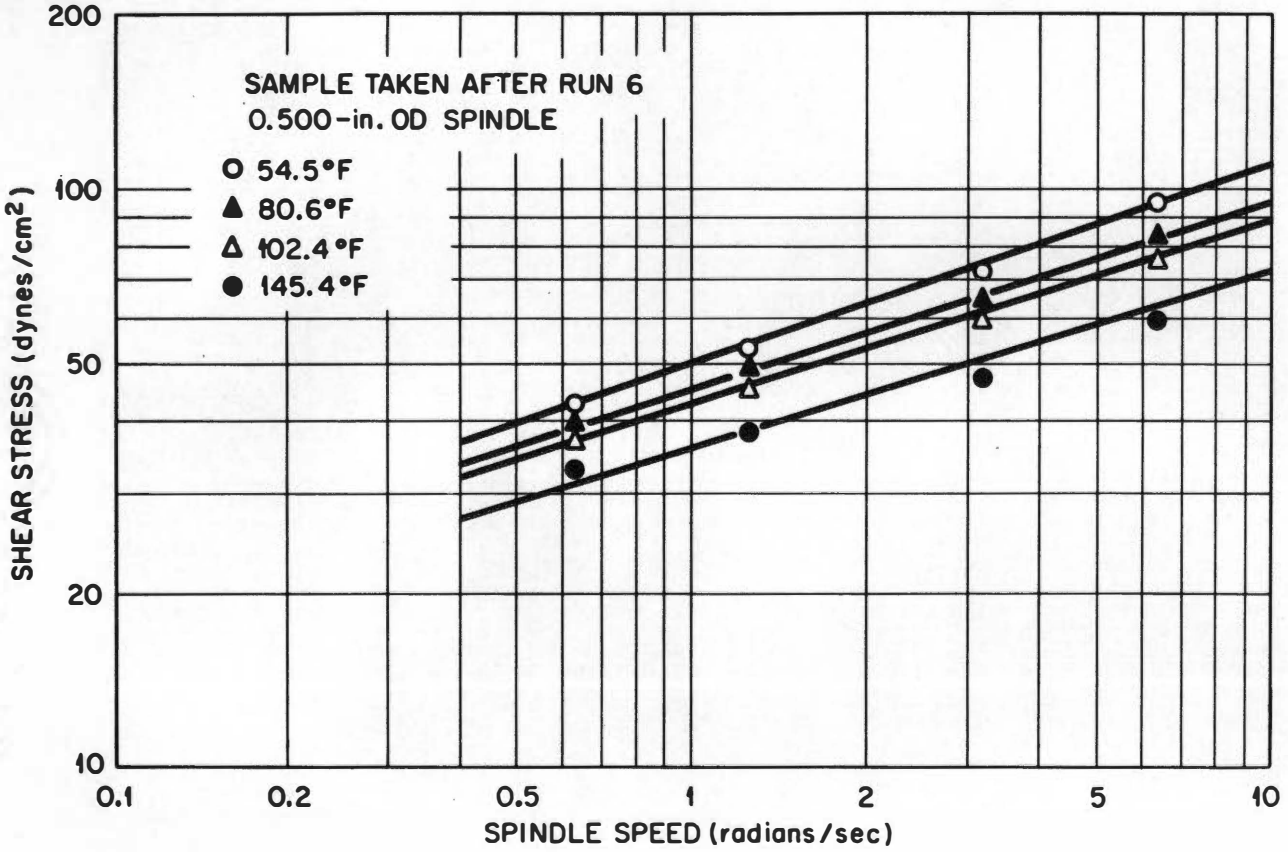


FIGURE B.4

TYPICAL LOG-LOG PLOT OF SHEAR STRESS VERSUS SPINDLE SPEED DATA, SAMPLE TAKEN AFTER RUN 6

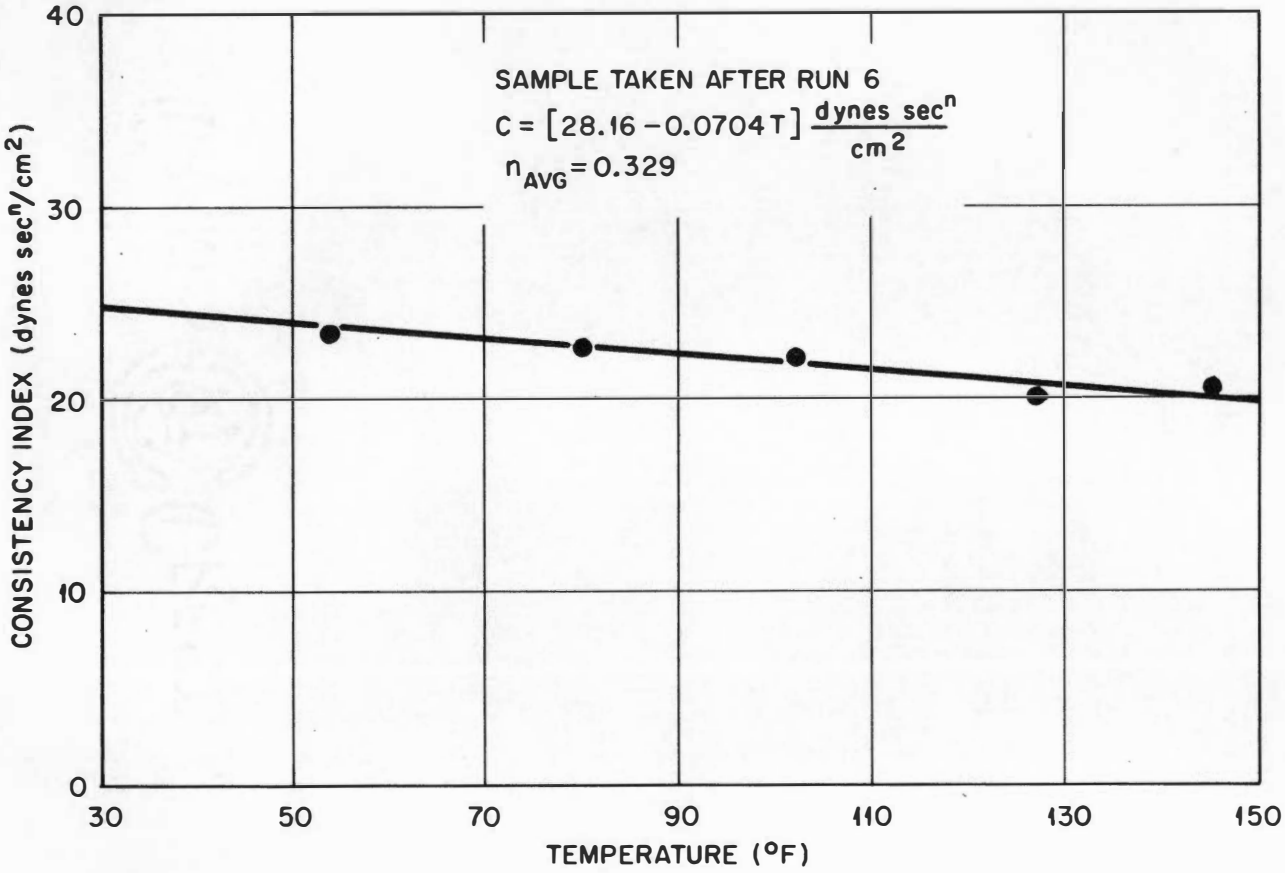


FIGURE B.5

TYPICAL CONSISTENCY INDEX VERSUS TEMPERATURE DATA,
SAMPLE TAKEN AFTER RUN 6

APPENDIX C

COMPUTER PROGRAMS

An IBM 1620 digital computer, located in the Computer Center of the University of Tennessee, was used to make many of the lengthy calculations required in this work. The machine was programmed in Fortran, an automatic coding system with a language closely resembling algebra. A list of the more common symbols and commands used in the Fortran programs for this investigation are given below.

Symbol	Meaning
+	denotes addition
-	denotes subtraction
*	denotes multiplication
/	denotes division
**	denotes exponentiation
LOG ( )	denotes Log_e of ( )
DO	denotes a command for a series of repeated calculations specified in the statement
Dimension	denotes a command to save space for certain items
Read	denotes a command to read input (tape) data
Print	denotes a command to type out results

I. PROGRAM (C-1)

This program was used to calculate: (a) reduced radial position (dimensionless), (b) point velocity (ft/min), (c) point shear stress lb_f/ft^2), (d) point temperature (^oF), and (e) point thermal conductivity (btu/hr-ft-^oF) for 101 equally spaced points from the pipe centerline

to its wall. Only 17 of the sets of numbers were actually printed because of the rather slow print out. The values printed were those corresponding to each 0.1 reduced radial increment and the three 0.01 reduced radial increments nearest the centerline and wall. The volumetric flow rate was also calculated in Program (C-1).

The data input symbols and their meanings for Program (C-1) are:

Symbol		Meaning
Runno	=	data identification number
TCL	=	T_{CL}, centerline temperature, Table I
A	=	A, a constant in the empirical temperature distribution, Table I
T	=	m, a constant in the empirical temperature distribution, Table I
PG	=	pressure gradient, Table III
B	=	B, an empirical constant in the temperature-dependent rheological equation, Table IV
AKO	=	C_o, an empirical constant in the temperature-dependent rheological equation, Table IV
S	=	1/n, an empirical constant in the temperature-dependent rheological equation, Table IV
DTCLZ	=	$\partial T_{CL} / \partial z$, Table II
DAZ	=	$\partial A / \partial z$, Table II
DMZ	=	$\partial M / \partial z$, Table II

The following additional constants were also supplied in the program:

R_w = 1.332 cm., pipe radius

CPR = 1.0116 cal/cc.$^{\circ}$C (Pure water data (39), calculated)

D = 0.0002 cal/cc.-$^{\circ}$C-$^{\circ}$F (Pure water data (39), calculated)

In the above, CPR and D are constants in the temperature-dependent expression for the product of heat capacity and density.

$$C_p \rho = (CPR - DT) \text{ cal/cc.}^{\circ}C \qquad (C\text{-}1)$$

where T is in $^{\circ}F$.

Program (C-1)
Calculation of
Dynamic Thermal Conductivities

```
DIMENSION F(101), G(101), P(101), U(101), V(101)
CPR=1.0116
D=0.0002
RW=1.332
1 READ,RUNNO,TCL,A,PG,B,AKO,DTCLZ,DAZ,DMZ,S,T
RWT=RW**T
AA=DTCLZ*(CPR-2.*D*TCL)
AB=RWT*(2.*D*TCL*DAZ+2.*A*D*DTCLZ-CPR*DAZ)
AC=-RWT*RWT*2.*A*D*DAZ
AD=RWT*DMZ*(2.*A*D*TCL-A*CPR)
AE=-2.*A*A*D*RWT*RWT*DMZ
C=((PG/(2.*A*B))**S)*(RW**(S-S(T+1.))*1.9685
CO=(AKO-B*TCL)/(A*B*RWT)
DA=122.8974*((RW**(2.-T))/(A*T))
W=A*RWT
PGS=PG**S
PRINT, RUNNO, PG, S, PGS
DO 5 N=1, 101
Q=N
```

```
F(N)=0.01*(Q-1.)
P(N)=F(N)**T
5 G(N)=((F(N)/(P(N)+CO))**S)*C
U(101)=0.
DO 8 N=1, 101
N1=101-N
N2-102-N
8 U(N1)=0.005 *(G(N1)+G(N2))+U(N2)
G(1)=0.
DO 11 N=2,101
XT=P(N)
BLNRX=LOG(RW*F(N))
G(N)=AA+AB*XT+AC*XT*XT+AD*XT*BLNRX+AE*XT*XT*BLNRX
11 V(N)=G(N)*U(N)*F(N)*DA
V(1)=0.
P(1)=TCL
DO 15 N=2,101
15 G(n)=(V(n)+V(N-1))*0.005+G(N-1)
DO 20 N=2,101
G(N)=-G(N)/P(N)
P(N)=TCL-W*P(N)
20 V(N)=0.00104428*PG*RW*F(N)
DO 23 N=1,4
PRINT,F(N),U(N),V(N),P(N),G(N)
23 CONTINUE
DO 25 N=11,91,10
```

```
PRINT,F(N),U(N),V(N),P(N),G(N)
25 CONTINUE
DO 27 N=98,101
PRINT,F(N),U(N),V(N),P(N),G(N)
27 CONTINUE
P(1)=0.
DO 29 N=2,101
29 P(N)=(U(N)*F(N)+U(N-1)*F(N-1))*RW*RW*0.00202895+P(N-1)
PRINT,P(101)
PAUSE
GO TO 1
END
```

II. PROGRAM (C-2)

This program was used to calculate the temperature profiles down stream from a point in the system where both temperature and velocity distributions were known (along with an approximate wall temperature distribution) by assuming a constant thermal conductivity. This solution was made with the use of finite difference increments and required 170 sets of repeated calculations per 0.75 ft. axial increment.

The data input symbols and their meanings for Program (C-2) are:

Symbol		Meaning
Runno	=	data identification number
TMJ	=	initial wall temperature
ATJ	=	wall temperature gradient
ALPHA	=	thermal conductivity/(heat capacity)(density)
W(i)	=	inlet temperatures
V(i)	=	inlet velocities

The increments used were:

DR	=	0.004371 ft., radial increment
DZ	=	0.004411 ft., axial increment.

Analysis Used to Compute Temperature Distributions in Program (C-2)

If one assumes thermal conductivity to be independent of position, the energy equation in cylindrical coordinates and Fourier's Law, Equations (3-2) and (3-4), can be combined into

$$\frac{\partial\left[r\left(\frac{\partial T}{\partial r}\right)\right]}{\partial r} = \frac{r}{K}\frac{\partial\left(w_z \rho C_p T\right)}{\partial T} \qquad \text{(C-2)}$$

If one further assumes that the density and heat capacity are independent of position while the radial velocity profile remains unchanged in the axial direction, the above equation becomes

$$\frac{1}{r}\left(\frac{\partial T}{\partial r}\right) + \left(\frac{\partial^2 T}{\partial r^2}\right) = \frac{w_z}{\alpha}\frac{\partial T}{\partial z} \qquad \text{(C-3)}$$

where $\alpha = \frac{K}{c_p \rho}$

Now, let the following finite-difference approximations be made:

$$\frac{\partial T}{\partial z} \simeq \frac{T(i,j+1) - T(i,j)}{\Delta z} \qquad (C\text{-}4)$$

$$\frac{\partial T}{\partial r} \simeq \frac{T(i+1,j) - T(i,j)}{\Delta r} \qquad (C\text{-}5)$$

$$\frac{\partial^2 T}{\partial r^2} \simeq \frac{T(i+1,j) - 2T(i,j) + T(i-1,j)}{(\Delta r)^2} \qquad (C\text{-}6)$$

Furthermore, at the centerline $\left(\frac{\partial T}{\partial r}\right) \to 0$ as $r \to 0$ and

$$2 \frac{\partial^2 T}{\partial r^2} = \frac{w_z}{\alpha} \frac{\partial T}{\partial z} \qquad (C\text{-}7)$$

By substituting equations (C-4), (C-5), and (C-6) into equations (C-3) and (C-7), the following are obtained

$$T(i,j+1) = \frac{\alpha \Delta z}{(\Delta r)^2 w_z(i)} \left[T(i+1,j) \left(\frac{i+1}{i}\right) + T(i,j) \left(\frac{(\Delta r)^2 w_z(i)}{\alpha \Delta z} \right) - \frac{2i+1}{i} + T(i-1,j) \right] \qquad (C\text{-}8)$$

and at the centerline

$$T(1,j+1) = \frac{\alpha \Delta z}{(\Delta r)^2 w_z(i)} \left[4T(i+1,j) + T(i,j) \left(\frac{(\Delta r)^2 w(i)}{\alpha \Delta z} - 4 \right) \right] \qquad (C\text{-}9)$$

Equations (C-8) and (C-9) can now be solved numerically to evaluate the temperature profile at axial positions downstream from some initial sets of temperature and velocity distributions when a wall temperature distribution is known or can be estimated.

Program (C-2)
Calculation of
Downstream Temperature Profiles

```
DIMENSION T(11),U(11),V(11),W(11)
DR=0.004371
DZ=0.004411
DRS=DR*DR
1 READ,RUNNO,TMJ,ATJ,ALPHA
READ,W(1),W(2),W(3),W(4),W(5),W(6),W(7),W(8),W(9)
READ,W(10),W(11),V(1),V(2),V(3),V(4),V(5),V(6),V(7)
READ,V(8),V(9),V(10),V(11)
ADZ=ALPHA*DZ
DO 10 J=1,3
OJ=J
RUNOP=RUNNO+0.001*(4.-OJ)
Z=170.0*DZ*OJ
PRINT,RUNOP,Z
DO 5 M=1,11
5 T(M)=W(M)
DO 25 N=1,170
Q=N
U(1)=(ADZ/(DRS*V(1)))*(4.*T(2)+(DRS*V(1)/ADZ-4.)*T(1))
```

```
U(11)=TMJ/ATJ*DZ*(170.0*(QJ-1.)+Q)
DO 15 M=2,10
P=M-1
R=((P+1.)/P)*T(M+1)+(DRS*V(M)/ADZ-(2.*P+1.)/P)*T(M)
15 U(M)=ADZ*(R+T(M-1))/(DRS*V(M))
DO 20 M=1,11
20 T(M)=U(M)
25 CONTINUE
DO 30 M=1,11
W(M)=T(M)
PRINT,M,T(M)
30 CONTINUE
10 CONTINUE
PAUSE
GO TO 1
END
```

PROGRAM (C-3)

This program was used to evaluate the flow system parameters: (a) bulk temperature, (b) liquid temperature gradient at the wall, (c) the temperature drop across the wall, (d) the point film coefficient, (e) the point heat flux, and (f) the apparent fluid viscosity at the wall. The following dimensionless groups were also calculated:

Group	Definition
Reynolds Number, (Bulk)	$\frac{D^n V^{2-n} \rho}{g_c C \theta^{n-1}}$
Prandtl Number, (Bulk)	$\frac{C_p g_c C \theta^{n-1}}{K_B} \left(\frac{V}{D}\right)^{n-1}$
Prandtl Number, (Wall)	$\frac{C_p}{K_w} \left[\frac{C_o - B T_w}{\tau_w^{1/n-1}}\right]^{1/n}$
Nusselt Number, (Wall)	$\frac{D \left(\frac{\partial T}{\partial r}\right)_w}{T_{Bulk} - T_{Wall}}$

The data input symbols and their meanings for Program (C-3) are:

Symbol		Meaning
Rumno	=	data identification number
A	=	1/n, Table IV
B	=	B, Table IV
AKO	=	C_o, Table IV
WSS	=	wall shear stress, calculated in Program (C-1)
T(i)	=	point temperatures, smoothed and in Table I
U(i)	=	point velocities, calculated and in Tables XXI through XXVIII

The following additional constants were also supplied in the program:

DF	=	inside pipe diameter, 0.087411 ft.
DC	=	inside pipe diameter, 2.664 cm.
OD	=	outside pipe diameter, 0.109583 ft.
PI	=	3.14159, a constant
AQKW	=	estimated thermal conductivity of the test fluid at the wall temperature, 0.34 Btu/hr-ft-^{o}F

AQKB = estimated thermal conductivity of the test fluid at the bulk temperature, 0.36 Btu/hr-ft-^{o}F

SSK = approximate thermal conductivity of the stainless steel pipe wall, 9.4 Btu/hr-ft-^{o}F

DR = 0.1 reduced radius unit, 0.004371 ft.

Newton's formula for backward interpolation and a system of numberical differentiation (45) were employed to estimate the fluid temperature gradient at the wall in Program (C-3).

Program (C-3)
Heat Transfer Data and
Dimensionless Groups

```
DIMENSION G(11),H(11),T(11),U(11),Y(5)
DF=0.087417
DC=2.664
OD=0.109583
P1=3.14159
AQKW=0.34
AQKB=0.36
SSK=9.4
ALND1=LOG(OD/DF)/(2.*P1*SSK)
DR=0.004371
1 READ,RUNNO,A,B,AKO,WSS
READ,T(1),T(2),T(3),T(4),T(5),T(6),T(7)
READ,T(8),T(9),T(10),T(11),U(1),U(2),U(3)
READ,U(4),U(5),U(6),U(7),U(8),U(9),U(10)
U(11)=0.0
DO 2 M=1,11
```

```
Q=M-1
G(M)=Q*U(M)
2 H(M)=G(M)*T(M)
DO 3 M=2,10,2
H(M)=4.*H(M)
3 G(M)=4.*G(M)
DO 4 M=3,9,2
H(M)=2.*H(M)
4 G(M)=2.*G(M)
TU=0.0
U=0.0
DO 5 M=1,11
TU=TU+H(M)
5 U=U+G(M)
TCUP=TU/U
UMEAN=1.3547*DR*DR*U/(DF*DF)
Y(1)=T(11)-T(10)
Y(2)=T(11)-2.*T(10)+T(9)
Y(3)=T(11)-3.*T(10)+3.*T(9)-T(8)
Y(4)=T(11)-4.*T(10)+6.*T(9)-4.(T(8)+T(7)
Y(5)=T(11)-5.*T(10)+10.*T(9)-10.*T(8)+5.*T(7)-T(6)
DTDRW=(Y(1)+0.5*Y(2)+2.*Y(3)/3.+0.75*Y(4)+0.8*Y(5))/DR
DELTA=TCUP-T(11)
PRINT,RUNNO,TCUP
ANUNO=-DF*DTDRW/DELTA
HI=AQKW*ANUNO/DF
```

```
FLUX=HI*DELTA
DTW=HI*ALNDI
AN=1./A
DN=DC**AN
FU=UMEAN**(2.-AN)
GAMMA=0.125*(AKO-B*TCUP)*(6.+2.*A)**AN
RENO=DN*FU/GAMMA
PRNOA=241.905*GAMMA*(DC/UMEAN)**(1.-AN)
PRNOA=PRNOA/AQKB
WSS=498.81*WSS
AMUAP=((AKO-B*T(11))**A)/(WSS**(A-1.))
PRNOB=241.905*AMUAP/AQKW
PRINT,RENO,ANUNO,PRNOA,PRNOB
PRINT,DTDRW,DTW,HI,FLUX,AMUAP
PAUSE
GO TO 1
END
```

APPENDIX D

EXPLANATION OF TABULATED DATA AND RESULTS

Table I summarized the experimental temperature profiles in terms of the three constants of an empirical equation. One constant, T_{CL} (Item (3)), was evaluated directly from the centerline temperature of the smoothed experimental data while the other two constants, A (Item (4)) and m (Item (5)), were evaluated from the slope and intercept of a log-log graph of $T_{CL} - T$ versus r, the radial position. The original temperature distribution data were used to make these graphs.

Table II is a summary of the constants required to evaluate the axial temperature gradients from the following relations.

Empirical Temperature Profile

$$T = T_{CL} - Ar^{m} \tag{D-1}$$

Axial Temperature Gradient

$$\left(\frac{\partial T}{\partial z}\right)_{z,r} = \left(\frac{\partial T_{CL}}{\partial z}\right)_{z} - r^{m_z}\left(\frac{\partial A}{\partial z}\right)_{z} - A_z r^{m_z} \ln r \left(\frac{\partial m}{\partial z}\right)_{z} \tag{D-2}$$

where the subscript z refers to the value of the parameter at some particular axial location. $(\partial T/\partial z)$, $(\partial A/\partial z)$, and $(\partial m/\partial z)$ were graphically evaluated from smoothed graphs of the constants T_{CL} (Item (3), Table I), A (Item (4), Table I), and m (Item (5), Table I)

versus cooling length (0.75 ft. between measuring ports) and tabulated in Table II for four axial positions as Items (3), (4), and (5). With these tabulated values it is now possible to calculate the axial temperature gradient at any axial and radial position.

Table III is a tabulation of the measured pressure gradient for each run and corresponding values of pressure gradients along the test section calculated by assuming: (a) that the volumetric flow rate was constant (continuity) and (b) that the measured pressure gradient corresponded to the actual pressure gradient at position (2), 15 inches from the downstream pressure tap. The second assumption is based on a few experimental measurements of the pressure gradient through the thermocouple ports. These data indicated that the pressure gradient (slope of a pressure versus length graph) increased along the axial flow direction such that the average (measured) value was reached at a position corresponding to position (2). The actual calculations of the corrected point pressure gradients were made with Computer Program (C-1), from which the volumetric flow rates were evaluated, and a desk calculator.

Table IV is a compilation of the temperature-dependent, power-law parameters for each run. These values were determined by the method outlined in Appendix B.

Table V lists non-Newtonian dimensionless groups and the bulk temperature for each run at four positions. These values were calculated by Computer Program (C-3), and the method is indicated in Appendix C. Table VI is a compilation of two types of "average" Nusselt and Graetz numbers that were compared with data of other

investigators. The first pair of Nusselt-Graetz numbers are average values of the "point" values of Nusselt numbers listed in Table V for each run with a corresponding average Graetz number. The second pair are based on the bulk temperature change and the over-all cooling length of the test sections.

Table VII is a tabulation of reduced temperature and radial position calculated for the experimental temperature data from runs 5 and 8. These data were compared with similar theoretical data.

Table VIII is explained in Appendix A where it appears.

Table IX through XII are explained in Appendix B where they appear.

Tables XIII through XX are the tabulated experimental temperature profiles. The reduced radius, Items (1), (3), (5), (7), and (9), is the measured radial distance, r, divided by the pipe radius, R_w = 1.332 cm. The temperature data were evaluated to the nearest 0.1°F in all cases while the radial position was measured to the nearest 0.1 mm. (0.0075 reduced radial units) with a vernier caliper.

Tables XXI through XXVIII contain the radial thermal conductivity and velocity profiles which were calculated for four positions in each run by Computer Program (C-1).

Tables XXIX through XXXVI are tabulations of the calculated temperature profiles (based on an assumed constant thermal conductivity). The technique used is outlined in Appendix C along with Computer Program (C-2).

TABLE XIII

EXPERIMENTAL TEMPERATURE DISTRIBUTION, RUN 1

(1) Inlet		(2)		(3) Middle		(4)		(5) Outlet	
Reduced Radius, X	Temp., °F.	Reduced Radius, X	Temp., °F.	Reduced Radius, X	Temp., °F.	Reduced Radius, X	Temp., °F.	Reduced Radius, X	Temp., °F.
(1)	(2)	(3)	(4)	(5)	(6)	(7)	(8)	(9)	(10)
-0.878	86.6	-0.863	79.2	-0.871	77.0	-0.871	76.0	-0.856	73.5
- .841	89.1	- .811	84.2	- .833	82.0	- .773	83.0	- .788	78.1
- .796	96.6	- .593	112.8	- .683	95.8	- .616	96.9	- .698	85.4
- .683	114.1	- .661	103.6	- .533	111.2	- .525	104.3	- .585	92.5
- .570	126.6	- .450	123.7	- .345	122.7	- .413	112.5	- .518	98.3
- .413	134.8	- .353	129.8	- .225	125.8	- .353	115.2	- .390	106.5
- .255	137.0	- .240	133.5	- .098	128.8	- .255	118.1	- .308	110.3
- .068	137.9	- .150	135.4	.030	129.8	- .165	120.7	- .233	112.0
.045	137.9	- .060	136.3	.150	129.0	- .023	122.0	- .158	114.9
.128	137.1	- .008	136.2	.233	127.0	.105	122.1	- .038	116.6
.263	136.0	.135	135.7	.315	124.5	.218	119.0	.113	115.5
.608	123.5	.210	134.0	.458	116.0	.323	115.3	.285	113.4
.353	134.5	.300	131.2	.533	110.3	.443	108.6	.338	108.6
.428	132.6	.435	124.8	.676	97.0	.585	100.3	.450	102.6
- .503	133.3	.510	119.5	.713	92.5	.713	89.3	.548	96.8
						.841	80.0	.653	90.7
								.773	81.0
								.841	76.4

TABLE XIV

EXPERIMENTAL TEMPERATURE DISTRIBUTION, RUN 2 (DOWNWARD)

(1) Inlet		(2)		(3) Middle		(4)		(5) Outlet	
Reduced Radius, X	Temp., °F.	Reduced Radius, X	Temp., °F.	Reduced Radius, X	Temp., °F.	Reduced Radius, X	Temp., °F.	Reduced Radius, X	Temp., °F
(1)	(2)	(3)	(4)	(5)	(6)	(7)	(8)	(9)	(10)
-0.826	88.0	-0.863	81.3	-0.893	76.3	-0.856	74.7	-0.886	73.3
- .721	107.7	- .826	82.5	- .751	80.3	- .796	83.2	- .706	86.1
- .585	120.4	- .638	105.1	- .518	112.5	- .668	92.6	- .480	105.1
- .398	127.7	- .518	116.4	- .398	120.5	- .555	102.1	- .585	94.7
- .278	128.9	- .383	123.3	- .188	125.8	- .413	112.1	- .353	109.0
- .420	127.8	- .240	126.8	- .090	126.5	- .308	116.1	- .203	115.0
- .158	129.4	- .165	127.3	- .023	126.1	- .188	119.9	- .090	116.8
.023	129.5	.038	128.1	.098	126.4	- .083	121.6	- .008	117.5
.195	128.9	.165	126.8	.473	118.5	.038	122.0	.135	116.1
.330	128.0	.345	123.4	.616	111.1	.135	120.5	.225	113.5
.533	124.1	.540	114.8	.818	82.2	.203	120.0	.293	111.0
.706	111.3	.773	92.6	.683	89.4	.293	116.4	.368	108.1
.848	94.5					.420	111.7	.458	102.8
						.563	101.3	.600	94.3
						.668	92.1	.743	83.4
						.886	74.5		

TABLE XV

EXPERIMENTAL TEMPERATURE DISTRIBUTION, RUN 3 (DOWNWARD)

(1) Inlet		(2)		(3) Middle		(4)		(5) Outlet	
Reduced Radius, X	Temp., °F	Reduced Radius, X	Temp., °F.	Reduced Radius, X	Temp., °F.	Reduced Radius, X	Temp., °F	Reduced Radius, X	Temp., °F.
(1)	(2)	(3)	(4)	(5)	(6)	(7)	(8)	(9)	(10)
-0.893	93.2	-0.878	88.5	-0.893	82.8	-0.886	78.9	-0.878	77.2
- .833	104.2	- .758	105.0	- .773	102.1	- .781	94.5	- .788	85.2
- .676	132.0	- .631	127.3	- .585	126.0	- .563	123.3	- .713	95.4
- .563	140.5	- .443	142.4	- .473	136.0	- .428	132.5	- .600	111.1
- .450	143.1	- .263	145.7	- .338	143.1	- .315	140.2	- .420	127.1
- .330	144.4	- .128	146.5	- .135	145.0	- .105	142.4	- .293	134.4
- .158	145.5	.090	146.7	- .015	145.0	- .015	142.4	- .135	137.6
- .045	145.6	.195	146.0	.075	144.0	.113	141.3	.000	138.3
.083	145.5	.315	144.6	.323	140.8	.360	134.5	.120	137.2
.188	144.8	.450	140.9	.540	129.2	.570	123.8	.285	132.7
.315	143.7	.548	134.8	.713	108.0	.616	114.5	.443	124.4
.398	142.4	.683	121.3	.826	92.0	.878	80.8	.616	109.2
.548	138.8	.818	95.0					.721	97.3
.653	132.0							.751	92.0
.781	112.1								
.833	101.8								

TABLE XVI

EXPERIMENTAL TEMPERATURE DISTRIBUTION, RUN 4

Reduced Radius, X	Temp., °F.	Reduced Radius, X	Temp., °F.	Reduced Radius, X	Temp., °F.	Reduced Radius, X	Temp., °F.	Reduced Radius, X	Temp., °F.
(1)	(2)	(3)	(4)	(5)	(6)	(7)	(8)	(9)	(10)
-0.901	85.5	-0.863	79.7	-0.908	75.9	-0.871	75.2	-0.871	72.8
- .803	100.6	- .766	83.3	- .803	86.7	- .796	86.0	- .766	82.7
- .706	121.1	- .683	111.5	- .668	108.4	- .585	113.1	- .540	112.4
- .631	123.2	- .495	135.5	- .443	125.3	- .480	123.6	- .428	124.0
- .563	139.0	- .293	144.9	- .203	143.8	- .330	136.3	- .293	133.0
- .323	145.2	- .188	146.1	- .038	144.6	- .173	141.3	- .150	137.0
- .180	146.3	- .083	146.8	.075	143.8	- .060	142.7	- .008	138.3
- .098	146.8	.075	146.6	.188	142.2	.083	141.9	.143	136.8
.008	146.8	.218	145.2	.353	137.5	.180	139.8	.248	132.6
.135	146.4	.405	140.8	.518	124.4	.360	132.0	.375	125.3
.300	144.9	.683	113.6	.638	110.0	.563	116.3	.503	115.2
.458	141.5	.856	84.9	.826	84.2	.698	98.9	.608	101.8
.570	135.4					.841	80.5	.788	79.7
.833	95.7							.818	75.1

TABLE XVII

EXPERIMENTAL TEMPERATURE DISTRIBUTION, RUN 5 (DOWNWARD)

(1) Inlet		(2)		(3) Middle		(4)		(5) Outlet	
Reduced Radius, X	Temp., °F.	Reduced Radius, X	Temp., °F.	Reduced Radius, X	Temp., °F.	Reduced Radius, X	Temp., °F.	Reduced Radius, X	Temp., °F.
(1)	(2)	(3)	(4)	(5)	(6)	(7)	(8)	(9)	(10)
-0.871	86.3	-0.863	81.6	-0.893	77.6	-0.886	74.5	-0.871	74.4
- .758	104.8	- .736	98.5	- .766	88.9	- .788	84.6	- .788	81.0
- .661	119.7	- .616	115.7	- .676	104.1	- .631	102.9	- .578	104.0
- .570	127.3	- .540	120.9	- .503	120.6	- .570	109.2	- .405	117.2
- .465	130.6	- .405	129.0	- .338	128.8	- .443	119.9	- .225	125.0
- .330	132.0	- .323	130.6	- .195	131.3	- .360	125.1	- .045	127.4
- .225	132.5	- .180	132.1	- .083	132.0	- .225	128.6	.113	126.4
- .098	132.9	- .098	132.4	.090	131.7	- .090	130.2	.368	122.0
.098	132.6	.030	132.5	.240	130.0	.075	129.8	.450	114.5
.195	132.3	.173	130.0	.405	125.3	.285	126.0	.638	98.7
.368	130.8	.270	131.0	.533	117.7	.488	115.7	.826	79.4
.473	128.9	.435	127.9	.683	103.3	.676	98.7		
.653	122.2	.510	124.5	.826	86.7	.863	76.6		
.743	112.8	.661	113.8						
.856	93.5	.773	99.8						
		.826	91.0						

TABLE XVIII

EXPERIMENTAL TEMPERATURE DISTRIBUTION, RUN 6

(1) Inlet		(2)		(3) Middle		(4)		(5) Outlet	
Reduced Radius, X	Temp., °F.	Reduced Radius, X	Temp., °F.	Reduced Radius, X	Temp., °F.	Reduced Radius, X	Temp., °F.	Reduced Radius, X	Temp., °F
(1)	(2)	(3)	(4)	(5)	(6)	(7)	(8)	(9)	(10)
-0.863	93.0	-0.871	85.4	-0.916	80.9	-0.878	81.2	-0.871	76.5
- .758	110.9	- .788	114.1	- .788	93.0	- .781	90.0	- .743	90.8
- .616	137.4	- .540	138.3	- .653	114.9	- .676	107.5	- .503	122.7
- .458	147.5	- .270	149.3	- .525	133.5	- .563	122.7	- .210	130.7
- .368	149.2	.030	150.1	- .278	147.6	- .458	135.6	.030	145.8
- .203	151.0	.285	147.6	- .128	149.3	- .345	142.7	.203	142.2
- .075	151.9	.465	142.8	.045	149.2	- .180	148.0	.270	137.5
.090	152.2	.653	124.8	.203	147.4	- .045	149.1	.488	125.2
.210	151.6	.856	90.9	.353	143.8	.023	149.2	.608	111.9
.398	149.2			.525	132.7	.158	147.8	.856	81.1
.578	143.4			.728	108.0	.278	143.6		
.863	104.5			.848	91.1	.495	131.0		
						.646	109.3		
						.841	83.7		

TABLE IX

EXPERIMENTAL TEMPERATURE DISTRIBUTION, RUN 7 (DOWNWARD)

(1) Inlet		(2)		(3) Middle		(4)		(5) Outlet	
Reduced Radius, X	Temp., °F.	Reduced Radius, X	Temp., °F.	Reduced Radius, X	Temp., °F.	Reduced Radius, X	Temp., °F.	Reduced Radius, X	Temp., °F.
(1)	(2)	(3)	(4)	(5)	(6)	(7)	(8)	(9)	(10)
-0.856	90.7	-0.863	85.1	-0.886	78.3	-0.848	77.6	-0.871	75.9
- .788	108.8	- .811	90.7	- .796	88.1	- .721	95.9	- .751	89.4
- .691	131.8	- .721	106.7	- .570	122.6	- .706	119.0	- .578	113.8
- .480	152.8	- .585	131.0	- .465	136.8	- .465	129.8	- .435	129.4
- .360	155.3	- .480	143.6	- .285	148.1	- .323	140.9	- .293	139.3
- .218	156.6	- .315	152.0	- .173	151.6	- .195	146.4	- .128	144.7
- .060	156.9	- .188	154.2	- .038	152.9	- .060	149.0	.008	145.7
.113	156.4	- .038	155.0	.113	152.3	.068	148.8	.203	141.8
.255	155.4	.083	154.7	.240	150.0	.263	143.6	.398	129.7
.390	153.5	.195	153.6	.368	144.0	.435	132.2	.548	116.6
.548	149.0	.330	151.1	.510	135.1	.608	115.9	.706	97.0
.646	139.6	.458	145.2	.736	107.2	.736	94.4	.826	82.3
.781	117.6	.661	125.1	.871	87.7	.893	78.2		
.871	99.8	.841	95.3						

TABLE XX

EXPERIMENTAL TEMPERATURE DISTRIBUTION, RUN 8

(1) Inlet		(2)		(3) Middle		(4)		(5) Outlet	
Reduced Radius, X	Temp., °F.	Reduced Radius, X	Temp., °F.	Reduced Radius, X	Temp., °F.	Reduced Radius, X	Temp., °F.	Reduced Radius, X	Temp., °F.
(1)	(2)	(3)	(4)	(5)	(6)	(7)	(8)	(9)	(10)
-0.886	93.9	-0.878	84.8	-0.901	82.5	-0.863	82.1	-0.886	75.7
- .833	101.0	- .803	98.9	- .766	99.3	- .796	89.6	- .773	88.0
- .751	121.1	- .585	141.3	- .661	117.9	- .706	103.3	- .623	109.3
- .623	148.0	- .480	154.8	- .510	144.3	- .540	128.3	- .420	137.1
- .473	162.3	- .233	167.7	- .345	159.9	- .405	146.1	- .143	156.2
- .278	167.7	- .068	169.2	- .180	166.1	- .300	155.6	- .300	151.7
- .053	169.9	.135	168.3	- .053	166.5	- .150	162.2	.030	157.4
.090	169.5	- .023	169.2	.090	165.7	.030	162.8	.150	155.5
.270	167.4	.233	166.7	.218	161.4	.150	160.8	.300	148.2
.428	162.6	.398	159.3	.435	147.4	.248	156.4	.443	136.5
.631	144.9	.585	135.0	.585	130.8	.420	144.4	.555	121.1
.826	102.5	.713	114.5	.728	106.7	.600	122.8	.676	103.1
		.841	89.3	.788	98.0	.743	101.3	.758	91.2
						.856	85.8	.833	81.7

TABLE XXI

CALCULATED VELOCITY AND THERMAL CONDUCTIVITY DISTRIBUTION, RUN 1

Position	(2)		(3) Middle		(4)		(5) Outlet	
Reduced Radius, X	Velocity Ft/Min	Thermal Conductivity Btu/Hr-Ft-°F	Velocity Ft/Min	Thermal Conductivity Btu/Hr-Ft-°F	Velocity Ft/Min	Thermal Conductivity Btu/Hr-Ft-°F	Velocity Ft/Min	Thermal Conductivity Btu/Hr-Ft-°F
(1)	(2)	(3)	(4)	(5)	(6)	(7)	(8)	(9)
0.000	1.378	-----	1.368	-----	1.363	-----	1.361	-----
0.100	1.378	0.286	1.368	0.247	1.362	0.246	1.361	0.241
0.200	1.375	.283	1.365	.274	1.360	.270	1.358	.264
0.300	1.363	.300	1.353	.300	1.348	.286	1.347	.278
0.400	1.330	.318	1.321	.321	1.317	.297	1.318	.286
0.500	1.262	.329	1.256	.334	1.253	.302	1.252	.290
0.600	1.145	.327	1.142	.334	1.141	.300	1.142	.289
0.700	0.966	.308	0.968	.319	0.970	.291	0.971	.282
0.800	0.717	.274	0.723	.291	0.727	.273	0.729	.266
0.900	0.394	.228	0.401	.251	0.405	.246	0.407	.242
1.000	0.000	-----	0.000	-----	0.000	-----	0.000	-----

TABLE XXII

CALCULATED VELOCITY AND THERMAL CONDUCTIVITY DISTRIBUTION, RUN 2 (DOWNWARD)

Position	(2)		(3) Middle		(4)		(5) Outlet	
Reduced Radius, X	Velocity Ft/Min	Thermal Conductivity Btu/Hr-Ft-°F	Velocity Ft/Min	Thermal Conductivity Btu/Hr-Ft-°F	Velocity Ft/Min	Thermal Conductivity Btu/Hr-Ft-°F	Velocity Ft/Min	Thermal Conductivity Btu/Hr-Ft-°F
(1)	(2)	(3)	(4)	(5)	(6)	(7)	(8)	(9)
0.000	1.594	-----	1.573	-----	1.562	-----	1.552	-----
0.100	1.593	0.477	1.573	0.305	1.562	0.280	1.552	0.240
0.200	1.590	.356	1.569	.307	1.559	.322	1.548	.279
0.300	1.574	.331	1.554	.321	1.544	.355	1.534	.304
0.400	1.531	.328	1.513	.335	1.505	.379	1.496	.322
0.500	1.446	.323	1.432	.340	1.428	.391	1.420	.333
0.600	1.302	.306	1.296	.329	1.300	.391	1.292	.336
0.700	1.087	.272	1.091	.303	1.098	.376	1.096	.332
0.800	0.795	.224	0.808	.261	0.821	.346	0.822	.317
0.900	0.430	.170	0.444	.213	0.456	.305	0.458	.292
1.000	0.000	-----	0.000	-----	0.000	-----	0.000	-----

TABLE XXIII

CALCULATED VELOCITY AND THERMAL CONDUCTIVITY DISTRIBUTION, RUN 3 (DOWNWARD)

Position	(2)		(3) Middle		(4)		(5) Outlet	
Reduced Radius, X	Velocity Ft/Min	Thermal Conductivity Btu/Hr-Ft-°F	Velocity Ft/Min	Thermal Conductivity Btu/Hr-Ft-°F	Velocity Ft/Min	Thermal Conductivity Btu/Hr-Ft-°F	Velocity Ft/Min	Thermal Conductivity Btu/Hr-Ft-°F
(1)	(2)	(3)	(4)	(5)	(6)	(7)	(8)	(9)
0.000	2.729	-----	2.685	-----	2.676	-----	2.672	-----
0.100	2.728	2.027	2.685	0.676	2.675	0.678	2.672	0.638
0.200	2.720	0.792	2.677	.473	2.667	.510	2.664	.481
0.300	2.687	.507	2.644	.425	2.634	.450	2.630	.409
0.400	2.600	.404	2.559	.414	2.548	.421	2.545	.363
0.500	2.425	.354	2.393	.407	2.383	.399	2.381	.328
0.600	2.137	.317	2.122	.389	2.115	.375	2.115	.298
0.700	1.723	.276	1.735	.353	1.734	.342	1.736	.269
0.800	1.201	.227	1.238	.300	1.242	.299	1.246	.238
0.900	0.610	.173	0.649	.238	0.655	.250	0.660	.205
1.000	0.000	-----	0.000	-----	0.000	-----	0.000	-----

TABLE XXIV

CALCULATED VELOCITY AND THERMAL CONDUCTIVITY DISTRIBUTION, RUN 4

Position	(2)		(3) Middle		(4)		(5) Outlet	
Reduced Radius, X	Velocity Ft/Min	Thermal Conductivity Btu/Hr-Ft-°F	Velocity Ft/Min	Thermal Conductivity Btu/Hr-Ft-°F	Velocity Ft/Min	Thermal Conductivity Btu/Hr-Ft-°F	Velocity Ft/Min	Thermal Conductivity Btu/Hr-Ft-°F
(1)	(2)	(3)	(4)	(5)	(6)	(7)	(8)	(9)
0.000	2.550	-----	2.492	-----	2.479	-----	2.473	-----
0.100	2.549	1.250	2.491	0.388	2.478	0.355	2.473	0.369
0.200	2.541	0.580	2.483	.351	2.471	.359	2.465	.319
0.300	2.508	.428	2.451	.368	2.438	.390	2.433	.292
0.400	2.422	.381	2.368	.392	2.356	.420	2.352	.272
0.500	2.252	.357	2.209	.406	2.201	.437	2.198	.254
0.600	1.974	.330	1.955	.399	1.952	.431	1.951	.236
0.700	1.583	.289	1.597	.367	1.601	.400	1.602	.215
0.800	1.098	.234	1.139	.314	1.149	.347	1.152	.192
0.900	0.554	.173	0.599	.250	0.609	.282	0.612	.166
1.000	0.000	-----	0.000	-----	0.000	-----	0.000	-----

TABLE XXV

CALCULATED VELOCITY AND THERMAL CONDUCTIVITY DISTRIBUTION, RUN 5 (DOWNWARD)

Position	(2)		(3) Middle		(4)		(5) Outlet	
Reduced Radius, X	Velocity Ft/Min	Thermal Conductivity Btu/Hr-Ft-°F	Velocity Ft/Min	Thermal Conductivity Btu/Hr-Ft-°F	Velocity Ft/Min	Thermal Conductivity Btu/Hr-Ft-°F	Velocity Ft/Min	Thermal Conductivity Btu/Hr-Ft-°F
(1)	(2)	(3)	(4)	(5)	(6)	(7)	(8)	(9)
0.000	2.939	-----	2.911	-----	2.882	-----	2.881	-----
0.100	2.939	0.986	2.910	0.485	2.881	0.387	2.880	0.504
0.200	2.932	.437	2.903	.361	2.874	.348	2.873	.412
0.300	2.901	.349	2.872	.352	2.843	.347	2.842	.365
0.400	2.818	.342	2.789	.368	2.763	.355	2.762	.333
0.500	2.650	.348	2.625	.381	2.604	.360	2.603	.306
0.600	2.364	.341	2.349	.378	2.340	.354	2.339	.281
0.700	1.940	.311	1.944	.352	1.950	.334	1.950	.255
0.800	1.382	.259	1.406	.304	1.426	.299	1.426	.226
0.900	0.719	.194	0.749	.242	0.771	.252	0.772	.195
1.000	0.000	-----	0.000	-----	0.000	-----	0.000	-----

TABLE XXVI

CALCULATED VELOCITY AND THERMAL CONDUCTIVITY DISTRIBUTION, RUN 6

Position	(2)		(3) Middle		(4)		(5) Outlet	
Reduced Radius, X	Velocity Ft/Min	Thermal Conductivity Btu/Hr-Ft-°F	Velocity Ft/Min	Thermal Conductivity Btu/Hr-Ft-°F	Velocity Ft/Min	Thermal Conductivity Btu/Hr-Ft-°F	Velocity Ft/Min	Thermal Conductivity Btu/Hr-Ft-°F
(1)	(2)	(3)	(4)	(5)	(6)	(7)	(8)	(9)
0.000	3.053	-----	2.999	-----	2.959	-----	2.951	-----
0.100	3.053	1.263	2.998	0.493	2.959	0.288	2.951	0.306
0.200	3.044	0.559	2.990	.359	2.950	.260	2.942	.258
0.300	3.005	.424	2.951	.345	2.912	.264	2.905	.234
0.400	2.903	.393	2.852	.355	2.817	.274	2.810	.217
0.500	2.700	.379	2.659	.362	2.633	.280	2.628	.204
0.600	2.365	.354	2.345	.350	2.336	.276	2.334	.191
0.700	1.892	.307	1.903	.317	1.915	.258	1.917	.176
0.800	1.305	.241	1.343	.264	1.372	.228	1.378	.159
0.900	0.654	.171	0.696	.202	0.725	.189	0.731	.139
1.000	0.000	-----	0.000	-----	0.000	-----	0.000	-----

TABLE XXVII

CALCULATED VELOCITY AND THERMAL CONDUCTIVITY DISTRIBUTION, RUN 7 (DOWNWARD)

Position	(2)		(3) Middle		(4)		(5) Outlet	
Reduced Radius, X	Velocity Ft/Min	Thermal Conductivity Btu/Hr-Ft-°F	Velocity Ft/Min	Thermal Conductivity Btu/Hr-Ft-°F	Velocity Ft/Min	Thermal Conductivity Btu/Hr-Ft-°F	Velocity Ft/Min	Thermal Conductivity Btu/Hr-Ft-°F
(1)	(2)	(3)	(4)	(5)	(6)	(7)	(8)	(9)
0.000	3.054	-----	3.011	-----	2.993	-----	2.983	-----
0.100	3.053	0.974	3.011	0.488	2.992	0.413	2.982	0.510
0.200	3.043	.568	3.000	.396	2.982	.358	2.972	.435
0.300	3.000	.472	2.958	.381	2.940	.340	2.930	.394
0.400	2.892	.447	2.852	.383	2.835	.331	2.827	.365
0.500	2.681	.434	2.650	.384	2.638	.321	2.632	.339
0.600	2.343	.412	2.330	.372	2.328	.305	2.324	.313
0.700	1.876	.371	1.886	.343	1.893	.281	1.895	.284
0.800	1.302	.312	1.332	.298	1.346	.248	1.351	.252
0.900	0.661	.243	0.692	.244	0.706	.209	0.711	.217
1.000	0.000	-----	0.000	-----	0.000	-----	0.000	-----

TABLE XXVIII

CALCULATED VELOCITY AND THERMAL CONDUCTIVITY DISTRIBUTION, RUN 8

Position	(2)		(3) Middle		(4)		(5) Outlet	
Reduced Radius, X	Velocity Ft/Min	Thermal Conductivity Btu/Hr-Ft-°F	Velocity Ft/Min	Thermal Conductivity Btu/Hr-Ft-°F	Velocity Ft/Min	Thermal Conductivity Btu/Hr-Ft-°F	Velocity Ft/Min	Thermal Conductivity Btu/Hr-Ft-°F
(1)	(2)	(3)	(4)	(5)	(6)	(7)	(8)	(9)
0.000	2.854	-----	2.827	-----	2.805	-----	2.792	-----
0.100	2.853	0.400	2.826	0.495	2.804	0.519	2.791	0.583
0.200	2.843	.285	2.815	.398	2.793	.441	2.780	.493
0.300	2.797	.271	2.769	.373	2.748	.410	2.736	.446
0.400	2.683	.278	2.656	.365	2.638	.390	2.628	.411
0.500	2.467	.285	2.447	.358	2.435	.372	2.429	.380
0.600	2.134	.279	2.125	.341	2.123	.349	2.122	.349
0.700	1.688	.257	1.695	.311	1.704	.319	1.708	.316
0.800	1.157	.220	1.177	.269	1.193	.282	1.200	.279
0.900	0.581	.175	0.601	.221	0.616	.239	0.622	.239
1.000	0.000	-----	0.000	-----	0.000	-----	0.000	-----

TABLE XXIX

CALCULATED TEMPERATURE PROFILES WITH ASSUMED CONSTANT THERMAL CONDUCTIVITY, RUN 1

Position	(3) Middle	(4)	(5) Outlet
Reduced Radius, X	Temperature, °F	Temperature, °F	Temperature, °F
(1)	(2)	(3)	(4)
0.000	129.99	121.71	112.55
0.100	129.29	120.84	111.68
0.200	127.49	118.64	109.52
0.300	124.23	114.78	105.84
0.400	119.21	109.18	100.68
0.500	112.11	101.91	94.26
0.600	102.75	93.27	86.95
0.700	91.43	83.79	79.23
0.800	79.03	74.16	71.59
0.900	66.71	65.00	64.45
1.000	55.33	56.67	58.0

TABLE XXX

CALCULATED TEMPERATURE PROFILES WITH ASSUMED CONSTANT THERMAL CONDUCTIVITY, RUN 2 (DOWNWARD)

Position	(3) Middle	(4)	(5) Outlet
Reduced Radius, X	Temperature, °F	Temperature, °F	Temperature, °F
(1)	(2)	(3)	(4)
0.000	124.05	117.63	110.29
0.100	123.44	116.83	109.47
0.200	121.84	114.82	107.42
0.300	118.89	111.27	103.92
0.400	114.27	106.07	98.99
0.500	107.66	99.26	92.84
0.600	98.93	91.12	85.80
0.700	88.43	82.18	78.35
0.800	76.99	73.10	71.01
0.900	65.71	64.48	64.17
1.000	55.33	56.67	58.00

TABLE XXXI

CALCULATED TEMPERATURE PROFILES WITH ASSUMED CONSTANT THERMAL CONDUCTIVITY, RUN 3 (DOWNWARD)

Position	(3) Middle	(4)	(5) Outlet
Reduced Radius, X	Temperature, °F	Temperature, °F	Temperature, °F
(1)	(2)	(3)	(4)
0.000	145.47	142.45	138.07
0.100	145.04	141.73	137.14
0.200	143.85	139.82	134.74
0.300	141.38	136.18	130.39
0.400	136.92	130.27	123.82
0.500	129.61	121.65	114.96
0.600	118.74	110.30	104.14
0.700	104.32	96.93	92.13
0.800	87.69	82.78	79.93
0.900	70.88	69.12	68.42
1.000	55.33	56.67	58.00

TABLE XXXII

CALCULATED TEMPERATURE PROFILES WITH ASSUMED CONSTANT THERMAL CONDUCTIVITY, RUN 4

Position	(3) Middle	(4)	(5) Outlet
Reduced Radius, X	Temperature, °F	Temperature, °F	Temperature, °F
(1)	(2)	(3)	(4)
0.000	144.99	141.02	135.71
0.100	144.44	140.17	134.68
0.200	142.94	137.96	132.83
0.300	139.92	133.84	127.46
0.400	134.67	127.39	120.67
0.500	126.50	118.40	111.79
0.600	115.01	107.06	101.24
0.700	100.69	94.17	89.81
0.800	84.98	80.87	78.37
0.900	69.52	68.19	67.67
1.000	55.33	56.67	58.00

TABLE XXXIII

CALCULATED TEMPERATURE PROFILES WITH ASSUMED CONSTANT THERMAL CONDUCTIVITY, RUN 5 (DOWNWARD)

Position	(3) Middle	(4)	(5) Outlet
Reduced Radius, X	Temperature, °F	Temperature, °F	Temperature, °F
(1)	(2)	(3)	(4)
0.000	132.04	129.86	126.67
0.100	131.70	129.30	125.93
0.200	130.77	127.81	124.01
0.300	128.82	124.93	120.50
0.400	125.26	120.17	115.10
0.500	119.35	113.09	107.69
0.600	110.40	103.55	98.46
0.700	98.23	92.51	88.03
0.800	83.83	79.68	77.32
0.900	69.05	67.64	67.17
1.000	55.33	56.67	58.00

TABLE XXXIV

CALCULATED TEMPERATURE PROFILES WITH ASSUMED CONSTANT THERMAL CONDUCTIVITY, RUN 6

Position	(3) Middle	(4)	(5) Outlet
Reduced Radius, X	Temperature, °F	Temperature, °F	Temperature, °F
(1)	(2)	(3)	(4)
0.000	149.13	146.35	142.38
0.100	148.69	145.62	141.42
0.200	147.43	143.67	138.97
0.300	144.80	139.92	134.49
0.400	140.05	133.76	127.66
0.500	132.27	124.75	118.36
0.600	120.75	112.85	106.93
0.700	105.66	98.81	94.20
0.800	88.46	83.97	81.26
0.900	71.23	69.68	69.05
1.000	55.33	56.67	58.00

TABLE XXXV

CALCULATED TEMPERATURE PROFILES WITH ASSUMED CONSTANT THERMAL CONDUCTIVITY, RUN 7 (DOWNWARD)

Position	(3) Middle	(4)	(5) Outlet
Reduced Radius, X	Temperature, °F	Temperature, °F	Temperature, °F
(1)	(2)	(3)	(4)
0.000	153.32	149.81	145.25
0.100	152.70	148.93	144.18
0.200	151.03	146.64	141.47
0.300	147.72	142.35	136.59
0.400	142.09	135.56	129.28
0.500	133.43	125.93	119.52
0.600	121.24	113.54	107.70
0.700	105.79	99.18	94.69
0.800	88.47	84.17	81.55
0.900	71.22	69.77	69.18
1.000	55.33	56.67	58.00

TABLE XXXVI

CALCULATED TEMPERATURE PROFILES WITH ASSUMED CONSTANT THERMAL CONDUCTIVITY, RUN 8

Position	(3) Middle	(4)	(5) Outlet
Reduced Radius, X	Temperature, °F	Temperature, °F	Temperature, °F
(1)	(2)	(3)	(4)
0.000	166.41	161.59	153.60
0.100	165.59	160.49	154.32
0.200	163.41	157.65	151.07
0.300	159.21	152.42	145.29
0.400	152.31	144.34	136.78
0.500	142.04	133.14	125.63
0.600	127.99	119.08	112.39
0.700	110.63	103.12	98.02
0.800	91.54	86.66	83.66
0.900	72.68	70.96	70.19
1.000	55.33	56.67	58.00

APPENDIX E

NOMENCLATURE

A - constant used in Equation (D-1)

a - constant in Equation (A-15)

B - constant defined for Table IV

b - constant in Equation (A-15)

C - consistency index of power-law

C_o - constant defined for Table IV

C' - modified consistency index defined in Equation (2-7)

C_p - heat capacity

D - pipe diameter

d - constant in Equation (A-15)

E - defined by Equation (A-12)

f_{iso} - isothermal Fanning friction factor

f_{ni} - non-isothermal Fanning friction factor

G - 0.944, a differencing constant

$\vec{g}$ - external force vector

g - acceleration of gravity

g_c - units constant

H - measured couple per unit height

h - $z' - z'_o$

h_A - heat transfer film coefficient based upon arithmetic-mean temperature difference

h_i - driving height at $t = 0$

K - thermal conductivity

L - length

m - constant used in Equation (D-1)

n - exponent in power-law

n' - modified exponent in power-law defined in Equation (2-6)

P - static pressure

Q - volumetric flow rate

$\vec{q}$ - heat flux vector

q_r - radial heat flux

R - upper limit corresponding to radial position

R_C - radius of capillary

R_M - radius of manometer tube

R_R - radius of the reservoirs in the capillary unit

R_w - pipe radius

r - radius

r_C - radius of container

r_s - radius of spindle

s - height of sample column

T - temperature

$T(i,j)$ - temperature at radial position i and axial position j

t - time

V - average linear velocity

w - velocity

$\vec{w}$ - velocity vector

w_z - axial velocity

$w_z(i)$ - axial velocity at radial position i

X - reduced radius

y - height of mercury column in capillary unit reservoir

y_o - hydrostatic balance height

y_r - dummy integration symbol for distance from centerline

z - cooled length

z_1 - spindle immersion depth

z' - height of mercury column in manometer

z'_o - hydrostatic balance height

α - defined by Equation (C-3)

β - reciprocal Graetz number

μ - viscosity

μ_b - viscosity at bulk temperature

μ_w - viscosity at wall temperature

ν - shear rate

π - 3.1415----

ρ - density

ρ_m - density of mercury

ρ_s - density of test liquid

τ - shear stress

$\vec{\tau}$ - shear stress tensor

τ_r - shear stress at radius r

τ_{rz} - rz component of shear stress

θ - reduced temperature

Ω - angular velocity

Ω_s - angular velocity at spindle radius

Δ - difference notation

$\frac{D}{Dt}$ - Substantial derivative

∇ - Del operator

f( ) - functional notation

COMPUTER SYMBOLS

A - A, a constant in the empirical temperature distribution

AKO - C_o, an empirical constant in the temperature-dependent rheological equation

ALPHA - thermal conductivity

AQKB - estimated thermal conductivity of test fluid at bulk temperature

AQKW - estimated thermal conductivity of test fluid at wall temperature

ATJ - wall temperature gradient

B - B, an empirical constant in temperature-dependent rheological equation

CPR - a constant in Equation (C-1)

D - a constant in Equation (C-1)

DAZ - partial derivative for Equation (D-2)

DC - inside pipe diameter, cm.

DF - inside pipe diameter, ft.

DMZ - partial derivative for Equation (D-2)

DR - radial increment

DTCLZ - partial derivative for Equation (D-2)

DZ - axial increment

OD - outside pipe diameter

PG - pressure gradient

PI - 3.14159, a constant

Runno - data identification number

S - 1/n, an empirical constant in the temperature-dependent rheological equation

SSK - approximate thermal conductivity of stainless steel

T - m, a constant in the empirical temperature distribution

T(i) - point temperatures

TCL - T_{CL}, centerline temperature

TMJ - initial wall temperature

U(i) - point velocities

V(i) - inlet velocities

W(i) - inlet temperatures

WSS - wall shear stress

DIMENSIONLESS GROUPS

ANUNO - Nusselt Number (Wall), see page 99

N_{GZ} - Graetz Number, Equation (7-1)

N_{NU} - Nusselt Number based on arithmetic-mean temperature difference, Equation (7-1)

PRNOA - Prandtl Number (Bulk), see page 99

PRNOB - Prandtl Number (Wall), see page 99

RENO - Reynolds Number, see page 99

VITA

VITA

George Marshall Drake, Jr. was born in Goodlettsville, Tennessee on July 25, 1932. He attended public schools in Old Hickory, Tennessee and graduated from Du Pont High School in June, 1951. He entered the University of Tennessee in September, 1951 and has since received both his B. S. (August, 1955) and M. S. (March, 1957) degrees in chemical engineering from the University.

Upon completion of the requirements for the Ph. D. degree (August, 1961), the author and his wife will move to Richmond, Virginia where he will be employed by E. I. du Pont de Nemours and Company.

COMMENTARY

The existance of fully developed laminar flow is required before one is justified in determining the velocity distribution from experimental temperature and rheological data. An equation for estimating the transition length required for fully developed laminar flow is given below (39):

$$L_{entrance} = 0.065\ D\ N_{Re}$$

where: $L_{entrance}$ is the entrance length,

D is the inside pipe diameter, and

N_{Re} is the Reynolds number.

This equation has been shown to give conservative estimates for pseudoplastic power-law fluids by Bogue*. The maximum transition lengths required in this investigation were less than 1.5×10^{-3} ft as compared to the 0.75 ft spacing between temperature measuring ports, therefore; it is concluded that fully developed laminar velocity profiles did exist in the test section and that their calculation from experimental temperature and rheological data was justified.

---

* Bogue, D. C., "Entrance Effects and Prediction of Turbulence in Non-Newtonian Flow", Ind. Eng. Chem. 51, 874 (1959).